SUMMARY

ProQuest LLC.
789 East Eisenhower Parkway
P.O. Box 1346
Ann Arbor, MI 48106 – 1346

"Thermodynamic and Structural Properties of Zinc/Copper Alloys"

Summary

The thesis, entitled as above, is concerned with the measurement of thermodynamic properties of zinc copper alloys in the liquid and solid states, and with the interpretation of these in terms of alloy structure.

A conventional dew-point technique was used to determine, initially, the vapour pressure of the zinc component at a number of temperatures and, from these values, partial and integral thermodynamic functions were calculated. For evaluation of the vapour pressures, the equations of Kubaschewski and Evans[+], relating the vapour pressure of pure zinc, in solid and liquid states, to temperature were used as a basis. The results of other workers were recalculated, wherever possible, to the same basis for comparison.

In general, the present results show fair agreement with previous work but with certain differences. For liquid alloys, for instance, a change from negative to positive deviation

---

[+] O. Kubaschewski and E.L. Evans, "Metallurgical Thermochemistry" Pergamon Press (1958).

from ideality is shown by the thermodynamic activity of the zinc as high zinc contents are approached. Previously, the results of other workers have indicated negative deviation over the whole compositional range.

Also, characteristic minima and maxima were obtained in the curves when $\Delta\bar{S}^{x}_{Zn}$ values from the present work on liquid and solid alloys were plotted against composition. One of these minima, viz. that occurring at 0·43 N_{Zn} in the solid alloys, is considered difficult to explain and probably spurious. Otherwise, the minima occur at compositions corresponding approximately to the centre of the β and γ-phase fields and are associated with the critical electron/atom ratios (1·48 and 1·615 respectively) required, by electron theory for the formation of the appropriate electron compounds. The peak positive value (i.e. highest maximum) in the $\Delta\bar{S}^{x}_{Zn}$ curve for liquid alloys, which occurs at 0·68 N_{Zn}, has analogies in at least two other binary systems, viz. Zn/Sb and Cd/Sb. This positive value of excess entropy is considered to be associated with an increased vibrational contribution to entropy, and linked with the previously reported defect structure of the δ-phase.

Quantitative application of quasi-chemical theory to

the partial and integral thermodynamic functions was attempted but, after comparison with other systems, reasons are advanced for the limited applicability. However, qualitative application, particularly when integral properties are considered, is possible.

The partial thermodynamic functions of the second component, i.e. copper, were calculated from the Gibbs-Duhem relationship, and thus integral properties obtained. For the liquid alloys, both of the partial and the integral functions are compared and the conclusion drawn that, in certain compositional regions there is build up of "excess" enthalpy (stored probably as vibrational energy) which is released again to allow the "minimum" value to be attained at fixed compositions. Two of these fixed compositions co-incide approximately with the critical electron/atom ratios necessary, according to electron theory, for the formation of the β and γ-phases in solid alloys, but it is postulated that the true "critical" compositions are those corresponding to the maximum build-up of excess enthalpy. In addition, the variation of the partial properties in the region of these critical compositions suggests that the release of the excess enthalpy is accompanied by a redistribution of the vibrational energy between the two components of the solution.

Because of the close approximation of the compositions, at which the minimal values occur, to the centres of the solid β, γ and ε- phase fields, a fourth minimum, corresponding to the unexplored δ-phase field region is predicted. Also, the existence of these min in plots referring to liquid alloys, is taken as an indication of the extent to which "solid" structures persist above liquidus temperatures.

The above postulations and the link with electron theory are less clearly applicable to the solid alloys, but sufficient similarity exists to suggest that complete analogy may be established by further study.

"THERMODYNAMIC AND STRUCTURAL PROPERTIES of ZINC/COPPER ALLOYS"

Thesis presented to the

UNIVERSITY OF GLASGOW

by

DAVID B. DOWNIE, B. Sc., A.R.C.S.T.

for the

DEGREE OF DOCTOR OF PHILOSOPHY

METALLURGY DEPARTMENT,

THE ROYAL COLLEGE OF SCIENCE AND TECHNOLOGY,

GLASGOW.

April, 1963.

CONTENTS

Page

LIST OF SYMBOLS

A	an atomic species, also area and equation constant
a	activity
B	an atomic species and equation constant
E	electromotive force
F	faraday
$\Delta\overline{G}$	partial molar free energy
ΔG_m	integral " " "
$\Delta\overline{G}^X$	excess partial molar free energy
ΔG^X_m	" integral " " "
H	enthalpy
$\Delta\overline{H}$	partial molar enthalpy
ΔH_m	integral " "
K	equilibrium constant
°K	degrees Kelvin
ln	Naperian logarithm
log	logarithm to base 10
No	Avogadro's number
P	number of bonds
p	partial vapour pressure of metal in alloy
p_o	vapour pressure of pure metal
R	the gas constant per gram-molecule
$\Delta\overline{S}$	partial molar entropy
ΔS_m	integral " "

$\Delta\bar{S}^{x}$	excess partial molar entropy
ΔS^{x}_{m}	" integral " "
T	temperature
$\Delta\bar{Y}$	partial molar thermodynamic function
ΔY	integral " " "
Z	co-ordination number
γ	activity coefficient
ν	interaction energy

PART - 1

INTRODUCTION

PART 1 - INTRODUCTION

Considerable attention, extending over many years, has been given to the measurement of the thermodynamic properties of alloys in binary metallic systems. A wide variety of experimental methods has been employed in these measurements but little attempt has been made, until recently, to collate and assess the relative reliability of the various results. However, in 1952 Lumsden (1)* reviewed the data on two or three alloy systems and later, in 1956, Kubaschewski and Catterall (2) assessed a much larger number of systems.

In addition, despite the plethora of results available, it is only comparatively recently that some attention has been given to the use of thermodynamic data in the interpretation of alloy structures in both solid and liquid states. Thus, the earlier solution theory of Guggenheim, Rushbrooke, Hildebrand and others has been developed and applied to metallic systems by, for example, Hilliard, Averbach and Cohen (3) and Kleppa (4), making use of thermodynamic measurements for qualitative and quantitative interpretation.

Examination of the relevant literature, including the assessments of Lumsden and Kubaschewski and Catterall referred to above, showed that, although some attention had been given to the determination of the thermodynamic properties of zinc-copper alloys, there was need for

---

*Numbers in brackets relate to references which are listed on pages 127 and 128.

further measurements, particularly in the liquid state, before a reasonable attempt at correlation with structure could be made. Since this system is an important, if not a key one in the application of electron theory to alloys, it was decided to carry out an investigation with an attempt at this correlation as objective.

Previous workers on the thermodynamics of the zinc/copper system have used a wide variety of experimental methods. These include measurement of electrode potentials (5,6), of vapour pressure by transportation (7), dew point (8, 9, 10), isopiestic (11) and absorption spectra (12) techniques, and by calorimetry (13, 14, 15). The general application of these methods in the metallurgical field has been described by Kubaschewski and Evans (16) and will not be discussed further at this stage. However, in view of the high measurement temperatures necessary, particularly for the liquid alloys of higher copper content, it was considered desirable to use a vapour pressure method to evaluate, in the first instance, the partial thermodynamic properties of the zinc component. Also, by making measurements over a range of temperature for each alloy, an estimate of the partial entropy term could be obtained. Of the three vapour pressure methods mentioned above, the dew-point technique seemed best suited to determinations in both solid and liquid states over the necessary ranges of composition and temperature and, consequently, was adopted for the present investigation.

In the dew-point technique the sample is enclosed in a clear fused-quartz tube which is subsequently evacuated and sealed. At each end of the quartz tube are small diameter re-entrant tubes of the same material which carry thermocouples. In operation, the tube with the sample located at one end, is heated to the measurement temperature and, while maintaining the sample end at this temperature (T_1), the other end is cooled slowly until the dew-point of the vapour in equilibrium with the sample is reached (T_2). Thus the vapour pressure of the alloy at temperature T_1 is the same as that of pure zinc at T_2. The method requires, therefore, a pre-knowledge of the vapour pressure of pure zinc over the temperature range covered by the investigation. The adoption of appropriate values for this is discussed in Part 4.2.

In all estimations by the above method the vapour pressure o f the second component, viz. copper, is assumed to be negligible compared with that of zinc. This assumption is justified by the known thermodynamic behaviour of Zn/Cu alloys and by comparison of accepted values for the vapour pressures of the two pure metals which, even at the highest temperatures used in this work, are in the ratio of 10^7 : 1.

Detailed descriptions of the apparatus and experimental procedure follow in Parts 2 and 3 respectively.

PART 2

DESCRIPTION OF APPARATUS

PART 2 - Description of Apparatus

2.1 General

An isometric view of the assembled apparatus is shown in Fig. 1. It consisted essentially of four main items, viz.-

(i) a dew-point tube containing the alloy sample,

(ii) a multi-winding furnace to contain the dew-point tube and provide means of applying a variable heat gradient,

(iii) a panel of variable transformers, ammeters, switches, etc., to facilitate furnace control, and

(iv) a twin thermocouple arrangement to measure temperatures T_1 and T_2.

In general, the apparatus was similar to that used by previous workers using the dew-point technique and closely resembled that described by Underwood and Averbach (17).

2.2. Dew-point Tube

A sketch of this item is shown in Fig. 2. The main tube was made from clear fused-silica ware of 10 mm. bore and 1·5 mm wall with a closed end thermocouple sheath of the same material, 4 mm bore by 1·2 mm wall, sealed into each end. The main tube, below the end of the thermocouple sheath at one end, was blown out to form a well to accommodate the sample. Finally, a small side-tube of dimensions similar to the thermocouple sheathing was fixed to allow evacuation and sealing of the tube. Invariably, the apparatus was made in two parts, the sample inserted and the parts joined before evacuation and sealing.

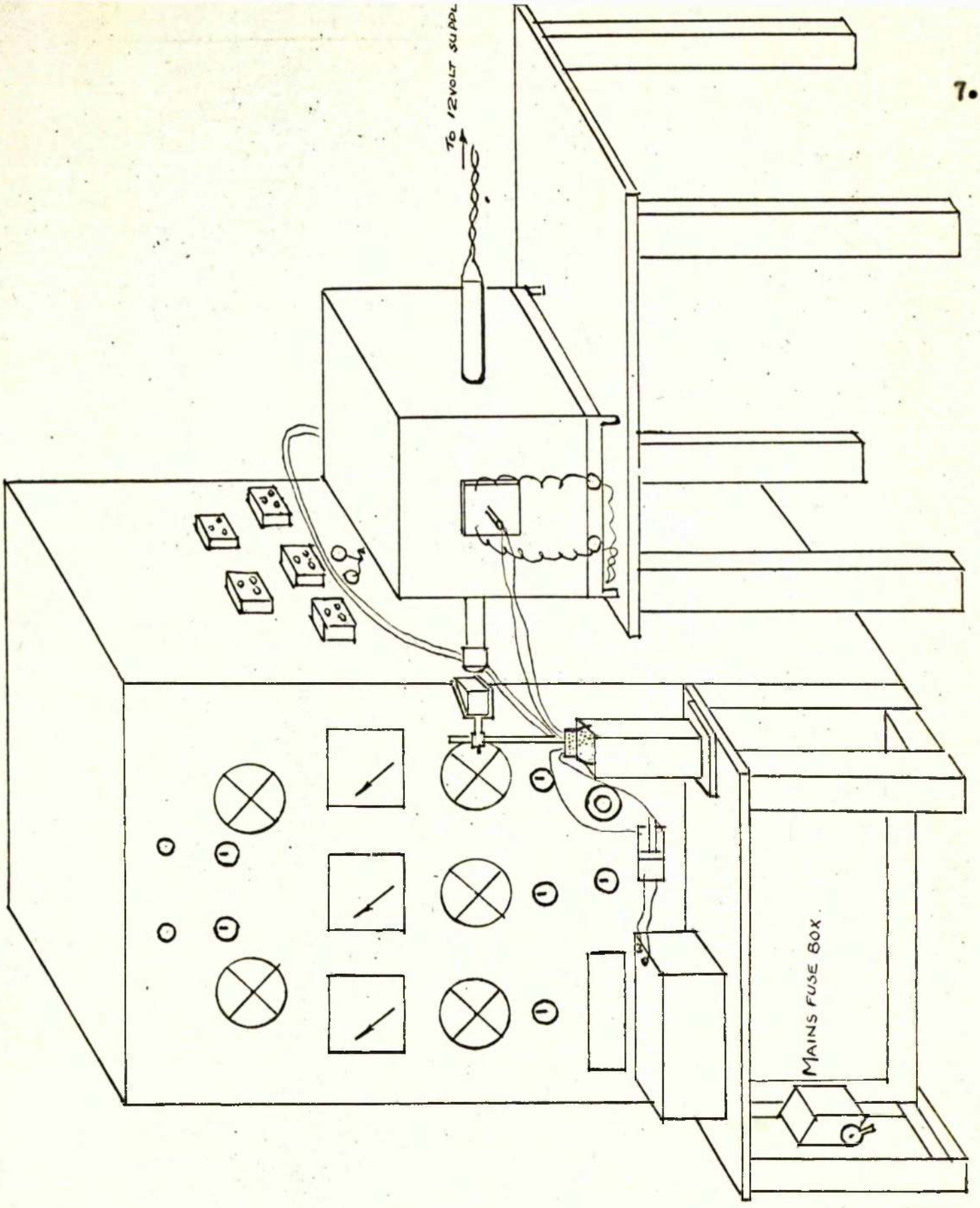

FIG. 1.

Previous workers whose determinations were confined to the solid state used a sample in the form of a hollow cylinder which slipped over the end of one of the thermocouple sheaths. This was done to ensure accurate temperature determination and to provide a large free surface area. However, the sample-well method adopted for these investigations allowed determination of vapour pressures in both liquid and solid states on the same sample. Results obtained with this design of apparatus (10, 18) appear to compare satisfactorily with those obtained from the other (9, 17).

The important dimensions of the dew-point tube were found to be the distance between the sheath tips ("x" in Fig. 2) and the distance from the tip of the sheath at the cold end to the closed end of the tube ("y" in Fig. 2). It was desirable to have the sample positioned at the point of maximum temperature in the furnace when the tip of the termocouple measuring T_s was opposite the viewing aperture. Thus, distance "x" was dictated by the temperature gradient characteristics of the furnace, i.e. the distance between the viewing aperture and the position of maximum temperature. It was likewise desirable not to have distance "y" too great since, even with the auxiliary heater in position, it was possible to have the closed end at a lower temperature than the tip of the thermocouple measuring T_s. Thus, condensation could take place away from the thermocouple point and out of sight. During vapour pressure determinations the dew-point tube was located inside/heating chamber of the multi-winding
the

furnace (A in Fig. 3).

Strict cleanliness during blowing and handling of the clear silica-ware was observed as far as possible, but it was found, during use, that the tube gradually became opaque and had to be replaced. However, it was normally possible to cut open the dew-point tube and replace the sample with another two or three times before the tube became unusable. In most instances, the sample filled the well so completely that, when solid, it could not be removed except by partly dissolving it with nitric acid.

2.3 Multi-winding Furnace

The general requirements for heating in dew-point determination are those of a chamber which can be controlled to give a temperature gradient along its length and which provides means of observing the condensate end of the dew-point tube. Thus, a multi-resistance wound refractory tube, carrying two side-tubes for illumination and observation respectively, was found suitable when enclosed in an insulated case carrying terminals for the various electrical connections.

A sketch of the furnace used is shown in Fig. 3. The main tube, 60 mm. o/d by 5 mm. wall thickness by 400 mm. in length, was of fused alumina. Two holes, about 25 mm. in diameter, were drilled opposite each other in the wall about 130 mm. from one end. The drilling was achieved fairly conveniently and accurately using a diamond impregnated steel tubular bit of the appropriate diameter.

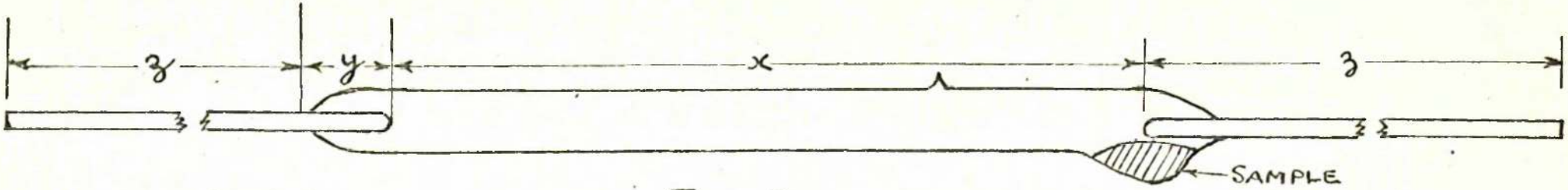
z
y
x
3
SAMPLE

FIG. 2.

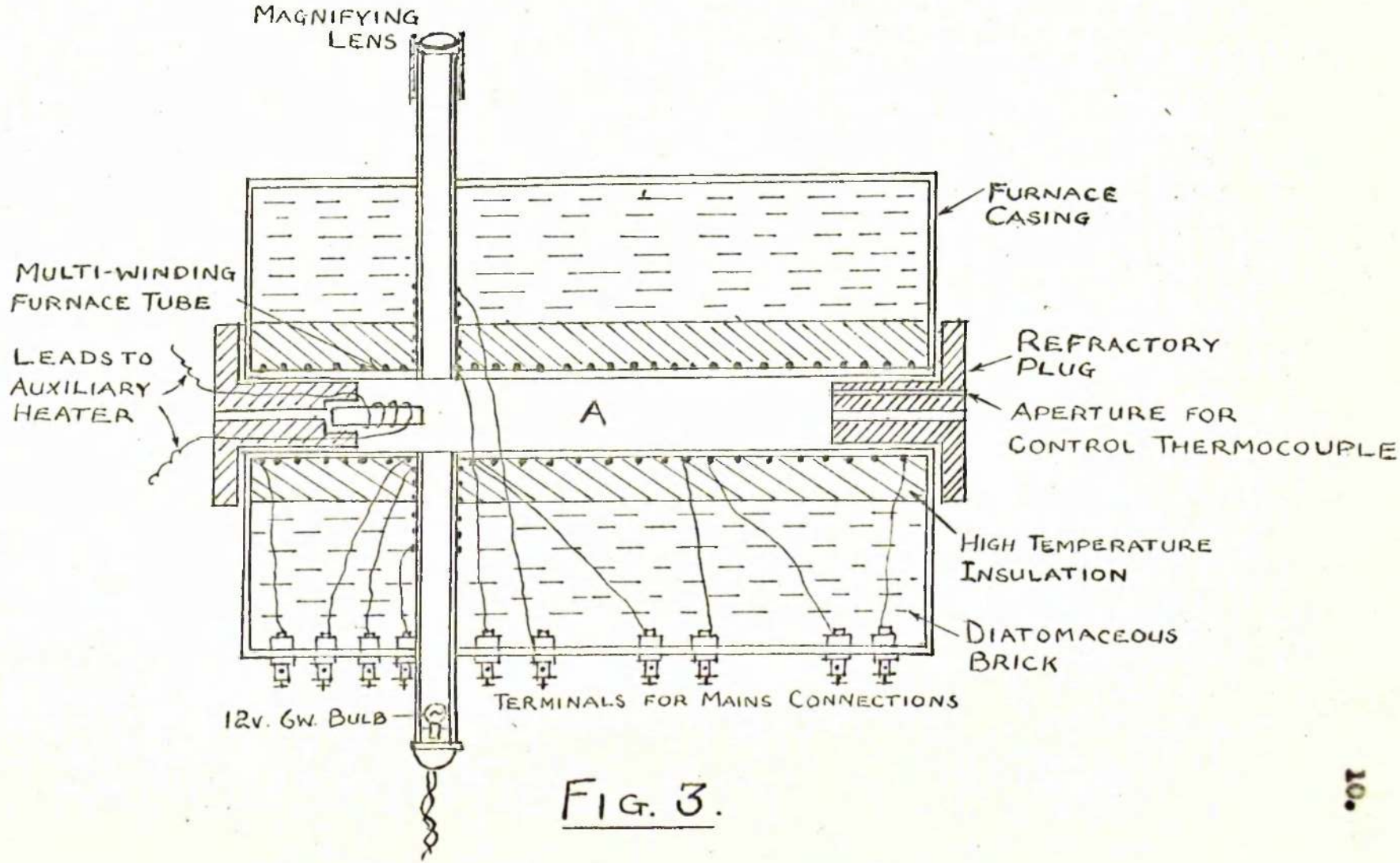
MAGNIFYING LENS
FURNACE CASING
MULTI-WINDING FURNACE TUBE
LEADS TO AUXILIARY HEATER
REFRACTORY PLUG
A
APERTURE FOR CONTROL THERMOCOUPLE
HIGH TEMPERATURE INSULATION
DIATOMACEOUS BRICK
12v. 6w. BULB
TERMINALS FOR MAINS CONNECTIONS

FIG. 3.

Flood lubrication with water was employed.

The three main furnace windings, each of which covered approximately a one-third length of the tube, were disposed two on one side of the side-tubes and one on the other. The spacing of the turns of wire was aimed at compensating for heat losses from the furnace ends. Thus the two end windings were graded from the open ends of the tube in the sequence 16 turns at approximately 3 turns per cm., 14 turns at approximately 2·5 turns per cm. and 5 turns at approximately 2 turns per cm., while the centre winding was of constant spacing at approximately 1·5 turns per cm. Nichrome wire of 22 s.w.g. (0·711 mm.) diameter was used for all three windings.

The side-tubes, approximately 25 mm. o/d by 5 mm. wall thickness by 175 mm. in length, were made from alundum cement and wound separately with 26 s.w.g. (0·457 mm.) diameter nichrome wire over an 80 mm. length from one end. When the main furnace tube had been located in the partly filled casing the side-tubes were fixed in position with alundum cement, the wound ends being placed next to the wall of the main tube and the unwound ends penetrating through holes to the outside of the furnace case. During operation of the apparatus a small current (0·5 to 1·0 amp.) in each side-tube winding minimised localised heat loss at the holes in the main tube. General heat losses were reduced by surrounding the main tube with shaped high-temperature insulating brick and packing the rest of the casing with diatomaceous

blocks. The ends of the main tube were also plugged with shaped insulating brick which was drilled to accommodate the thermocouple sheaths and leads for the auxilliary heater.

This last, auxilliary heater consisted of a 150 mm. length of silica tubing wound over two-thirds of its length from one end with 35 s.w.g. (0·213 mm) diameter nichrome wire. When in position, the wound portion covered the condensation end of the dew-point tube but left the tip of the thermocouple sheath uncovered for observation. The unwound end rested in a hole cut in the corresponding end-plug. While adjustments of the currents in the main furnace windings were used to establish the desired heat gradient approximately, final and more flexible control was achieved by the auxilliary heater.

To provide illumination of the condensation area one of the side-tubes was fitted with a 6-watt bulb connected to a 12-volt supply. Observations were made through the opposite side-tube which carried a magnifying lens and a prism to facilitate viewing.

In operation, the furnace was given a slight inclination downwards towards the high temperature end to ensure retention of the molten sample in the well.

As indicated previously, it was desirable to know the nature of the temperature gradient established in the furnace at any given setting. For this reason, tests were carried out using a long thermocouple and sheath in place of the dew-point tube inside the furnace.

The thermocouple was moved back and forth along the length of the furnace, temperature readings being noted at one or two centimetre intervals. A typical plot of temperature against distance from centre of viewing tube is shown in Fig. 5. It was found that little change in location of maximum and minimum temperatures occurred with change in setting, thus allowing the distance between the tips of the thermocouple sheaths in the dew-point tube to be fixed at about 197 mm. Further checks on the temperature gradient were made from time to time, particularly following repairs to, or replacement of, any of the main windings.

2.4 Electrical Circuits

The wiring arrangements necessary to control the heating elements of the apparatus were made through a central control panel which is shown in Fig. 4. This consisted essentially of a board to which were fixed the variable transformers, ammeters, pilot lights, switches and temperature controller. The board was mounted vertically on a Dexion frame which rested on the floor and carried a horizontal shelf suitable for holding the portable-type potentiometer which was used for temperature measurement. Below this shelf, and to one side, was fitted a fuse box carrying a mains switch, while behind the vertical board were located the control resistance (see below) and all connecting leads.

The wiring diagram is shown in Fig. 4. Main winding

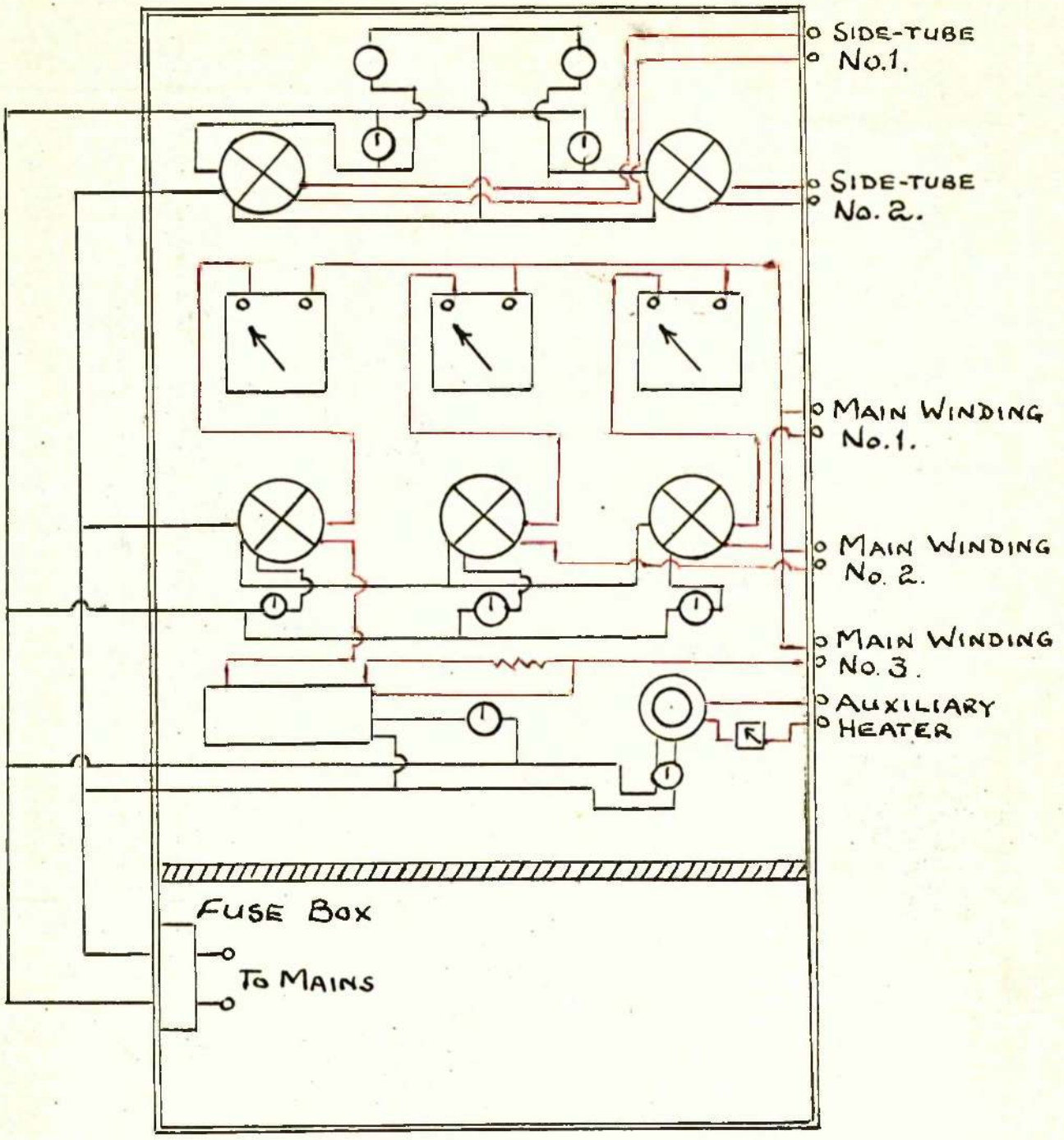

8-AMP. VARIACS.

CONTROLLER.

PILOT LIGHTS.

2-AMP. VARIAC.

SWITCHES.

PLUG SOCKETS.

AMMETERS.

CONTROL RESISTANCE.

INPUT CIRCUITS.

OUTPUT CIRCUITS.

FIG. 4.

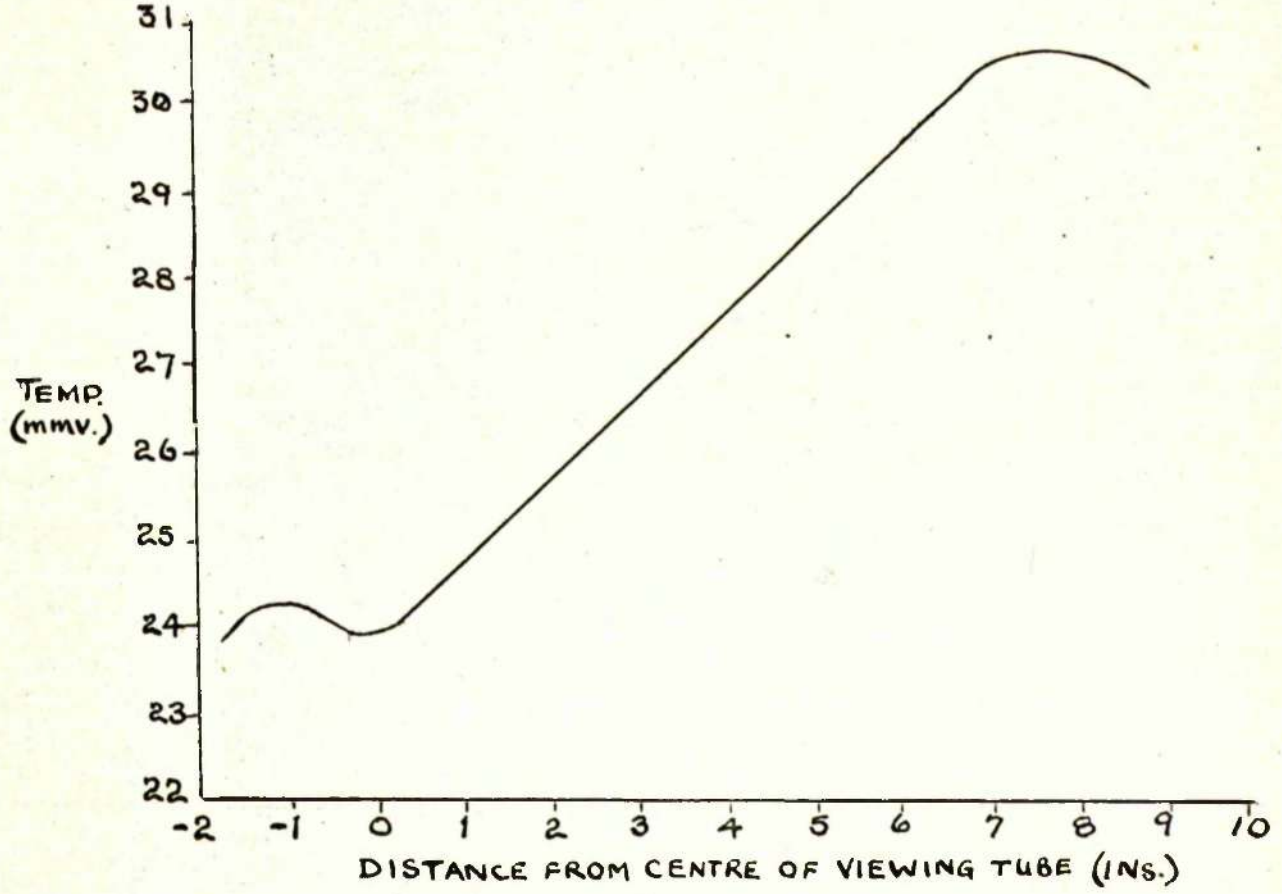
TEMP. (mmv.)
31
30
29
28
27
26
25
24
23
22
-2
-1
0
1
2
3
4
5
6
7
8
9
10
DISTANCE FROM CENTRE OF VIEWING TUBE (INS.)

FIG. 5.

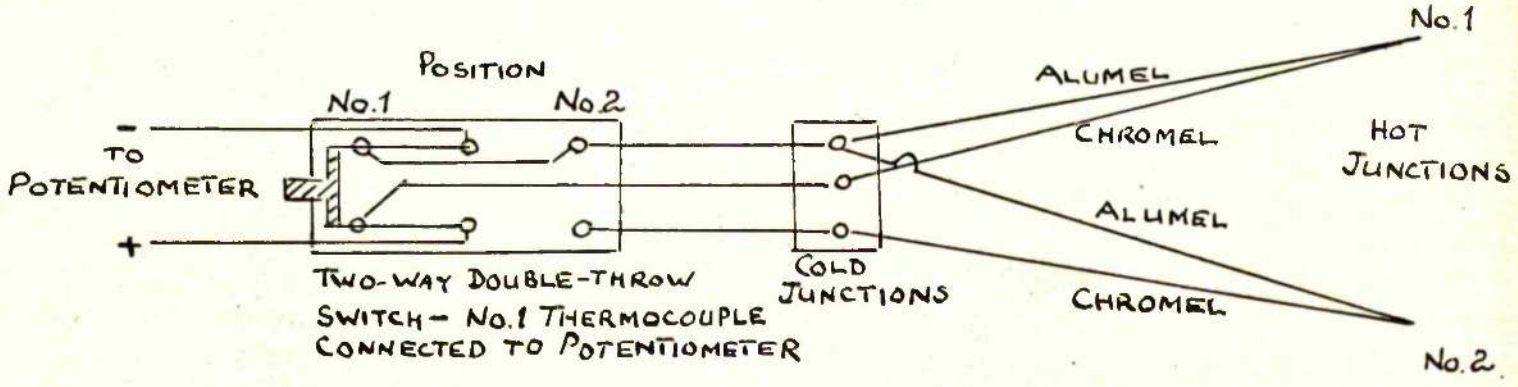
POSITION
No.1
No.2
-
TO POTENTIOMETER
+
TWO-WAY DOUBLE-THROW SWITCH - No.1 THERMOCOUPLE CONNECTED TO POTENTIOMETER
COLD JUNCTIONS
ALUMEL
CHROMEL
ALUMEL
CHROMEL
No.1
HOT JUNCTIONS
No.2

FIG. 6.

No. 1 (at the "hot" end of the furnace) was the only winding connected through a temperature controller as well as a variable transformer. A Kelvin and Hughes Proportional Controller Mk. 4, operated by a chromel/alumel thermocouple located near the sample, was used and the wiring arranged so that, instead of cutting the current off completely on a rising temperature, a small fixed resistance was switched into the circuit. This reduced the current in the winding by 0·5 to 1·0 amp. and the whole arrangement resulted in a degree of control of the order of $\pm$ 1°C in the temperature of the sample.

It will be noted from Fig. 4 that ammeters were incorporated in the circuits for windings 1, 2 and 3, and for the auxiliary heater. Ammeters in the side-tube circuits were omitted since little alteration of the current in these was necessary. However, pilot lights in the input circuits served to give an indication of "on" or "off".

Leads from the output terminals of the variable transformers were taken to sockets screwed to the panelling on one side of the frame. Plugs, with leads to the winding terminals on the furnace casing were then inserted into the appropriate sockets. It was found desirable to ensure that, where first and last turns of adjacent windings were close together, the leads were given the same polarity to minimise potential difference and hence arcing between the turns.

All furnace terminals, furnace leads, output sockets and control panel switches were labelled to provide rapid identification.

2.5 Temperature Measurement

Originally, Chromel/Alumel thermocouples were used to measure T_1 and T_2. Due, however, to the almost continuous use to which they were subjected, oxidation and breakage necessitated frequent calibration. This standardisation was carried out by determination of the zinc and aluminium points using Tadanac zinc and B.A.C. Super-purity aluminium. Conversion of the indicated freezing points from millivolts to degrees centigrade was made using the British Standard relationship for Chromel/Alumel thermocouples and the required corrections obtained by subtraction from the true melting points, viz. 419·5 and 660·1°C respectively. These two corrections were plotted on squared paper against indicated temperature and a straight line through them extrapolated to the highest temperature registered in the investigation. This straight line graph was then used to correct all indicated temperatures, the maximum connection required being about 6°C.

Later, Platinum/Platinum-13% Rhodium thermocouples were substituted, these being calibrated against a N.P.L. standarised thermocouple (also of Pt/Pt -13% Rh) as well as, initially, the zinc and aluminium points. The working and standard thermocouples were compared over the full range of temperature used in the experimental work, thus avoiding the necessity for extrapolated corrections. It was found that only small corrections (0·010 - 0·020 mav), which were constant over the full working temperature range, were required. Moreover, the noble metal thermocouples were much more stable in

calibration.

The wiring arrangement of the base metal thermocouples is shown in Fig. 6. It will be noted that from the cold junction to the potentiometer the thermocouples had a common negative lead. Thus, the two Alumel wires were joined to one copper lead, while the two Chromel wires were attached to separate copper leads. All three joints were soldered and these, the cold junctions, maintained at 0°C. by means of pure, melting ice in a vacuum flask. The copper leads were taken from the cold junction to a two-way switch connected, again by copper leads, to the portable-type potentiometer used for measuring temperature. Operation of the two-way switch allowed either thermocouple to be read at will.

The same wiring arrangements were used with the precious metal thermocouples except that, since very long thermocouple wires were necessary, an economy was effected by using short lengths of Pt and Pt/Rh wire which were connected to the cold junction via standard compensating leads.

Calibration against the freezing points of the pure metals was carried out in a small vertical furnace into which was inserted an alundum crucible carrying a fused alumina thermocouple sheath closed at one end. The pure metal in the crucible was melted and cooled at about 1°C per minute until an arrest was registered by the test thermocouple in the alumina sheath. This procedure was repeated at least once before the first thermocouple was replaced by the

second and again two checking results obtained.

When calibration of the precious metal thermocouples was made by comparison with the N.P.L. standard, all three hot junctions were enclosed in thin-walled alumina sheaths which, in turn, were inserted into holes drilled in the end of a cylinder of austenitic stainless steel. This cylinder, about 25 mm diameter by 50 mm in length, acted as a heat reservoir and minimised temperature variation across the diameter of the furnace tube. The cold junctions of the standard thermocouple were connected, without intervening compensating cable, by copper leads, via a second two-way switch, to the potentiometer.

All calibrations were carried out with the connections and wiring arrangements as close as possible to those used under experimental working conditions.

PART 3

EXPERIMENTAL PROCEDURE

Part 3 - Experimental Procedure

3.1 Preparation of Alloys

The alloys used were prepared by accurately weighing out pure zinc (Tadanac A quality, containing 99·95% Zn) and pure copper (to B.S.S. 1861, containing 99·95% Cu) in the required proportions and melting the mixtures in sealed, evacuated fused silica tubes. After quenching in cold water to produce rapid solidification and minimise segregation, the alloys were annealed, still in their original sealed tubes, for two days to further reduce inhomogeneity.

It was found that ingots of about 50 grams weight provided ample material for vapour pressure determination samples and, if necessary, for analysis. Thus it was convenient to use satin surface silica tubing of 13 mm. bore and 1·5 mm wall thickness which gave an ingot about 50 mm. long for a weight of approximately 50 grams. The pure metals were cut into small pieces (about 3 mm. in diameter) before weighing so that fairly close packing in the melting tubes was obtained, thus keeping the total length of tubing to a minimum and reducing the furnace accommodation required for melting and annealing. This proved particularly advantageous in annealing during which it was essential to keep the whole length of the tube fairly evenly heated. Excessive heat gradients were liable to produce condensation of zinc vapour on the colder parts of the tube, thus changing the alloy composition. After making allowance for sealing,

a final tube length of about 150 mm (i.e. approximately three times the length of the final ingot) was obtained.

Furnace temperature during melting varied according to the melting point of the alloy. For alloys of high copper content temperatures of around 1100°C were necessary but this could be reduced progressively to about 900°C as the copper content was reduced to the low values of the zinc-rich alloys. Frequent agitation was carried out during melting with a final vigorous shake before plunging the melting-tube into the cold water quenching bath. Cracking of the melting-tube at this stage was sometimes experienced but was generally avoided by ensuring rapid immersion in the water.

The alloys were annealed, still in the silica melting tubes, in a nichrome wound furnace controlled to ± 5°C by a Kelvin and Hughes Proportional Controller. Micro-examination of sections from the annealed ingots showed that a treatment of 48 hours at 650°C (450°C in the case of the single alloy in the ε- field) was adequate to eliminate the coring produced by rapid solidification.

Analytical checks were carried out on some of the annealed ingots, samples from each end being analysed separately. In these estimations the copper content was found by electrolytic deposition and the zinc by difference. The results agreed, within the experimental accuracy of the analyses, with the as-weighed compositions.

3.2 Determination of Vapour Pressures

Between 5 and 6 grams of alloy, in the form of several small portions from top and bottom of the ingot, were placed in the well at one end of the dew-point tube and the other part of the tube fused on. The whole tube was then evacuated through the side arm to 0·05 mm Hg pressure and sealed.

The sealed dew-point tube was then fitted into the multi-winding furnace. First of all, the plug and auxiliary heater at the "cold" end of the furnace were removed and fitted over the thermocouple sheath at the condensation end of the dew-point tube. The end plug was then carefully inserted, at the same time feeding the dew-point tube into the furnace. When the first plug was fully home the second plug was pushed over the "hot" end thermocouple sheath. Finally, the thermocouples were placed in position. Before switching on, the leads from the auxiliary heater, which passed through the "cold" end plug, were connected to their terminals on the lower part of the furnace casing.

Initially, the sample was melted by raising the whole of the dew-point tube to above the melting point of the alloy. To ensure that all the sample entered the well the furnace was tilted to an angle of about 45° and then carefully returned to its normal angle of tilt before being allowed to cool. The dew-point tube was then

removed from the furnace to check the sample for completeness of melting and for position. The apparatus was reassembled and the determination of vapour pressures commenced.

When determinations were made with the alloy in the solid state about 16 hours at temperature were allowed (usually overnight) for equilibrium to be reached before condensation temperatures were measured, but only 3 to 4 hours were found to be necessary when the sample was molten. Thus, in many instances, it was possible to make one estimation in the solid and one in the liquid state every 24 hours. In general, estimations at successively increasing or decreasing temperatures were avoided so that any progressive errors could more readily be detected.

When changing the estimation temperature in the upward direction it was necessary to ensure that the temperature at the "cold" end of the dew-point tube was also raised at a similar or greater rate to prevent condensation due to increased vapour pressure at the "hot" end. However, it was advantageous to disturb the existing heat gradient as little as possible since many hours could elapse before the furnace became stabilised after an increase or decrease in power input.

Once the equilibrium vapour pressure had been reached the temperature of the condensation end of the dew-point tube (T_2) was gradually lowered until a clearly visible condensate was observed. This temperature was noted and immediately T_2 was raised again, using

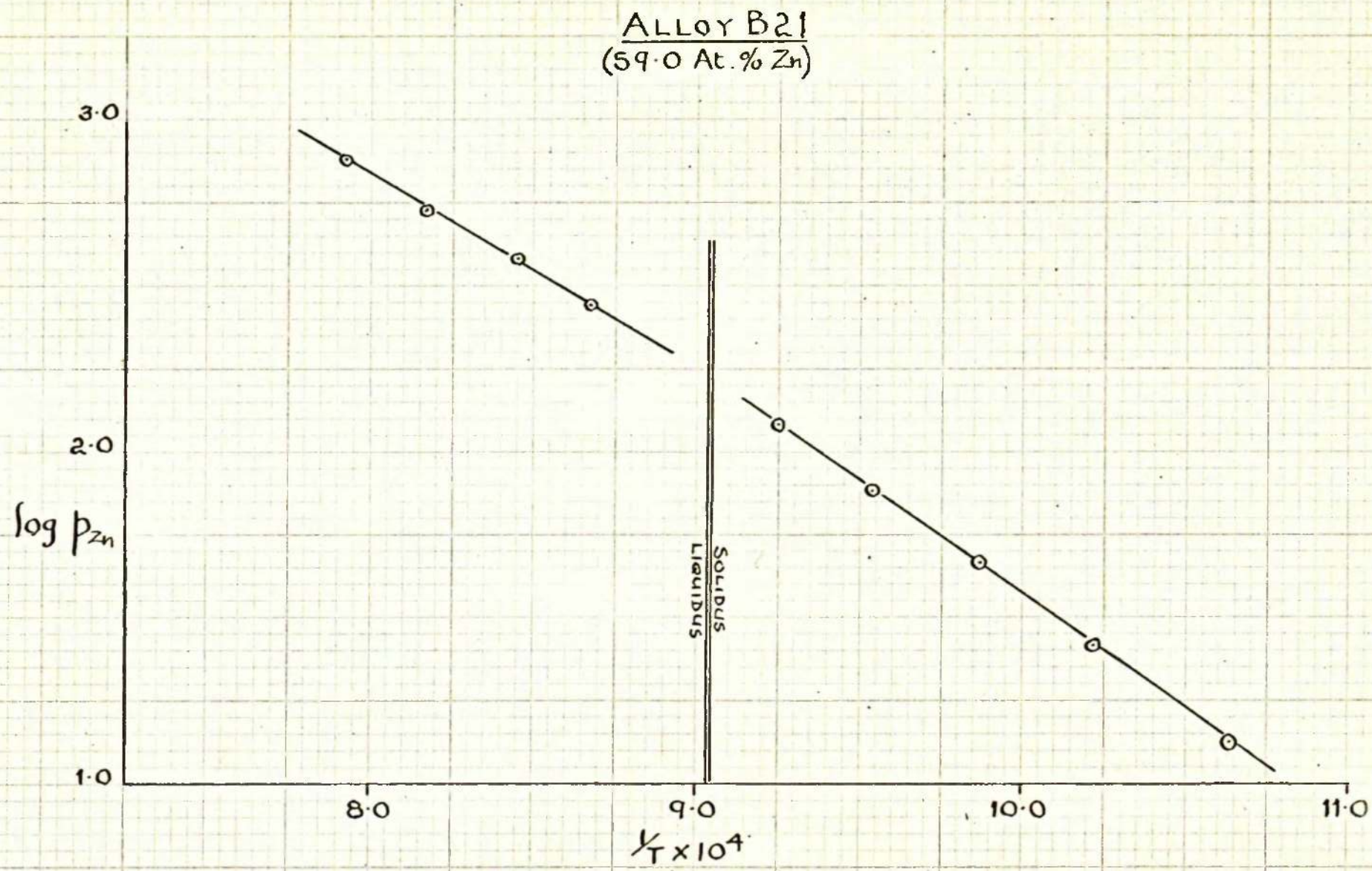
ALLOY B21
(59·0 At.% Zn)
3·0
2·0
1·0
log p_{Zn}
SOLIDUS
LIQUIDUS
8·0
9·0
10·0
11·0
$1/T \times 10^4$

FIG. 7.

the quick-response auxiliary heater until re-evaporation took place. Using these approximate condensation and evaporation temperatures as a guide, further, more closely-controlled cooling and heating cycles were made to reduce the difference between them. The final difference between the two temperatures varied considerably depending upon the measured vapour pressure, viz. from 16°C for low vapour pressures to 1·5°C for high vapour pressures. The values adopted for T_s was the mean of the closest condensation and evaporation temperatures measured.

The results for each alloy were plotted on a graph of log p_{Zn} against $1/T°K$. Normally, their consistency was such that four or five results each for the solid and liquid alloys were sufficient to establish close approximations to linear relationships. Plots for a typical alloy are shown in Fig. 7.

PART 4

THERMODYNAMIC CALCULATIONS

Part 4 - Thermodynamic Calculations

4.1 Partial Molar Properties of Zinc

In general, results from vapour pressure measurements by the dew-point technique, as described in Part 3, are expressed as two temperatures, viz. the temperature of the alloy (T_A) and the temperature at which the vapour, in equilibrium with the alloy, condenses (T_B). The vapour pressure of the volatile metal in the alloy is then that of the pure condensed metal at temperature T_B. From this known vapour pressure and that corresponding to pure volatile metal at T_A, assuming the vapour to behave as an ideal gas, the activity of the vaporised component in the alloy is obtained.

Therefore, in this investigation,

$$a_{Zn} = \frac{p_{Zn}}{p_{Zn_o}}$$

where a_{Zn} = thermodynamic activity of zinc in the alloy

p_{Zn} = vapour pressure of zinc in the alloy

p_{Zn_o} = vapour pressure of pure zinc at the same temperature

From this activity value other thermodynamic functions can be derived as follows:-

$$\gamma_{Zn} = \frac{a_{Zn}}{N_{Zn}}$$

$$\Delta G_{Zn} = RT \ln a_{Zn}$$

$$\Delta \overline{G}^{x}_{Zn} = \Delta G_{Zn} - RT \ln N_{Zn} = RT \ln \gamma_{Zn}$$

where γ_{Zn} = activity coefficient of zinc in alloy,

N_{Zn} = mole fraction of zinc in alloy,

$\Delta\bar{G}_{Zn}$ = partial molar free energy of zinc,

and $\Delta\bar{G}^{x}_{Zn}$ = excess partial molar free energy of zinc.

Knowledge of the variation of vapour pressure, and hence activity and partial free energy values with temperature, allows partial entropy values to be derived. Thus, the following further functions can be derived:-

$$\Delta\bar{S}_{Zn} = -\frac{d(\Delta\bar{G}_{Zn})}{dT}$$

$$\Delta\bar{S}^{x}_{Zn} = \Delta\bar{S}_{Zn} - \Delta\bar{S}^{i}_{Zn} = \Delta\bar{S}_{Zn} - R \ln N_{Zn}$$

and $$\Delta\bar{H}_{Zn} = \Delta\bar{G}_{Zn} + T\Delta\bar{S}_{Zn} = \Delta\bar{G}^{x}_{Zn} + T\Delta\bar{S}^{x}_{Zn}$$

where $\Delta\bar{S}_{Zn}$ = partial molar entropy of zinc,

$\Delta\bar{S}^{x}_{Zn}$ = excess partial molar entropy of zinc,

$\Delta\bar{S}^{i}_{Zn}$ = ideal partial molar entropy of zinc,

and $\Delta\bar{H}_{Zn}$ = partial molar enthalpy of zinc.

In the present investigation, therefore, vapour pressure determinations were carried out at several temperatures in both liquid and solid states.

If the heat of vaporisation is assumed to be constant over the temperature range spanning the set of results being considered, then a linear relationship between $\log p_{Zn}$ and the reciprocal of the absolute temperature $\left(\frac{1}{T^{o}K}\right)$ is obtained as follows:-

$$Zn\ (Cu\ :\ l) \quad = \quad Zn\ (g)$$

and, by Van't Hoff's relationship

$$\frac{d \ln K}{dT} = \frac{\Delta H^\circ}{RT^2}$$

or

$$\frac{d \ln K}{d\left(\frac{1}{T}\right)} = -\frac{\Delta H^\circ}{R}$$

i.e.

$$\frac{d \ln p_{Zn}}{d\left(\frac{1}{T}\right)} = \text{constant}$$

where ΔH° = enthalpy change for reaction

and K = equilibrium constant for reaction.

The best straight line relationship, therefore, representing the variation of $\log p_{Zn}$ with $\frac{1}{T}{}^\circ K$ was deduced by the method of least squares from the results for each alloy in both liquid and solid states. A sample calculation is shown in Appendix 1.

This method of calculation gave values for the constants A and B in the equation :

$$\log p_{Zn} = A + \frac{B}{T}$$

where $T = T_A$.

The temperatures T_A and T_B, together with $\log p_{Zn}$ values and the calculated constants A and B for all the alloys used in the present investigation, are shown in Table 1. These constants were used as a basis for calculation of the partial thermodynamic properties of zinc in the alloys. Details of the calculations are given in Appendix 3 and the values obtained for the liquid and solid alloys shown in Tables 2 and 4 respectively.

In addition to the partial thermodynamic functions mentioned above, Table 2 also includes calculated values of the α - function. This function, which equals $\frac{\Delta \bar{G}^{ex}_{Zn}}{RT_{Cu}}$, is used in assessing the adherence of the partial thermodynamic properties of the liquid solutions to quasi-chemical theory and receives more detailed attention in Part 7.3.

4.2 Standard States and Vapour Pressure/Temperature Relationships

Since vapour pressure determinations were made on both liquid and solid alloys it was considered desirable that two standard states should be chosen. Thus, in general, the partial properties of the liquid solutions were referred to those of their pure liquid components at 1200°K and the solid solutions to their solid components at 1000°K. The equations representing the various solutions are:

$Zn\ (L)_{1200\,°K} = Zn[Cu + L]_{1200\,°K}$,

$Zn(hex)_{1000\,°K} = Zn[Cu + fcc, bcc\ or\ \gamma\text{- cub}]_{1000\,°K}$,

$Cu(L)_{1200\,°K} = Cu[Zn + L]_{1200\,°K}$,

and $Cu(fcc)_{1000\,°K} = Cu[Zn + fcc, bcc\ or\ \gamma\text{- cubic}]_{1000\,°K}$

In accordance with the above standard states, therefore, the partial molar properties of zinc in Tables 2 and 4 have been calculated for 1200° and 1000°K respectively. Table 4 also includes values of $\Delta \bar{G}^{ex}_{Zn}$ at 1100°K. These last results were

used in deriving the partial molar properties of the copper component in the solid alloys and are considered further in Part 4. 3.

As indicated above, evaluation of the constants A and B requires knowledge of the variation with temperature of the vapour pressure over pure liquid zinc. Also, to relate the thermodynamic properties of the solid alloys to solid zinc at the two temperatures specified, implies known values of the vapour pressure over solid zinc at these two temperatures, viz. 1000°K and 1100°K. The following relationships, given by Kubaschewski and Evans (16), were used to obtain the required values.

$$\log p_{mm} = 12{\cdot}34 - \frac{6{,}620}{T} - 1{\cdot}255 \log T \quad \ldots\ldots\ldots 1A$$

$$\log p_{mm} = 11{\cdot}24 - \frac{6{,}650}{T} - 0{\cdot}755 \log T \quad \ldots\ldots\ldots 1B$$

Equation 1A refers to liquid zinc between melting point (692·5°K) and boiling point (1179°K), and equation 1B to solid zinc between 298°K and melting point. Thus, to obtain values for solid zinc at 1000°K and 1100°K, considerable extrapolation of equation 1B was necessary.

Recently Chiotti and Gill (19) compared the values given by the above equations with those by relationships derived by them from the data of Kelly (20) and Stull and Sinke (21). They found good agreement at temperatures near the boiling point but poor agreement near the melting point. The relationships of Chiotti and Gill, which are given in Appendix 2, along with others

which are discussed in Part 5, have been labelled 2A and 2B to correspond with equations 1A and 1B respectively. In Appendix 2 values from equation 2A are compared with those from equation 1A and it can be seen that log p_{Zn} values differ significantly at temperatures below about 900°K. This difference was ascribed by Chiotti and Gill to consideration given by Kubaschewski and Evans to effusion data of Vance and Whitman (22) who applied a new correction for use of a cylindrical aperture in this type of experiment. Chiotti and Gill prefer to neglect these results until confirmation is forthcoming. However, it would appear from references quoted by Kubaschewski and Evans that consideration was given to the results of Vance and Whitman only in constructing equation 1B. Moreover, the only results from this relationship used in the present investigation (viz. log p_{Zn} at 1000°K = 2·125 and at 1100°K = 2·717) are in good agreement with those found by extrapolation of equation 2B of Chiotti and Gill (Viz. 2·123 and 2·713 respetively). In view of the above arguments, therefore, it was decided to adhere to equations 1A and 1B, in preference to the more recent ones of Chiotti and Gill, throughout the present calculations.

4. 3 Partial Molar Properties of Copper

The partial molar properties of one component in a binary solution are connected with those of the other component by a Gibbs-Duhem type of relationship, viz :

$$N_A \, d(\Delta \bar{Y}_A) + N_B \, d(\Delta \bar{Y}_B) = 0$$

Where N_A = mole fraction of component A

N_B = mole fraction of component B

$\Delta \bar{Y}_A$ = partial molar property of component A

$\Delta \bar{Y}_B$ = partial molar property of component B

Thus, $$\Delta \bar{Y}_B = -\int \frac{N_A}{N_B} \, d(\Delta \bar{Y}_A) \qquad \text{.....(4.3.1)}$$

and, failing a relationship between $\frac{N_A}{N_B}$ and $\Delta \bar{Y}_A$ which can be integrated directly, the value of $\Delta \bar{Y}_B$ is found from the area between the curve and the abscissa when $\frac{N_A}{N_B}$ values are plotted as ordinates against $\Delta \bar{Y}_A$. In order that the integral be definite, a value for $\Delta \bar{Y}_B$ must be known at one composition and, in general, the integration is carried out from $\frac{N_A}{N_B} = 0$, i.e. $N_A = 0$ or $N_B = 1$, at which point $\Delta \bar{Y}_B = 0$.

This procedure involves extrapolation of $\Delta \bar{Y}_A$ values to $N_A = 0$ and accurate integration can only be performed if $\Delta \bar{Y}_A$ approaches a finite value at this composition. This is not true if $\Delta \bar{Y}_A$ represents $\Delta \bar{G}_A = RT \ln a_A$, since the value of $\ln a_A$ approaches minus infinity at $N_A = 0$. However, values of $\Delta \bar{G}^E_A = RT \ln \gamma_A$ can be used since $\gamma_A = \frac{a_A}{N_A}$ is always finite. Similarly, $\Delta \bar{S}_A$, $\Delta \bar{S}^E_A$ and $\Delta \bar{H}_A$ values can also be used.

Throughout the present work use was made of the Gibbs-Duhem

relationship, shown in equation (4.3.1), with graphical integration, to obtain the partial molar properties of the copper component from those of the zinc.

For the liquid alloys, integrations were carried out, as indicated in Graph 5 and Table 3, to find $\Delta\bar{S}^{ex}_{Cu}$ and $\Delta\bar{H}_{Cu}$ values at compositions corresponding to those of the alloys used in the present experimental work. (Since the points on the plots were joined by straight lines it was possible to calculate the ΔA values in Table 3 without actual reference to Graph 5). From the results obtained, other partial properties of copper were calculated, viz.

$$\Delta\bar{G}^{ex}_{Cu} = \Delta\bar{H}_{Cu} - T\Delta\bar{S}^{ex}_{Cu},$$

$$\Delta\bar{G}_{Cu} = \Delta\bar{G}^{ex}_{Cu} + RT \ln N_{Cu}$$

and $$a_{Cu} = \ln^{-1}\left(\frac{\Delta\bar{G}_{Cu}}{RT}\right) = \text{antilog}_{10}\left(\frac{\Delta\bar{G}_{Cu}}{5390}\right).$$

In the case of the solid alloys, since each phase had to be considered separately, a known value of $\Delta\bar{Y}_B$ was required at a datum point for each phase. For the α-phase, the two results from the present investigation were considered inadequate for extrapolation to $N_{Cu} = 1$, and, therefore, consideration was given to the results of other workers (see Part 5), which have been plotted in Graphs 12 and 13, when drawing the curves. Extrapolation of these curves in the other direction to the $\alpha/\alpha+\beta$ phase boundary for the two temperatures concerned (viz. 1000° and 1100°K respectively) allowed the calculation of the $\Delta\bar{G}^{ex}_{Cu}$ values at these compositions. From these values, the values of the conjugate alloys in the β-phase field were obtained as follows.

$$\Delta\bar{G}^{M}_{Cu\alpha} + RT \ln N_{Cu\alpha} = \Delta\bar{G}^{M}_{Cu\beta} + RT \ln N_{Cu\beta} \quad \ldots\ldots\ldots(4.3.2)$$

i.e. $$\Delta\bar{G}^{M}_{Cu\beta} = \Delta\bar{G}^{M}_{Cu\alpha} + RT \ln \frac{N_{Cu\alpha}}{N_{Cu\beta}} \quad \ldots\ldots\ldots(4.3.3)$$

where $N_{Cu\alpha}$ and $N_{Cu\beta}$ are conjugate compositions in the α and β-phase fields respectively, and the identity expressed in equation (4.3.2) assumes conjugate alloys to have equal chemical potentials, i.e. equal partial molar free energies of mixing.

Using the two values of $\Delta\bar{G}^{M}_{Cu\beta}$ so obtained, integration to find values for the experimental alloys in the β-phase field at both temperatures was possible (see Table 5 and Graph 14). From the $\Delta\bar{G}^{M}_{Cu}$ values at the two temperatures, a value for $\Delta\bar{S}^{M}_{Cu}$ for each composition was obtained by subtracting the $\Delta\bar{G}^{M}_{Cu}$ values and dividing by the temperature difference.

i.e. $$\Delta\bar{S}^{M}_{Cu} = -\frac{\Delta\bar{G}^{M}_{Cu_{1100}^{\circ}} - \Delta\bar{G}^{M}_{Cu_{1000}^{\circ}}}{1100 - 1000} \quad \ldots\ldots\ldots(4.3.4)$$

$\Delta\bar{H}_{Cu}$ values at 1000°K were then derived from

$$\Delta\bar{H}_{Cu} = \Delta\bar{G}^{M}_{Cu_{1000}^{\circ}} + T\Delta\bar{S}^{M}_{Cu} \quad \ldots\ldots\ldots(4.3.5)$$

For alloys in the γ-phase field a slightly different procedure was adopted. As before, $\Delta\bar{G}^{M}_{Cu}$ values at 1000°K were found by integration of the corresponding property of zinc, use being made of the measured activity/composition curves for both β and γ phases, shown in Graph 9, to obtain agreeing extrapolated values at the $\beta/\beta+\gamma$ and $\beta+\gamma/\gamma$ phase boundaries. At 1100°K the $\beta+\gamma/\gamma$ phase boundary occurs at a composition of 0·590 N_{Zn}, for which measurements of partial zinc properties have been made over a range of temperature in the present experimental work. Thus, a value of $\Delta\bar{G}^{M}_{Zn}$ for the conjugate composition in

the β-phase field at 1100°K was readily obtained and extrapolation of the integration of Graph 14 to this value made possible the determination of $\Delta\bar{G}^{M}_{Cu}$ for these conjugate compositions. Thus, values of $\Delta\bar{G}^{M}_{Cu}$ at 0·590 N_{Zn} for two temperatures were obtained, and, as before, a value of $\Delta\bar{S}^{M}_{Cu}$ calculated from equation (4.3.4). With this datum point, integration of the $\Delta\bar{S}^{M}_{Zn}$ curve in Graph 15 was used to obtain $\Delta\bar{S}^{M}_{Cu}$ values for the other experimental compositions in the γ-phase field. This procedure avoided the extrapolation of measured $\Delta\bar{G}^{M}_{Zn}$ values for the solid alloys in the γ-phase field to a temperature above the solidus. As before, $\Delta\bar{H}_{Cu}$ values at 1000°K were obtained using equation (4.3.5).

Further details of the above calculations can be found in Appendix 3 and the values obtained at the various stages are set out in Table 5.

4.4 Integral Molar Properties

The following relationship exists between any integral molar quantity and the corresponding partial molar quantities

$$\Delta Y = N_A \cdot \Delta\bar{Y}_A + N_B \cdot \Delta\bar{Y}_B$$

where ΔY = integral molar quantity.

This relationship was used to calculate the integral molar properties of the liquid and solid alloys which are shown in Tables 3 and 6 respectively.

The equations representing the liquid and solid solutions are respectively.

$$x\,Zn(L) + (1-x)Cu(L) = [xZn, (1-x)\,Cu](L)$$

and $$x\,Zn(hex) + (1-x)Cu(fcc) = [xZn, (1-x)Cu](fcc, bcc \text{ or } \gamma\text{-cubic})$$

PART B

RESULTS OF OTHER WORKERS

Part 5 - Results of Other Workers

5.1 General

When results obtained in this investigation were first compared with those of other workers it was found that significant differences could arise due to variations in the vapour pressure values used for pure zinc. It was decided, therefore, to recalculate, as far as possible, the results of other workers, used for comparison, to the basis of Kubaschewski and Evans' equation 1A (see Part 4.2.). All the vapour pressure/temperature relationships involved, the comparisons and the corrections made are shown in Appendix 2. Where determinations were carried out at more than one temperature plots of corrected values of log p_{Zn} against $\frac{1}{T}$ were used to obtain values for constants A and B, as in the present investigation.

All the values of thermodynamic quantities calculated from the results of other workers are shown in Table 7. Individually, the treatment of their results was as follows.

5.2 Everett, Jacobs and Kitchener (7) - Liquid Alloys

These investigators, using a transportation method, measured the vapour pressures of a large number of alloys ranging from N_Z = 0·165 to N_Z = 0·782. Determinations were confined

to one for each alloy at temperatures ranging from 1095° to 1303°K. Only their results measured at temperatures within 10°of 1200°K have been compared with the present work. The vapour pressure/temperature relationship for pure zinc which they used for finding p_{Zn_0} was found by them from measurements on the pure molten metal between 860° and 1010°K. Since their values for the vapour pressures of the alloys were found directly and did not depend upon their values for pure zinc, no correction was made to these figures. However, the values of p_{Zn_0} at their experimental temperatures were derived from equation 1A and used in place of their own to calculate the thermodynamic properties. It will be noted that use of their own equation in this respect involves considerable extrapolation.

5.3 Schneider and Schmid (10) - Liquid Alloys

In this case the vapour pressure values for pure zinc were stated to be taken from Landolt-Bornstein (24). These data are represented in Schneider and Schmid's paper by a straight line graph which, however, does not quite agree with that obtained by the present author from the same data (see Appendix 2). Nevertheless, since Schneider and Schmid's results were also taken from their graphs and, therefore, subject to the same possible errors in reading therefrom, their linear relationship was used in assessing corrections. As shown in Appendix 2, the values given by this

relationship are sufficiently close, at temperatures above 900°K, to those of equation 1A not to require correction. The values of the constants A and B found for the alloys from Schneider and Schmid's linear plots of log p_Z against $\frac{1}{T}$ were used in the same way as before to derive thermodynamic properties.

5.4 Leitgebel (25) - Liquid Alloys

Leitgebel measured the boiling points of several alloys in the copper/zinc system but only two of these were considered close enough to 1200°K to warrant their use for comparison with the present work. Taking the vapour pressures of these alloys as 760 mm at the temperature of boiling, thermodynamic properties were calculated using equation 1A.

5.5 Kleppa and Thalmeyer (6) - Liquid Alloys

The e.m.f. measurements of Kleppa and Thalmeyer were confined to a narrow range of alloys (0·800 to 0·915 N_{Zn}) at 900°K. In each case a temperature coefficient was reported and this was used to extrapolate the results to 1200°K and to calculate $\Delta\bar{S}_{Zn}$ values.

In these calculations the following relationships were used:

$$\Delta\bar{G}_{Zn} = -nFE = -46{,}120\,E \text{ cal} \quad \text{.....(5.6.1)}$$

and $$\Delta\bar{S}_{Zn} = -d\frac{\Delta\bar{G}}{dT} = +46{,}120\,\frac{dE}{dT} \text{ cal/deg} \quad \text{..... (5.6.2)}$$

where E = e.m.f. in volts, $46{,}120\,\frac{dE}{dT}$ cal/deg

5.6 Argent and Wakeman (9) - Solid Alloys

Using the dew-point technique, these investigators carried out vapour pressure determinations on a large number of alloys in the α-phase field. The vapour pressure/temperature relationship used for pure zinc was that given in an earlier edition of Kubaschewski and Evans' "Metallurgical Thermochemistry" (Appendix 2) and their results were reported as values of the constants A and B. Since it was not possible, therefore, to apply corrections to individual results and obtain new values for these constants, corrections at 1000°K only were applied.

5.7 Hargreaves (8) - Solid Alloys

Hargreaves, one of the first workers to use the dew-point technique, presented his results in graph form (log p_{Zn} against $\frac{1}{T}$) and also as a table of temperatures for each alloy corresponding to certain fixed values of vapour pressure. Pure zinc vapour pressure values were reported to have been taken from three sources (27, 28, 29) but no vapour pressure/temperature relationship was given. Using appropriate values from these sources, a best straight line relationship, which is shown in Appendix 2, was obtained. Comparison of this with equation 1A enabled corrections to be made to Hargreaves' fixed vapour pressures. The corrected results for each alloy were then plotted against $\frac{1}{T}$ and values for the constants A and B found by drawing the best straight line

through the plotted points. As before, these constants were used in calculating the thermodynamic properties.

5.6 Seith and Kraus (19) - Solid Alloys

Vapour pressure determinations, involving a continuous weighing technique, were made by Seith and Kraus on two different series of alloys at 1073 and 1123°K respectively. Their results were reported in graph form only as log p_{Zn} against composition. At certain compositional intervals (to suit Graphs) the log p_{Zn} values at both temperatures were corrected (see below) and extrapolated and interpolated to 1000°K and 1100°K for comparison with the present work. At the same time, a temperature coefficient was obtained for conversion to $\Delta\bar{S}_{Zn}$ values. It was found convenient to achieve this by finding, as in other cases, values for the constants A and B.

In the absence of any reference to the source of p_{Zn_o} values used, it was assumed to be Landolt-Bornstein and log p_{Zn} values corrected accordingly. In view of this, and the rather uncertain extrapolation to 1000°K, it is considered that values of thermodynamic properties calculated from their results should be treated with some reserve.

5.9 Herbener, Siebert and Ruffendeck (12) - Solid Alloys

X-ray absorption spectra were employed to measure the vapour pressures of six alloys in the α-phase field. Individual results at several temperatures for each alloy were reported and, after correction, were plotted, the best straight lines drawn, and hence values found for the constants A and B. The vapour pressure values obtained from the temperature relationship quoted do not appear to correspond to those given in Table III of their paper, but the latter have been used in assessing the corrections applied (Appendix 2).

5.10 Olander (5)- Solid Alloys

The results of Olander's e.m.f. measurements have been extrapolated from the temperature of measurement (773°K) to 1000°K using the temperature coefficients obtained in the course of their investigation.

In the calculation of partial thermodynamic properties from these results the relationship expressed in equations (5.6.1) and (5.6.2) were used. To refer the results to solid zinc at 1000°K, the free energy and entropy of fusion values at this temperature were added to the appropriate thermodynamic functions. The values used were -779 cal and +2.825 cal/deg respectively and were calculated from vapour pressure equations 1A and 1B as shown in Appendix 3.4.

PART 6

RESULTS OF PRESENT INVESTIGATION

Part 6 - RESULTS OF PRESENT INVESTIGATION

6. 1 - General

As indicated in Part 4, the compositions (expressed as atomic fraction of zinc, N_{Zn}), temperatures of measurements (T_1) and condensation temperatures (T_2) for both liquid and solid alloys are recorded in Table 1. Also included are the logarithms of the vapour pressures corresponding to T_2 and the values of the constants A and B in the linear equation, $\log p_{Zn} = A + \frac{B}{T}$, found by the method of least squares from the results for each alloy.

All the thermodynamic functions calculated from these results are shown in Tables 2 to 6 and in Graphs 1 to 19. Standard states for liquid and solid alloys are as described in Part 4. 2, viz. pure liquid components at 1200°K and pure solid components at 1000°K respectively. In certain instances results of other workers, suitably corrected, have been included in the graphs for comparison. Throughout this thesis temperatures are reported in degrees Kelvin, pressures in mm Hg and energies in calories.

6. 2 - Liquid Alloys

Graph 1 is a plot of zinc and copper activities against atomic fraction and illustrates the behaviour of liquid zinc-copper alloys with respect to Raoult's Law. The curve

representing the activity of zinc has been drawn using results obtained in the present investigation and that of the copper has been calculated from these using the Gibbs-Duhem relationship as described in Part 4.3.

The activity curves indicate that solutions of zinc in copper show negative deviation from Raoult's Law for zinc contents below about 70 atomic percent, while above this concentration there is slight positive deviation. This pattern of behaviour, at the temperature being considered (1200°K), is supported by the results of Schneider and Schmid(10), Leitgebel (25) and, to a lesser extent, by Kleppa and Thalmayer (6). This corroboration of positive deviation at high zinc contents is more clearly seen in Graph 2, in which α-function values are plotted against N_{Zn}. In this plot, the upper curve refers to results of the present work only and the lower to a combination of those derived from the vapour pressure measurements of Schneider and Schmid and the e.m.f. measurements of Kleppa and Thalmayer. The two curves also show similar trends and, in both instances, it is fairly certain that the values of the thermodynamic deviation become positive before N_{Zn} reaches a value of one. It should be stated that, although the results of Kleppa and Thalmayer have been extrapolated considerably beyond the

temperature of measurement (viz. 900°K), the values at the lower temperature also indicate positive deviation at high zinc contents. The two results attributed to Leitgebel are calculated from boiling point determinations, the actual temperatures being 1196° and 1188°K.

Everett, Jacobs and Kitchener, using the transportation method, made vapour pressure determinations on a wide range of liquid zinc/copper alloys, at single temperatures varying from 1069° to 1303°K. Those of their results obtained at temperatures within 10° of 1200°K were recalculated as indicated in Part 5.2 and are shown plotted in Graphs 1 and 2. As is evident in these Graphs the values so obtained are lower than any of the others plotted and do not indicate positive deviation from ideality at high zinc contents. In addition, the α-function values (Table 7, Graph 2) show no systematic variation with composition. The authors conclude that the thermodynamic deviation is constant within experimental error, and therefore, that solutions of zinc in copper are regular.

This conclusion is not substantiated by the results of the other workers shown in Graphs 1 and 2. The reason for the discrepancy may lie in the experimental method used by Everett, Jacobs and Kitchener. As demonstrated by Alcock and Hooper (30), satisfactory conditions for the accurate determination of vapour

pressures by the transportation method are difficult to fulfil for liquid metals, low results frequently being obtained due to restriction of surface area in contact with the transporting gas.

The plot of a_{Cu} against composition shows that deviations from Raoult's Law for solutions of copper in zinc are negative over the whole range of composition.

Values for the partial molar free energy ($\Delta\bar{G}$), the excess partial molar free energy ($\Delta\bar{G}^{E}$) and the partial molar entropy ($\Delta\bar{S}$) for zinc in the liquid solutions are plotted against N_{Zn} in Graph 3. As indicated by the smoothed curves drawn through $\Delta\bar{G}$ and $\Delta\bar{G}^{E}$ values, these two quantities show a progressive variation with composition, with $\Delta\bar{G}^{E}$ rising to a maximum at a small positive value at about 80 atomic percent and, presumably, falling again to zero at 100 atomic percent. This, of course, is consistent with the behaviour indicated in Graphs 1 and 2.

The variation of $\Delta\bar{S}_{Zn}$ with composition, however, shows further deviations from ideality. From Graph 3 it would appear that, instead of a progressive variation, $\Delta\bar{S}_{Zn}$ fluctuates about a value of approximately +1·0 with particularly large dips at about 48, 61 and 83 atomic percent zinc. When deviations from

ideal entropy are considered, however, a more systematic variation is apparent. This is shown more clearly in Graph 4 in which the partial molar excess entropy ($\Delta\bar{S}^{x}$) is plotted against zinc atomic fraction. Thus $\Delta\bar{S}^{x}$ appears to show an overall rise from a small negative value at about 30 atomic percent zinc to a small positive value about 70 atomic percent and then fall to approximately the ideal value of zero as N_{Zn} approaches unity. Superimposed on this general trend are two distinct drops at about 46 and 61 atomic percent.

Since $\Delta\bar{G}^{x}_{Zn}$ values, as indicated above, show a progressive variation with composition, these dips are reflected in the partial heat of mixing ($\Delta\bar{H}_{Zn}$) curve which is also shown in Graph 4. As can be seen from the few available results of other workers plotted in Graph 4, confirmation of the above pattern of $\Delta\bar{S}^{x}_{Zn}$ and $\Delta\bar{H}_{Zn}$ values is uncertain. Although the results of Schneider and Schmid show a similar overall trend (i.e. excluding the dips) to those of the present investigator, their numerical values are considerably lower. On the other hand, the compositions of the alloys used by Kleppa and Thalmayer are almost entirely beyond the present range but results from them are reasonably confirmatory in numerical size and trend in this limited region.

The partial molar properties of the copper component and the integral molar properties of the solution, calculated

from the partial zinc quantities, are reported in Table 3. Graph 6 is a plot of partial and integral enthalpies and shows their relative variations with composition. In the same plot, the broken line represents the nearest quasi-chemical curve to the present results (see Part 7.3), while the chain-dotted line represents a plot of $\triangle H_m = -8200\ N_{Cu} \cdot N_{Zn}$ which is the relationship derived by Kubaschewski and Catterall (2) from data of Samson-Himmelstjerna (13). It is obvious that the present results are considerably less negative than those of Kubaschewski and Catterall, showing a maximum discrepancy at $0{\cdot}82\ N_{Zn}$ of about 800 cal. However, as indicated by Kubaschewski and Catterall, their expression is only approximate, having been derived from the heat contents between 1273°K and 293°K and the heats of formation at room temperature. A further plot showing the values of $\triangle H_m$, $\triangle G^x_m$ and $\triangle S^x_m$ from the present investigation is contained in Graph 7. In this graph the chain-dotted line represents H_m values for the Zn/Sb system which is introduced for comparison with the Zn/Cu system.

The significance of the above plots, and also that of Graph 8, which shows $\triangle H_m$ and $\triangle S^x_m$ values on a larger scale, is discussed in Part 7.

6.2 - Solid Alloys

In the solid state the range of alloys cannot be

treated as a continuous series but only as a number of separate solid solutions between which equilibrium relationships exist at certain compositions. Thus, Graph 9, showing variation of activity with composition at 1000°K, is drawn with breaks in the curve where two-phase fields intervene.

The curves in Graph 9 have been drawn with consideration only for points obtained in the present investigation. Although only two experimental points are available from the present work in the α-phase field the curve is drawn through the origin and a fourth point, at the $\alpha/\alpha+\beta$ phase boundary, which must agree with the activity value at the corresponding limit of the β-phase field. For the range of composition covered, the graph indicates that solid solutions of zinc in copper show negative deviation from ideality with the deviation decreasing with rising zinc content. The shape of the curve suggests that ideality may not be achieved below 100 atomic percent, i.e. unlike the liquid alloys, the activity coefficient nowhere rises above unity.

Results of other workers have been superimposed on Graph 9. In the α-phase field, to avoid confusion, not all of the available data have been plotted. However, the large number of plotted points, involving several workers using a variety of experimental methods, shows good agreement with the drawn curve. In the β-phase field the scatter of results is somewhat greater, but again fair agreement with the present work

is exhibited. Confirmation in the γ-phase field depends solely upon the results of Olander. The plotted values, which have been extrapolated from Olander's e.m.f. measurements at 773°K show a similar trend to those of the present investigation but with a certain difference in numerical value, particularly at the extremities of the phase field.

Graph 10 shows plots of $\Delta\bar{G}_{Zn}$, $\Delta\bar{G}^{M}_{Zn}$ and $\Delta\bar{G}_{Zn}$ against N_{Zn}. The two partial free energy curves show no abnormalities and will not be discussed further. As with the liquid alloys, however, the partial molar entropy shows characteristic dips in the β and γ-phase fields. In this instance, two dips, at approximately 43·0 and 47·5 atomic percent zinc respectively, are present in the β-phase field, while that in the γ-field occurs at about 61·5 percent. This pattern is also apparent in the plots of partial excess entropy and partial heat of solution (Graph 11).

Thermodynamic properties of solid alloys in the α-field have been extensively studied, particularly in a recent publication by Argent and Hakeman (9). In the present investigation, therefore, only two α-alloys were included, primarily to show that the experimental technique gave results in satisfactory agreement with those of the many other workers

in this phase field (Graph 9). Consequently, in Graph 11 comparison of entropy and enthalpy values with those from other sources has been made only in the β and γ- fields. As with liquid alloys, confirmation of the trend of partial excess entropy and partial heat of solution values is uncertain. In the β-field the results of Hargreaves and those of Seith and Kraus (with one exception) show fairly good agreement with the present work. While the values calculated from Olander's e.m.f. measurements are much lower, they show a similar trend to those of the present investigation, with slight tendencies in the $\Delta\bar{S}^{x}_{Zn}$ curves to a double dip in the β-field and a single dip in the γ-field at similar compositions to those given above.

As for the liquid alloys, the partial functions of copper and the integral functions, for both phases, were calculated from the measured partial zinc values and are reported in Table 6. The enthalpy values for all three are plotted against N_{Zn} in Graph 16, along with the integral heats of mixing derived by Kubaschewski and Catterall (2), mainly from Olander's e.m.f. data. As anticipated from the comparison already made with the partial functions calculated from Olander's results, the integral values of Kubaschewski and Catterall are considerably lower than the presently obtained values. However,

the trends of the results within each phase field are fairly similar. This applies more particularly to the γ-phase field in which both sets of values show a minimum at approximately 0·61 N_{Zn}. The minimum in the present results is perhaps more clearly seen in Graph 17 which is plotted on a different scale and which includes also plots of the integral excess entropy values. The significance of the variations of the various partial and integral thermodynamic functions with composition is discussed in Part 7.5.

PART 7

CORRELATION OF THERMODYNAMIC PROPERTIES AND STRUCTURE

Part 7 CORRELATION OF THERMODYNAMIC PROPERTIES AND STRUCTURE

7.1 General

Explanations of alloy structure are based upon the premise that configurations tend to positions of lowest energy. The factors which limit this tendency are determined by the two main characteristics of the constituent atoms, viz. the atomic sizes and the electronic configurations. Thus, the interrelations of atoms in a condensed phase are generally held to fall into three categories, one arising from size considerations and two from electronic behaviour. The effects identified are (i) a strain energy effect arising from differences in atomic sizes, (ii) an electro-chemical effect controlling the tendency to bonding between the atoms and (iii) a valency effect which involves interaction of outer shell electrons.

Workers in the field of electron theory have sought to explain structural effects in terms of Brillouin-zones. In this theory structural changes are related to the filling of outer electronic energy levels within certain limited zones. When a zone, characteristic of a given structure, is filled to such an extent that it becomes unstable with respect to

that of a second structure, with lower, unfilled levels, then reversion to the second structure occurs. The rate at which the outer electron levels will be occupied, when one metal is alloyed with another, will depend upon the valency of the added metal. By this means, certain stable phase structures in a number of metallic systems, including the Zn/Cu system, have been associated with fixed electron/atom ratios, i.e. electron concentrations. The theory takes account, therefore, only of effect (iii) above, but appears to accord well with systems where the other two effects are small. However, direct experimental observation, e.g. quantitative measurement of electronic energies, is scarce and the theory rests mainly upon circumstantial evidence.

An alternative approach, that of quasi-chemical theory, considers only the bonding effect (i.e. item (ii) above). In this treatment of solutions, interactions between nearest neighbours only are considered and the accuracy of the results, therefore, will depend upon the relative importance of the other two factors. Strain energy effects, for example, must extend beyond immediate neighbours, particularly if there is a large difference in atomic dimensions. However, as far as the present investigation is concerned, since the atomic radii of

zinc and copper are relatively close (1·37 and 1·28 respectively on the Goldschmidt scale), this effect should not be great. In contrast to electron theory, at least limited quantitative application of the theory can be made to any system for which sufficient thermodynamic data are available. The limitations in this case, are to be found in the number of systems for which the available data do not accord with theory prediction. However, since it is intended to test, at least to a limited extent, the quantitative application of quasi-chemical theory to the Zn/Cu system, using the results of the present investigation, the theory is given further consideration below.

7. 2 Quasi-chemical Theory

When solid solutions of two metals A and B are formed it is considered that three types of bonds are present, viz. A - B, A - A and B - B, and the number of nearest neighbours to each atom (i.e. the Co-ordination Number) depends upon the crystal structure. Thus, atoms in a solution having a FCC lattice have 12 nearest neighbours, a BCC lattice 8 and a CPH 6, with 6 more only slightly further off.

Development of the quasi-chemical approach to binary solutions, which can be found elsewhere (e.g. Swalin (31), Guggenheim (32) and Kleppa (4)), results in the following expression for the heat of mixing for a reaction:-

N_A atoms pure A + N_B atoms pure B = $(N_A + N_B)$ atoms in solution

$$\Delta H_m = P_{AB}\left[H_{AB} - \tfrac{1}{2}(H_{AA} + H_{BB})\right]$$

where ΔH_m = enthalpy of mixing

H_{AB} = enthalpy associated with A-B bond

H_{AA} = enthalpy associated with A-A bond

H_{BB} = enthalpy associated with B-B bond

P_{AB} = number of A-B bonds.

For an ideal solution,

$\Delta H_m = 0$ and, therefore, $H_{AB} = \tfrac{1}{2}(H_{AA} + H_{BB})$

i.e. the changes in interatomic potential energy of the three types of bonds cancel out.

For a regular solution $\Delta S_m^x = 0$. In terms of quasi-chemical treatment this implies a completely random solution and, otherwise, also unchanged vibrational entropy of the components. Thus P_{AB} can be evaluated from simple statistical considerations. It can be shown that

$$P_{AB} = N_A N_B Z N_0$$

where N_A = atomic fraction of component A

N_B = atomic fraction of component B

N_0 = Avogadro's number

Z = co-ordination numbers for A and B (assumed equal)

Therefore, $\Delta H_m = N_A N_B Z N_o [H_{AB} - \frac{1}{2}(H_{AA} + H_{BB})]$

$= N_A N_B Z N_o \nu$

where $\nu = [H_{AB} - \frac{1}{2}(H_{AA} + H_{BB})]$ = interaction energy.

More generally, with strong interaction between unlike atoms ΔH_m is negative (i.e. $H_{AB} < \frac{1}{2}(H_{AA} + H_{BB})$) and can be made more negative by having "short range order" in the solution. Thus P_{AB} increases over random value, hence decreasing the mixing entropy. Repulsive action, on the other hand, tends to give positive values of ΔH_m (i.e. $H_{AB} > \frac{1}{2}(H_{AA} + H_{BB})$) which may be made less positive by "clustering" of like atoms, i.e. decreasing P_{AB} compared to random value, but again leading to a decrease in ΔS_m.

For non-regular solutions the relationships are more complicated, e.g.

$$P_{AB} = N_A N_B Z N_o [1 - N_A N_B \{\exp.(-2N_o\nu/RT)\} - 1]$$

Expansion of the exponential with elimination of terms of higher order than second gives:-

$$\Delta H_m \cong N_A N_B Z N_o \nu \left(1 - N_A N_B \frac{2N_o\nu}{RT}\right) \quad \ldots\ldots\ldots (7.2.1)$$

$$\Delta S^x_m \cong - N_A^2 N_B^2 z \frac{(N_o\nu)^2}{RT^2} \quad \ldots\ldots\ldots (7.2.2)$$

$$\Delta G^x_m \cong N_A N_B Z N_o \left(1 - N_A N_B \frac{N_o\nu}{RT}\right) \quad \ldots\ldots\ldots (7.2.3)$$

The corresponding partial properties are given by

$$\Delta\bar{H}_A = Z\omega\nu N_B^2 \left\{ 1 + \left(\frac{2\omega\nu}{RT}\right) N_A (1 - 3N_B) \right\} \quad \ldots\ldots\ldots(7.2.4)$$

$$\Delta\bar{S}^{ex}_A = \frac{Z\omega\nu}{T} N_B^2 \left\{ \frac{1}{2}\left(\frac{2\omega\nu}{RT}\right) N_A (1 - 3N_B) \right\} \quad \ldots\ldots\ldots(7.2.5)$$

$$\Delta\bar{G}^{ex}_A = Z\omega\nu N_B^2 \left\{ 1 + \frac{1}{2}\left(\frac{2\omega\nu}{RT}\right) N_A (1 - 3N_B) \right\} \quad \ldots\ldots(7.2.6)$$

these relationships being symmetrical for both components.

7.3 Application of Quasi-Chemical Theory

As pointed out by Hilliard et al. (3), with reference to equation (7.2.6), a plot of $\frac{\Delta\bar{G}^{ex}_A}{N_B^2}$, i.e. α-function for component A, against $N_A (1 - 3N_B)$ should give a straight line graph if the quasi-chemical treatment is applicable. The slope of this line is $\frac{Z}{RT}(\omega\nu)^2$, from which a value for $\omega\nu$ can be found. This value should agree with that found from $Z\omega\nu = \frac{\Delta\bar{G}^{ex}_A}{N_B^2}$ at $N_A(1 - 3N_B) = 0$

In order to test the applicability of this to the present results, and to results from other alloy systems, the plots shown in Graph 18 were made. α-fuction values for liquid alloys in the systems Zn/Cu, Zn/Sb, Cd/Sb and Tl/Au, and for solid α-phase alloys in the system Al/Zn, taking the first named metal as the A component in each case, were plotted against $N_A(1 - 3N_B)$. In addition, a plot for the Zn/Cu system was made considering copper as the A component.

The α-function values used for the two plots relating to the Zn/Cu system were taken from the present work i.e. from Tables 2 and 3, while those for the other systems were calculated from values of partial thermodynamic functions given by Kubaschewski and Catterall (2).

It will be appreciated that, since the plots representing the present work are derived from individual measurements and not, as in the other systems, from smoothed results, there is a greater degree of scatter with consequent greater difficulty in determining the straight line portion of the curve. However, in view of the fact that only limited application is attempted, it is considered that the straight lines drawn are reasonably representative.

Listed in Graph 18 are the values found for the interaction coefficient ($N_0\nu$) from the slope of the straight lines and from the intercepts at $N_A(1 - 3N_B) = 0$. In certain instances there are wide differences in the $N_0\nu$ values from the two sources. This applies particularly to the Zn/Cu and Zn/Sb systems. Also, although there is better agreement between the two values found for the copper component in the Zn/Cu system, there is again a wide difference between these and either of the values found for the zinc component. These

discrepancies are taken by the author as an indication of the limitations of quasi-chemical theory when applied to the systems concerned. It would appear from the plots in Graph 18 that, where a small value of N_0V (positive or negative) is forecast by the slope of the line, i.e. where the α-function values do not change rapidly with composition and the system is, therefore, not far from being regular (e.g. Tl/Au and Al/Zn), then reasonable agreement between the values from the two sources can be expected. On the other hand, for systems (e.g. Zn/Cu and Zn/Sb) showing strong interaction between unlike atoms (i.e. large negative values for N_0V), only limited application of quasi-chemical theory can be considered.

The foregoing has taken account only of partial thermodynamic properties, but the application of quasi-chemical theory can also be considered in terms of the integral properties of a solution. Thus it can be seen that, at high temperatures, the second term in equation (7.2.1) becomes very small and the equation approximates to that of a parabola in terms of N_{Zn}, if N_0V and Z remain constant.

Graph 6 includes a plot of ΔH_m values obtained from the present work, against N_{Zn}. It is obvious from this, and from Graph 7, that the results do not approximate to a parabolic relationship over the whole range of composition. This is

also true for the Zn/Sb system for which the ΔH_m curve has been drawn in Graph 7, again using values from Kubaschewski and Catterall (2).

A quasi-chemical type relationship, which is represented by the equation

$$\Delta H_m = -6100\ N_{Zn}N_{Cu} - 2583\ N_{Zn}^2 N_{Cu}^2$$

has been estimated as the best fit for the results of the present work and is shown plotted in Graph 6 as a broken line. It can be seen from this and from Graph 7 that the deviation of ΔH_m values, in both Zn/Cu and Zn/Sb systems, from the typical quasi-chemical relationship is greatest towards high zinc contents. Also, it is in this region of composition that both systems show, with respect to the activity of the zinc component, a change from negative to positive deviation from ideality. This connection between a_{Zn} and ΔH_m is to be expected since the behaviour of the zinc component must influence the properties of the solution as a whole, and result in a tendency to more positive values of ΔH_m. Thus, a changing value of interaction coefficient is obtained and quantitative expressions for evaluating thermodynamic properties, such as those in equations (7.2.1) to (7.2.6), are inapplicable. It seems probable also that similar variations of the interaction energy between the component metals is responsible for deviations from strict

quasi-chemical behaviour elsewhere in the composition range, thus accounting for the non-quantitative adherence to quasi-chemical theory of both partial and integral thermodynamic properties.

Notwithstanding the above conclusion, one of the values found for ω_V was used for substitution in equation (7.2.5) to obtain a quasi-chemical curve for excess entropy, for comparison with experimental values. The large negative value (viz. -1450) found from the slope of the zinc α-function plot in Graph 18 was adopted since this seemed consistent with a system showing, by the formation of several intermediate phases, a tendency to compound formation. As indicated by Kleppa (4), the quasi-chemical curve obtained, which is plotted along with the experimental $\Delta\bar{S}^{x}_{Zn}$ values in Graph 4, must follow a typical S-shape. Further discussion on the structural implications of these curves is made in Part 7.5.

7.4 Configurational and Vibrational Entropies

Another matter of relevance in this study is that the excess entropy of a system can be regarded as being made up of two parts, viz. a configurational part and a thermal or vibrational part. Thus the configurational part depends solely on the distribution of the A and B atoms and would be zero for

a completely random distribution, but lowered by the presence of either short range order or clustering, both of which represent a departure from randomness. Vibrational entropy, on the other hand, depends upon the thermal motion of the atoms, their frequency increasing (e.g. due to intermetallic bonding) to give negative entropy deviations, or decreasing (e.g. due to the presence of large foreign atoms or vacancies) to give positive deviations. It is possible to make estimations of these two types of entropy deviations separately, e.g. ΔS^{x}_{con} from determinations of short range order coefficients and ΔS^{x}_{vib} from calorimetric measurements.

7.5. Liquid Solutions of Zn/Cu Alloys

Since measurements of thermodynamic properties in this investigation have been confined to the partial functions of one component only, viz. zinc, it seems appropriate to discuss the structural implications of these values first.

The a_{Zn}/composition curve (Graph 1) shows somewhat unusual behaviour in that a change from negative to positive deviation from ideality at about 0·73 N_{Zn} is shown. In terms of quasi-chemical theory, this implies a change from association of unlike atoms and negative values of heats of solution to that of unlike atoms and positive values of heats of solution. This aspect has already been discussed in Part 7.3.

Of more significance, perhaps, are the fluctuating values of $\Delta\bar{S}^{x}_{Zn}$ (Graph 4). As indicated in Part 7.3, the quasi-chemical theory predicts an S-shaped curve when this quantity is plotted against composition. Comparison of the experimental and quasi-chemical excess entropy curves in Graph 4 indicates that, if a mean curve is drawn through the experimental values, the quasi-chemical prediction is followed fairly closely, with the exception of the positive peak at about $0.68N_{Zn}$. As shown by Kleppa (4), similar $\Delta\bar{S}^{x}$ curves to that of the zinc component in Zn/Cu alloys (without the dips) are obtained in the Zn/Sb and Cd/Sb systems. For comparison, all three systems, with the Zn/Cu dips in broken line, are shown in Graph 19. Thus it seems probable that the high positive value of $\Delta\bar{S}^{x}_{Zn}$ in the Zn/Cu system is a real effect which requires explanation.

It cannot, of course, be explained in terms of configurational entropy since both positive and negative deviations from ideality represent a departure from random mixings and hence a decrease in entropy. Thus, one must conclude that the vibrational contribution to the total excess entropy has suffered a sudden increase. This corresponds, as pointed out in Part 7.4. above, to a decrease in the vibrational frequency of the atoms which can be brought about by defects in the crystal lattice such as impurity atoms or vacant sites.

It is interesting to note, in this connection, that Hume-Rothery and Raynor (23) state that, in the solid alloys of copper and zinc, beyond the zinc-rich boundary of the γ-phase at about 1·7 electrons/atom (i.e. 0·70 N_{Zn}) a new phase (δ) forms which has a structure based on BCC lattice but with numerous atomic sites vacant.

Kleppa, with reference to the Zn/Sb and Cd/Sb curves, suggests that the configurational entropy deviations are superimposed on large positive excess entropy terms which, presumably, are due to vibrational considerations. If, therefore, an overall positive vibrational excess entropy of approximately 1·5 cals/degree were subtracted from the plotted values of the Zn/Cu system zero configurational excess entropy would occur at 0·68 N_{Zn} i.e. at approximately the composition in Graph 1 where γ_{Zn} (= $\frac{a_{Zn}}{N_{Zn}}$) is one. This implies consistency between the measured a_{Zn} and $\Delta\bar{S}_{Zn}$ values, at least at this point, since an ideal solution, for which γ is unity, must also be a regular one, for which $\Delta\bar{S}^{x}$ is zero.

This lowering of the $\Delta\bar{S}^{x}_{Zn}$ values by 1·5 units also obviates explanation of the small positive $\Delta\bar{S}^{x}_{Zn}$ value at 0·59 N_{Zn}. However, there is at present no experimental evidence to justify the subtraction of this arbitrary quantity

from the $\Delta\bar{S}^{x}_{Zn}$ values and it is only forwarded as a matter of interest.

The other features of the excess entropy curve which require explanation are the dips at 0·48 N_{Zn} and 0·62 N_{Zn}. It seems reasonable to assume that they show a tendency to compound formation which would reduce both configurational and vibrational excess entropies. Again, there appears to be here a distinct link with electron theory since these compositions correspond to the electron to atom ratios (i.e. 1·48 and 1·615), predicted by the filling of energy levels in the appropriate Billouin zones, necessary for the formation of the β and γ electron compounds respectively, in the solid state. Since the present results refer to liquid alloys it may also be taken as an indication of the extent to which "solid" structures persist above the melting point.

In spite of the foregoing discussion, the writer is of the opinion that it can be misleading to consider only the partial thermodynamic properties of a system when seeking structural enlightenment of the solution as a whole. Thus, when the integral excess entropy curve is plotted (Graph 7) it can be seen that the peak occurs at 0·83 N_{Zn} with small positive values obtaining between about 0·77 N_{Zn} and 1·00 N_{Zn}. One must, therefore, postulate an increasing contribution from vibrational entropy in this composition range, which, however,

does not fit so well with known structural changes(i.e. occurrence of δ-phase "defect" structure) as previously postulated for the partial values. On the other hand, the above composition range is very close to that in which the activity of the zinc component shows positive deviation from ideality and a connection between increasing activity and increasing vibrational properties is suggested.

Apart from this, the partial and integral thermodynamic properties of a solution are rigidly linked by the Gibbs-Duhem relationship and variation in one must inevitably be reflected in the other and explicable structurally in the same terms. In order to develop this discussion further it is proposed to examine the variation in $\triangle H_m$ values closely.

The values of partial and integral heats of mixing for zinc/copper solutions are shown in Graph 6, but, in order to show the variation of $\triangle H_m$ values more clearly, the larger scale plot shown in Graph 8 has been constructed. In this, a continuous line has been drawn through the results from the present investigation while the broken line, showing the overall trend of results, represents what the author proposes to call the "minimum enthalpy" curve. It will be noted that up to a composition of about 0·41 N_{Zn} both curves are co-incident while

beyond this they touch only at certain compositions. Thus, between about 0·41 N_{Zn} and 0·45 N_{Zn} the measured enthalpy values deviate increasingly in a positive fashion from the minimum curve. Beyond 0·45 N_{Zn} this deviation gradually diminishes until a composition of approximately 0·49 N_{Zn} is reached, when once more minimum enthalpy is achieved. Similarly, positive deviation is again registered at 0·55 N_{Zn}, rising to a maximum at 0·60 N_{Zn} before falling back to the minimum curve at 0·63 N_{Zn}. Minimum enthalpy is maintained to 0·65 N_{Zn} where, once more, positive deviation begins. Beyond this composition, due to lack of experimental points, the plot of the actual values is uncertain, except that it does appear to achieve a third minimum at about 0·83 N_{Zn}.

Since the first two minima in the experimental ΔH_m curve occur approximately at the centres of the β and γ-phase fields respectively, in the solid zinc/copper system, and the third approximately in the centre of the ε-phase field, it is suggested that there is also one co-incident with the δ-phase field i.e. at about 0·75 N_{Zn}. It can be seen that the values of 0·49, 0·63 and 0·75 N_{Zn} correspond approximately to the critical electron/atom ratios of 1·48, 1·615 and 1·75 postulated by Hume-Rothery for the formation of the β, γ and δ-phases respectively.

Included in Graph 8 is also an enlarged plot of integral excess entropy values. As expected, since the integral excess free energy values exhibit a smooth variation with composition, the $\triangle S^{x}_{m}$ curve shows a similar pattern of behaviour to that of $\triangle H_{m}$.

In terms of quasi-chemical theory, the positive deviations of H_{m} from the minimal values can be explained by postulating increases (i.e. decreases in negative value) of the interaction coefficient, which, of course, are equivalent to decreases in the number of A-B bonds. Thus, assuming the variations in $\triangle S^{x}_{m}$ to be due to configurational changes only, we find decreases in order, i.e. tendencies to more random distribution, between the compositions at which the enthalpy achieves a minimum value. It would appear, therefore, that the build-up of "excess" enthalpy between the stable phases is accommodated by establishing greater randomness of solution until sufficient enthalpy is accumulated to stabilise a new "ordered" structure.

Alternatively, the "excess" enthalpy could be accommodated by the electrons giving rise to increased vibrational entropy. On the basis of electron theory, filling of electron levels with increasing electron concentration results in raising the electronic energy, as a particular zone is filled, until new lower levels become available once the zone boundary has been overcome.

However, either explanation for the occurrence of "excess" enthalpy indicates that the critical compositions, or

electron concentrations, are those corresponding to the maximum deviations on the $\triangle H_m$ and $\triangle S^{x}_{m}$ curves. These compositions, at 0·45 N_{Zn}, 0·60 N_{Zn}, 0·68 N_{Zn} (?) and 0·79 N_{Zn}(?), mark the points at which reversion to the more stable arrangements begins. Also, it can be suggested that, for any given binary system, there may be a quantitative relationship between the minimum enthalpy values and the lowest energy levels available for electron accommodation.

To account for the variation of the partial thermodynamic properties on the same basis as the integral values, one is forced to think in terms of vibrational rather than configurational entropy since it does not seem possible to account for one component becoming more randomly dispersed while the other becomes less randomly dispersed, as suggested by the partial curves in Graph 6. On the other hand, it does seem reasonable to postulate that the increasing and decreasing of $\triangle H_m$ with respect to the minimum value is accompanied by redistribution of vibrational energy between the component atoms. Thus, graph 6 would indicate that, at the compositions corresponding to the critical electron/atom ratios, the copper atoms take more and the zinc atoms less than their weighted shares (i.e. according to the relative proportions of the two atoms present) of the total vibrational energy content. It is

more difficult to postulate, from the shape of the curves in Graph 6, that, at certain points between these compositions, the reverse holds, but this may also be true. Finally, therefore, it may prove profitable to attempt measurement of electronic energies with a view to discovering more about the possible changing potentials of the constituent atoms in the solution.

7.6. Solid Solutions of Zn/Cu Alloys

In general, the results obtained from the determination of partial thermodynamic properties of solid alloys show similar trends to those of the liquid alloys but with certain differences. For instance, although no alloys beyond 0·68 N_{Zn} were used in the determinations it would appear, from Graph 9, that a_{Zn} values continue to show negative deviation from ideality in the δ and ε-phase fields. Also, excess entropy values (Graph 11). while still exhibiting characteristic dips in the β and γ phase fields, tend to have more positive values than those of the corresponding liquid alloys. Indeed, it would seem that an overall vibrational contribution must be present, giving positive values to $\Delta\bar{S}^{M}_{Zn}$ except where, for configurational reasons, dips occur in the curves. Since, however, these excess entropy values are related to solid zinc while those of the liquid alloys are related to liquid zinc, the results for the two states are not directly numerically comparable.

Within the γ-phase field in the solid state, the values of both partial excess entropy ($\Delta\bar{S}^{x}_{Zn}$) and partial excess enthalpy ($\Delta\bar{H}_{Zn}$) show very similar trends to those of the corresponding liquid alloys. Thus, a minimum occurs at about 0·61 N_{Zn} (i.e. coincident with the critical electron/atom ratio required for the formation of the appropriate electron compound) and a very high value at 0·68 N_{Zn}. This latter peak can again be explained by postulating that the defect structure, said to occur just beyond the zinc-rich boundary of this phase-field, results in an increase in vibrational entropy.

On the other hand, the pattern of results in the β-phase field is more difficult to explain. In this case there are two dips, at 0·43 and 0·46 N_{Zn} respectively. It seems logical to associate the second of these, as in the liquid alloys, with the electron compound predicted at the electron/atom ratio of 1·46, but the first does not correspond to any previously postulated critical concentration. Although it is possible to postulate a double build-up of enthalpy, each followed by a release to lower energy levels, within this single phase field, it is considered more likely that the first dip is spurious. It will be noted from Graph 10 that the formation of this dip depends solely upon the determined entropy value of only one alloy in this investigation and its existence, therefore, is somewhat doubtful. In view of this, and the previously discussed discrepancies with

Olander's results, it is considered that further experimentation with β-phase alloys is desirable.

However, as before, it seems more relevant to discuss the partial properties of both components only in their relations to the integral values. Thus, the three sets of enthalpy values are shown plotted in Graph 16 for both β and γ-phases. As in the liquid alloys, the fluctuations of the partial properties must surely be explained by changes in the distribution of vibrational energy between the components. On the other hand, due to the intervening two-phase fields between solid phases in a system, it is not possible to discuss variations in the integral properties in the same manner as the liquid alloys. Integral enthalpy and excess entropy values are shown plotted on a different scale in Graph 17. From this, and from Table 6, it is clear that there are only slight tendencies to minima in the curves and agreement between the minima in enthalpy and entropy values is not close. Thus, in the β-phase field the minimum enthalpy occurs at about 0·46 N_{Zn} and minimum excess entropy at 0·43 N_{Zn}, while in the γ-phase field the minima occur at 0·61 and 0·63 N_{Zn} respectively. Also, it will be noted that the integral excess entropy values for the β-phase alloys are slightly positive throughout, while those for the γ-phase alloys are slightly negative throughout. It may be construed from this, assuming equal contributions from

vibrational sources, that the γ-phase alloys have lower configurational entropies, i.e. increased order, consistent with their stronger intermetallic bonding tendencies.

The foregoing shows that it has not been possible to subject the results from the determinations made on solid alloys to the same detailed analysis as those from the liquid alloys. Nevertheless, the similarities which do exist between both sets of results suggest that the analogy is valid and a future closer study of the solid alloys is considered worthwhile.

PART B

SUMMARY AND CONCLUSIONS

Part 8 - SUMMARY AND CONCLUSIONS

8.1. Summary

The present investigation has been concerned with the measurement of thermodynamic properties of zinc/copper alloys in the liquid and solid states, and with the interpretation of these in terms of alloy structure.

A conventional dew-point technique was used to determine, initially, the vapour pressure of the zinc component at a number of temperatures and, from these values, thermodynamic functions were calculated. For evaluation of the vapour pressures the equations of Kubaschewski and Evans (16), relating the vapour pressure of pure zinc in solid and liquid states to temperature, were used as a basis. Comparison with the results of other workers, recalculated, wherever possible, to the same basis, was made. In general, fair agreement with previous work was obtained but with certain differences. In the liquid state, for instance, a change from negative to positive deviation from ideality was noted in the a_{Zn}/N_{Zn} curve at high zinc contents. Previously, negative deviation over the whole compositional range had been reported.

Also, characteristic minima and maxima were obtained when $\Delta\bar{S}^{x}_{Zn}$ values for liquid and solid alloys were plotted against composition. One of these minima, viz. that occurring at 0·43 N_{Zn} in the solid alloys was considered difficult to explain and probably spurious. Otherwise, the minima occurred at compositions corresponding approximately to the centre of the β and γ-phase fields and were associated with the critical electron/atom ratios (1·48 and 1·615 respectively) required, by electron theory, for the formation of the appropriate electron compounds. The peak positive value (i.e. the highest maximum) in the $\Delta\bar{S}^{x}_{Zn}$ curve for liquid alloys, which occurred at 0·68 N_{Zn}, was found to have analogies in at least two other binary systems. (viz. Zn/Sb and Cd/Sb). This positive value of $\Delta\bar{S}^{x}_{Zn}$ was associated with an increased vibrational contribution to entropy and linked with the previously reported defect structure of the δ-phase.

Quantitative application of quasi-chemical theory to the partial and integral thermodynamic functions was attempted and, after comparison with other systems, reasons advanced for the limited applicability. However, qualitative application, particularly when integral properties were considered, was possible.

The partial thermodynamic functions of the second

component, viz copper, were calculated from the Gibbs-Duhem relationship and, thus, integral properties obtained. For the liquid alloys all three functions were compared and the conclusion drawn that, in certain compositional regions, there was a build-up of "excess" enthalpy (stored, probably, as vibrational energy) which was released again to allow the "minimum" value to be reached at fixed compositions. These compositions were found to co-incide approximately with the critical electron/atom ratios necessary, according to electron theory, for the formation of the β and γ-phases in solid alloys, but it was postulated that the true "critical" compositions were those corresponding to the maximum build-up of excess enthalpy. In addition the variation of the partial properties in the region of these critical compositions suggested that the release of the excess enthalpy was accompanied by a redistribution of the vibrational energy between the two components of the solution. Because of the close approximation of the compositions at which minimal values occurred, to the centres of the β, γ and ε-phase fields, a fourth minimum, corresponding to the unexplored δ-phase field region was predicted. Also, the existence of these minima were taken as an indication of the extent to which "solid" structures persist above liquidus temperatures.

The above postulations and the link with electron theory were less clearly applicable to the solid alloys, but sufficient similarity existed to suggest that complete analogy may be established by further study.

8. 2. Conclusions

Structural features arising from the alloying of zinc and copper are reflected in the thermodynamic properties of the solutions formed. As far as the partial functions are concerned, the correlation is somewhat limited and may be misleading but the patterns of the integral enthalpy and excess entropy values are very characteristic and capable of close correlation with structure.

There is evidence that, in the liquid state "solid" structures persist and, for the formation of liquid, and probably solid solutions, a minimum enthalpy can be postulated. Positive deviation from this, which is associated with an increase in the vibrational energy of the solution results from the necessity to fill the higher electron energy levels in a Brillouin zone of a particular structure before further lower levels become available, with the stabilising of a new atomic arrangement. In addition, accompanying the formation of the

new structure, there is a marked redistribution of vibrational energy between the two components of the solution.

In terms of quasi-chemical theory, the positive deviation of the enthalpy is equivalent to a decrease in the negative value of the interaction coefficient but, due to a systematic variation of this coefficient over the whole range of composition, no quantitative calculations, on this basis, can be made.

APPENDICES

APPENDIX 1

Calculation of Best Straight Line for $\log p_{Zn} = A + \frac{B}{T}$

Example : Alloy B21 $N_{Zn} = 0.590$

Result No	T_1 (°K)	X $(\frac{1}{T} \times 10^4)$	Y $(\log p_{Zn})$	XY (10^4)	X^2 $(\times 10^8)$	State	Constants Found
9	1262	7.923	2.893	22.921	62.774	L	
8	1225	8.164	2.742	22.386	66.651	I	A = 7.573
3	1183	8.453	2.578	21.792	71.453	Q U I D	B = -5911
5	1154	8.666	2.451	21.240	75.100		
n = 4		Σ 33.206	10.664	88.339	275.978		
2	1081	9.251	2.085	19.288	85.561	S	
4	1048	9.543	1.893	18.065	91.069	O	A = 8.504
1	1004	9.863	1.667	16.442	97.279	L	B = -6933
6	978	10.220	1.422	14.533	104.448	I	
7	941	10.630	1.130	12.012	112.997	D	
n = 5		Σ 49.507	8.197	80.340	491.374		

$$\Sigma XY = A\Sigma X + B\Sigma X^2$$
$$\Sigma Y = nA + B\Sigma X$$

For solid state,

$$80.340 = 49.507A + 491.374 \times 10^{-4} B \times 5$$
$$8.197 = 5A + 49.507 \times 10^{-4} B \times 49.507$$

$$401.700 = 247.535A + 0.2456870\ B$$
$$405.809 = 247.535A + 0.2450943\ B$$

$$-4.109 = .0005927\ B$$

$$B = \frac{-4.109}{.0005927} = \underline{\underline{-6933}}$$

$$A = \frac{8.197 + (49.507 \times 10^{-4} \times 6933)}{5}$$

$$= \underline{\underline{8.504}}$$

Similarly for liquid state.

APPENDIX 2

Determination of Corrections to Results of Other Workers

1. Vapour Pressure Relationships

Relationships $\log p_{Zn(mm)} = A + \frac{B}{T} + C \log T + D \times 10^{-3} T$

No.	A	B	C	D	Source
1A	12·34	-6620	-1·255	-	Kubaschewski and Evans (16)
1B	11·24	-6850	-0·755	-	" " "
2A	12·449	-6678	-1·274	-	Chiotti and Gill (19)
2B	9·824	-6865	-0·1913	-0·262	" " "
3	12·00	-6670	-1·126	-	Kubaschewski and Evans (26)-1951
4	8·095	-6150	-	-	Landolt - Bornstein (24)
5*	8·168	-6220	-	-	I.C.T. (27) and U.S. Bureau of Mines (2)
6	7·998	-6050	-	-	Schneider and Schmid (10)
7	8·140	-6193	-	-	Everett, Jacobs and Kitchener (7)
8	Values of $\log p_{Zn}$ from their Table III used for corrections				Herbenar, Siebert and Duffendack (12)

* Relationships used in obtaining constants A and B:-

$\log p_{Zn(mm)} = 12·0181 - \frac{6789·5}{T} - 1·051 \log T - 1·255 \times 10^{-3} T$ .... (Evaporation)

$\log p_{Zn(mm)} = 8·108 - \frac{6163}{T}$ .....(liquid 873° -1258°K)

$\log p_{Zn(mm)} = 12·84 - \frac{6633}{T} - 1·203 \log T$(" 692° - 898°K)

2. Comparison of $\log p_{Zn}$ values.

T°K	$\log p_{Zn(mm)}$ from relationship							
	1A	2A	3	4	5*	6	7	8
650	-0·950		-0·999					
730	-0·322	-0·346	-0·361	-0·331	-0·356	-0·290	-0·343	
765	0·067							0·056
786								0·269
800	0·422	0·401	+0·393	0·407	0·388	0·435	0·399	
849	0·866							0·847
850	0·876		+0·855					
900	1·276	1·265	+1·263	1·262	1·252	1·276	1·259	
912	1·366							1·351
940	1·565							
950	1·633		1·626					
972	1·779							1·776
1000	1·955	1·949	1·952	1·945	1·943	1·948	1·947	
1100	2·717							
1200	2·959	2·961	2·977	2·970	2·980	2·956	2·979	
1300	3·339	3·345	3·361	3·363	3·378	3·343	3·376	

3. Corrections to p_{Zn} values

Results of	Relation-ship	log p_{Zn} range	Correction applied
Argent and Wakeman	3	-0·999 to -0·361	+0·045
		-0·361 " 0·393	+0·035
		0·393 " 0·855	+0·025
		0·855 " 1·263	+0·015
		1·263 " 1·626	+0·010
		1·626 " 1·952	+0·005
Seith and Kraus	4	0·307 " 2·007	+0·010
Hargreaves	5	-0·263 " 2·009	Results recalculated from known values of T_a
Schneider and Schmid	6	2·261 " 2·872	nil
Everett et al.	7		Values of p_{Zn} only corrected
Herbenaret al.	8	0·056 " 0·269	+0·015
		0·269 " 0·847	+0·020
		0·847 " 1·351	+0·015
		1·351 " 1·555	+0·010
		1·555 " 1·776	+0·005

APPENDIX 3

Details of Thermodynamic Calculations

Using Kubaschewski and Evans' equations 1A and 1B (see Part 4.2. and Appendix 2) -

$\log p_{Zn\,1200°K}$ (liquid state) = 2·959 mm

$\log p_{Zn\,1100°K}$ (solid ") = 2·717 mm

$\log p_{Zn\,1000°K}$ (" ") = 2·125 mm

1. Activity of Zinc

$$\log a_{Zn} = \log \frac{p_{Zn}}{p_{Zno}} = \log p_{Zn} - \log p_{Zno}$$

$$= A_L + \frac{B_L}{1200} - 2·959 \quad \text{...(for liquid alloys at 1200°K)}$$

$$= A_S + \frac{B_S}{1100} - 2·717 \quad \text{...(" solid " " 1100°K)}$$

$$= A_S + \frac{B_S}{1000} - 2·125 \quad \text{...(" " " " 1000°K)}$$

where A_L and B_L = constants in equation $\log p_{Zn} = A + \frac{B}{T}$ for any given alloy in liquid state.

A_S and B_S = constants in equation $\log p_{Zn} = A + \frac{B}{T}$ for any given alloy in solid state.

2. Partial Free Energy of Zinc

$$\Delta \bar{G}_{Zn} = RT \ln a_{Zn}$$

$$= 5,490 \log a_{Zn} \quad \text{...(for liquid alloys at 1200°K)}$$

$$= 5,033 \log a_{Zn} \quad \text{...(" solid " " 1100°K)}$$

$$= 4,575 \log a_{Zn} \quad \text{...(" " " " 1000°K)}$$

3. Partial Entropy of Zinc

$$\Delta \bar{S}_{Zn} = -\frac{d(\Delta \bar{G}_{Zn})}{dt}$$

$$= -\frac{d[4{\cdot}575\ T\ (\log p_{Zn} - \log p_{Zno})]}{dt}$$

$$= -\frac{d[4{\cdot}575\ T\ (\log p_{Zn} - \text{equation 1A})]}{dt}$$

$$= -\frac{d[4{\cdot}575T(A + \frac{B}{T} - 12{\cdot}34 + \frac{6620}{T} + 1{\cdot}255 \log T)]}{dt}$$

$$= -4{\cdot}575\ A + 56{\cdot}456 - 5{\cdot}742 \log T - (0{\cdot}4343 \times 5{\cdot}742 \frac{T}{T})$$

$$= \underline{\underline{-4{\cdot}575\ A + 36{\cdot}281}} \quad \text{.....(for liquid alloys at 1200°K)}$$

or

$$-\frac{d[4{\cdot}575\ T\ (A + \frac{B}{T} - \text{equation 1B})]}{dt}$$

$$= -\frac{d[4{\cdot}575T\ (A + \frac{B}{T} - 11{\cdot}24 + \frac{6850}{T} + 0{\cdot}755 \log T)]}{dt}$$

$$= \underline{\underline{-4{\cdot}575\ A + 39{\cdot}561}} \quad \text{....(for solid alloys at 1000°K)}$$

4. Free Energy and Entropy of Fusion of pure Zinc at 1000°K

$$\Delta \bar{G}_{(L)} = RT \ln \frac{p_{Zn}}{p_{Zno}} = 4{\cdot}575\ T(\log p_{Zn} - \text{equation 1A})$$

$$= 4{\cdot}575\ T\ [A + \frac{B}{T} - 12{\cdot}34 + \frac{6620}{T} + 1{\cdot}255 \log T]$$

Similarly,

$$\Delta \bar{G}_{(s)} = 4{\cdot}575\ T[A + \frac{B}{T} - 11{\cdot}24 + \frac{6,850}{T} + 0{\cdot}755 \log T]$$

$$\therefore \Delta \bar{G}_{(S-L)} = 4{\cdot}575\ T[-1{\cdot}10 - \frac{230}{T} + 0{\cdot}500 \log T]$$

$$= -779 \text{ cal} \quad \text{.....(at 1000°K)}$$

$$\Delta \bar{S}_{(L)} = -4{\cdot}575\ A + 56{\cdot}456 - 5{\cdot}742 \log T - 2{\cdot}494 \quad \text{...(see 3 above)}$$

$$= -4{\cdot}575\ A + 36{\cdot}736 \quad \text{.....(at 1000°K)}$$

$$\Delta \bar{S}_{(s)} = -4{\cdot}575\ A + 39{\cdot}561 \quad \text{.....(see 3 above)}$$

$$\therefore \underline{\underline{\Delta \bar{S}_{(S-L)} = +2{\cdot}825}}$$

5. Partial Excess Free Energy of Copper in Solid Alloys

From Raynor's equilibrium diagram for the zinc/copper system (23) the following conjugate compositions are in equilibrium -

Phases	1000°K			1100°K		
	N_{Zn}	N_{Cu}	$\frac{N_{Zn}}{N_{Cu}}$	N_{Zn}	N_{Cu}	$\frac{N_{Zn}}{N_{Cu}}$
α	0·350	0·650	0·538	0·333	0·667	0·499
β	0·405	0·595	0·681	0·383	0·617	0·621
β	0·523	0·477	1·095	0·554	0·446	1·242
γ	0·575	0·425	1·350	0·590	0·410	1·439

α - phase:- At phase boundary,

$$\Delta\bar{G}^{x}_{Cu} = -\begin{cases} N_{Zn}/N_{Cu} = y \\ N_{Zn}/N_{Cu} \cdot d(\Delta\bar{G}^{x}_{Zn}) \\ N_{Zn}/N_{Cu} = 0 \end{cases}$$

$$= -[\text{Area}]^{N_{Zn}/N_{Cu} = 0\cdot538}_{N_{Zn}/N_{Cu} = 0\cdot000} \quad \ldots(\text{at } 1000^{\circ}K)$$

$$= \underline{\underline{-685 \text{ cal}}} \quad \ldots\ldots(\text{from Graph 12})$$

or $$-[\text{Area}]^{N_{Zn}/N_{Cu} = 0\cdot499}_{N_{Zn}/N_{Cu} = 0\cdot000} \quad \ldots(\text{at } 1100^{\circ}K)$$

$$= \underline{\underline{-630 \text{ cal}}} \quad \ldots\ldots (\text{From Graph 13})$$

β-phase:- At $\alpha/$ phase boundary,

$$\Delta\bar{G}^{x}_{Cu} = \Delta\bar{G}^{x}_{Cu\alpha} + RT \ln \frac{N_{Cu\alpha}}{N_{Cu\beta}} \quad \text{....(see Part 4.3.)}$$

$$= -885 + 4{,}575 \log \frac{0.650}{0.595} \quad \text{....(at 1000°K)}$$

$$= \underline{\underline{-709 \text{ cal}}}$$

or $$-830 + 5{,}033 \log \frac{0.667}{0.617} \quad \text{....(at 1100°K)}$$

$$= \underline{\underline{-660 \text{ cal}}}$$

For other compositions in β-phase field

$$\Delta\bar{G}^{x}_{Cu} = -709 - \int_{N_{Zn}/N_{Cu}=0.681}^{N_{Zn}/N_{Cu}=y} d(\Delta\bar{G}^{x}_{Zn}) \quad \text{....(at 1000°K)}$$

$$= -709 - [\text{Area}]^{N_{Zn}/N_{Cu}=y}_{N_{Zn}/N_{Cu}=0.681} \quad \text{.....(Graph 14)}$$

$$\underline{\underline{\qquad\qquad}}$$

or $$-660 - \int_{N_{Zn}/N_{Cu}=0.621}^{N_{Zn}/N_{Cu}=y} d(\Delta\bar{G}^{x}_{Zn}) \quad \text{.....(at 1100°K)}$$

$$= -660 - [\text{Area}]^{N_{Zn}/N_{Cu}=y}_{N_{Zn}/N_{Cu}=0.621} \quad \text{.....(Graph 14)}$$

$$\underline{\underline{\qquad\qquad}}$$

e. g. at $\beta/\beta+\gamma$ phase boundary

$$\Delta\bar{G}^{x}_{Cu} = -709 - [\text{Area}]^{N_{Zn}/N_{Cu}=1.095}_{N_{Zn}/N_{Cu}=0.681}$$

$$= -709 - 1089$$

$$= \underline{\underline{-1798 \text{ cal}}} \quad \text{....(at 1000°K)}$$

or $$-660 - [\text{Area}]^{N_{Zn}/N_{Cu}=1.242}_{N_{Zn}/N_{Cu}=0.621}$$

$$= -660 - 1360$$

$$= \underline{\underline{-2020 \text{ cal}}} \quad \text{....(at 1100°K)}$$

γ-phase:- At β-phase boundary,

$$\Delta\bar{G}^{x}_{Cu} = \Delta\bar{G}^{x}_{Cu\beta} + RT \ln \frac{N_{Cu\beta}}{N_{Cu\gamma}} \quad \text{....(see Part 4.3.)}$$

$$= -1798 + 4{,}575 \log \frac{0.477}{0.425} \quad \text{....(at 1000°K)}$$

$$= \underline{-1569 \text{ cal}}$$

or $$= -2020 + 5{,}033 \log \frac{0.446}{0.410} \quad \text{....(at 1100°K)}$$

$$= \underline{-1{,}835 \text{ cal}}$$

For other compositions in γ-phase field at 1000°K

$$\Delta\bar{G}^{x}_{Cu} = -1569 - \int_{N_{Zn}/N_{Cu}=1.350}^{N_{Zn}/N_{Cu}=y} N_{Zn}/N_{Cu} \cdot d(\Delta\bar{G}^{x}_{Zn})$$

$$= -1569 - [\text{Area}]_{N_{Zn}/N_{Cu}=1.350}^{N_{Zn}/N_{Cu}=y} \quad \text{.....(Graph 15)}$$

e. g. at $N_{Zn} = 0.590$

$$\Delta\bar{G}^{x}_{Cu} = -1569 - [\text{Area}]_{N_{Zn}/N_{Cu}=1.350}^{N_{Zn}/N_{Cu}=1.439}$$

$$= -1569 - 210$$

$$= \underline{-1{,}779 \text{ cal}}$$

and, making use of equation (4.3.3)

$$\Delta\bar{S}^{x}_{Cu} = -\frac{(\Delta\bar{G}^{x}_{Cu1100°K} - \Delta\bar{G}^{x}_{Cu1000°K})}{1100 - 1000}$$

$$= \frac{+1835 - 1779}{100} = \underline{+0.56 \text{ cal/deg}}$$

For other compositions,

$$\Delta\bar{S}^{x}_{Cu} = +0.56 - \int_{N_{Zn}/N_{Cu}=1.439}^{N_{Zn}/N_{Cu}=y} N_{Zn}/N_{Cu} \cdot d(\Delta\bar{S}^{x}_{Zn})$$

$$= +0.56 - [\text{Area}]_{N_{Zn}/N_{Cu}=1.439}^{N_{Zn}/N_{Cu}=y} \quad \text{(Graph 15)}$$

TABLES

Note:- The units used in the following tables are as follows:-

Temperature	°K
Vapour Pressure	mm Hg
Free Energy	calories
Enthalpy	calories
Entropy	calories per degree

TABLE I - Results of Vapour Pressure Determination on Zn/Cu Alloys

N_{Zn}	Temp. °K. V.P.(mm)	Liquid Alloys							Solid Alloys							
		Results						Constants	Results							Constants
		1	2	3	4	5	6		1	2	3	4	5	6	7	
0·254	T_1	1391	1343	1314	1291	1256			1138	1078	1031	979	934			
	$1/T_1 \times 10^4$	7·190	7·446	7·610	7·747	7·962		A= 7·603	8·788	9·274	9·701	10·21	10·71			A = 7·882
	T_2	1129	1097	1071	1055	1026		B= -6886	956	904	865	823	789			B = -7082
	log p_{Zn}	2·644	2·491	2·357	2·272	2·117			1·675	1·303	1·001	0·638	0·314			
0·304	T_1	1303	1271	1249	1233				1121	1071	1014	964				
	$1/T_1 \times 10^4$	7·676	7·868	8·007	8·112			A= 7·737	8·921	9·337	9·863	10·37				A = 8·279
	T_2	1094	1069	1051	1038			B= -6854	969	924	874	830				B = -7306
	log p_{Zn}	2·476	2·346	2·249	2·175				1·761	1·454	1·073	0·700				
0·412	T_1	1281	1247	1213	1188				1140	1093	1054	999	963			
	$1/T_1 \times 10^4$	7·807	8·021	8·245	8·416				8·776	9·149	9·486	10·01	10·39			
	T_2	1128	1099	1074	1049			A= 7·643	1013	973	935	886	853			A = 8·214
	log p_{Zn}	2·637	2·501	2·374	2·237			B= -6409	2·031	1·785	1·531	1·169	0·900			B = -7039
0·433	T_1	1302	1272	1237	1201	1182			1106	1070	1037	992	945			
	$1/T_1 \times 10^4$	7·683	7·861	8·085	8·328	8·459			9·028	9·346	9·645	10·08	10·58			
	T_2	1153	1129	1097	1068	1052		A= 7·660	998	962	931	889	842			A = 8·541
	log p_{Zn}	2·748	2·644	2·491	2·341	2·254		B= -6389	1·943	1·715	1·506	1·193	0·807			B = -7301
0·448	T_1	1318	1267	1267	1236	1213	1180		1136	1079	1050	1025	992	945		
	$1/T_1 \times 10^4$	7·588	7·769	7·893	8·078	8·245	8·474	A=7·731	8·788	9·266	9·523	9·757	10·08	10·58		A = 8·071
	T_2	1175	1146	1132	1107	1084	1058	B= -6429	1039	978	954	926	902	853		B = -6754
	log p_{Zn}	2·855	2·732	2·660	2·538	2·426	2·286		2·124	1·817	1·660	1·467	1·292	0·900		
0·460	T_1	1254	1205	1171					1055	1013	1000	958				
	$1/T_1 \times 10^4$	7·975	8·301	8·546				A =7·843	9·477	9·874	10·00	10·43				A = 8·136
	T_2	1132	1090	1058				B= -6498	965	927	910	876				B = -6753
	log p_{Zn}	2·660	2·455	2·286					1·735	1·473	1·351	1·089				
0·477	T_1	1295	1264	1241	1213	1171			1122	1080	1039	999	970	938		
	$1/T_1 \times 10^4$	7·721	7·911	8·060	8·245	8·538		A= 7·895	8·910	9·260	9·627	10·01	10·30	10·66		A = 8·367
	T_2	1170	1145	1122	1096	1062		B= -6552	1032	992	954	914	884	857		B = -6961
	log p_{Zn}	2·632	2·719	2·612	2·495	2·300			2·141	1·905	1·660	1·361	1·153	0·936		
0·493	T_1	1261	1241	1200	1176				1121	1067	992	948	912			
	$1/T_1 \times 10^4$	7·807	8·060	8·333	8·503			A= 7·816	8·921	9·371	10·08	10·55	10·96			A = 8·15
	T_2	1164	1128	1093	1071			B= -6420	1031	983	912	872	837			B = -673
	log p_{Zn}	2·805	2·644	2·469	2·357				2·137	1·849	1·366	1·057	0·762			

TABLE I (cont'd) - Results of Vapour Pressure Determination on Zn/Cu Alloys

N_{Zn}	Temp. °K. / V.P.(mm)	Liquid Alloys: Results 1	2	3	4	5	6	Liquid Alloys: Constants	Solid Alloys: Results 1	2	3	4	5	6	7	Solid Alloys: Constants
0·550	T_1 °	1263	1233	1192	1167	1140			1036	1022	1010	998	979	953		
	$1/T_1 \times 10$	7·918	8·112	8·389	8·569	8·772		A= 7·684	9·654	9·786	9·902	10·02	10·21	10·49		A = 8·714
	T_2	1175	1149	1112	1091	1066		B= -6102	980	962	953	937	920	893		B = -7141
	$\log p_{Zn}$	2·855	2·738	2·563	2·460	2·331			1·827	1·715	1·654	1·544	1·426	1·225		
0·590	T_1 °	1262	1225	1183	1154				1061	1046	1004	978	941			
	$1/T_1 \times 10$	7·923	8·164	8·453	8·666			A= 7·573	9·251	9·563	9·863	10·22	10·63			A = 8·504
	T_2	1184	1150	1115	1069			B= -5911	1022	990	955	919	881			B = -6933
	$\log p_{Zn}$	2·893	2·742	2·578	2·451				2·085	1·893	1·667	1·422	1·130			
0·602	T_1 °	1263	1190	1155	1130	1109			1095	1067	1053	1032	1003	977	946	
	$1/T_1 \times 10$	7·918	8·405	8·658	8·849	9·020		A= 7·702	9·131	9·371	9·497	9·692	9·972	10·23	10·57	A = 8·627
	T_2	1195	1129	1097	1074	1056		B= -6018	1046	1017	1005	982	952	926	889	B = -7005
	$\log p_{Zn}$	2·939	2·644	2·491	2·374	2·276			2·221	2·055	1·964	1·843	1·648	1·467	1·193	
0·613	T_1 °	1250	1201	1156	1115				1085	1061	1018	966	912	855		
	$1/T_1 \times 10$	8·000	8·328	8·650	8·971			A= 7·825	9·215	9·426	9·826	10·14	10·96	11·69		A = 8·652
	T_2	1191	1145	1102	1065			B= -6133	1045	1018	977	949	865	806		B = -6954
	$\log p_{Zn}$	2·921	2·719	2·514	2·326				2·216	2·060	1·811	1·627	1·001	0·498		
0·628	T_1 °	1256	1223	1173	1123				1072	1015	967	912	864			
	$1/T_1 \times 10$	7·962	8·177	8·525	8·906			A= 7·729	9·328	9·854	10·34	10·96	11·57			A = 8·521
	T_2	1200	1171	1126	1078			B= -5987	1040	986	935	879	827			B = -6768
	$\log p_{Zn}$	2·959	2·836	2·630	2·393				2·168	1·868	1·531	1·114	0·673			
0·652	T_1 °	1265	1197	1161	1129				1055	1027	980	928				
	$1/T_1 \times 10$	7·905	8·354	8·604	8·859			A= 7·668	9·477	9·736	10·21	10·77				A = 8·209
	T_2	1208	1147	1113	1086			B= -5916	1030	1003	953	904				B = -6412
	$\log p_{Zn}$	2·994	2·727	2·567	2·435				2·131	1·972	1·654	1·307				
0·680	T_1 °	1240	1191	1181	1176	1132	1123		999	964	934	904				
	$1/T_1 \times 10$	8·065	8·397	8·416	8·503	8·833	8·906	A= 7·477	10·01	10·37	10·71	11·06				A = 8·000
	T_2	1189	1146	1141	1137	1095	1086	B= -5659	981	948	917	889				B = -6155
	$\log p_{Zn}$	2·914	2·724	2·702	2·681	2·480	2·435		1·837	1·620	1·404	1·193				
0·827	T_1 °	1238	1208	1184	1136	1099										
	$1/T_1 \times 10$	8·078	8·275	8·445	8·803	9·097		A= 7·893								
	T_2	1220	1192	1170	1122	1085		B= -6004								
	$\log p_{Zn}$	3·040	2·926	2·832	2·612	2·429										

Table 2 - Partial Thermodynamic Properties of Zinc in Zn/Cu Alloys - Liquid State - 1200°K

N_{Zn}	Constants		$\log p_{Zn}$	$\log a$	a_{Zn}	$\Delta\bar{G}_{Zn}$	$\Delta\bar{S}_{Zn}$	$\Delta\bar{H}_{Zn}$	γ_{Zn}	$\Delta\bar{G}^{x}_{Zn}$	$\Delta\bar{S}^{x}_{Zn}$	α-function	$\Delta\bar{S}^{i}_{Zn}$	N_{Cu}	$N_{Zn}(1-3N_{Cu})$
	A	B													
0·254	7·603	-6886	1·865	$\bar{2}$·908	0·081	-6,006	+1·497	-4.210	0·317	-2,749	-1·226	-4,940	2·723	0·746	-0·31
0·304	7·737	-6854	2·025	$\bar{1}$·066	0·116	-5,128	+0·855	-4,102	0·382	-2,289	-1·511	-4,725	2·366	0·696	-0·33
0·412	7·643	-6409	2·302	$\bar{1}$·343	0·220	-3,607	+1·314	-2,030	0·534	-1,492	-0·448	-4,316	1·762	0·588	-0·31
0·433	7·660	-6389	2·336	$\bar{1}$·377	0·238	-3,420	+1·236	-1,937	0·550	-1,426	-0·427	-4·435	1·663	0·567	-0·30
0·448	7·731	-6429	2·373	$\bar{1}$·414	0·259	-3,217	+0·912	-2,123	0·578	-1,308	-0·683	-4,276	1·595	0·552	-0·29
0·460	7·843	-6498	2·428	$\bar{1}$·469	0·294	-2,915	+0·399	-2,436	0·639	-1,063	-1·144	-3,645	1·543	0·540	-0·28
0·477	7·895	-6552	2·435	$\bar{1}$·476	0·299	-2,877	+0·161	-2,684	0·627	-1·112	-1·310	-4,065	1·471	0·523	-0·27
0·493	7·818	-6420	2·468	$\bar{1}$·509	0·323	-2,696	+0·514	-2,079	0·655	-1,010	-0·891	-3,930	1·405	0·507	-0·25
0·550	7·684	-6102	2·599	$\bar{1}$·640	0·437	-1,976	+1·127	- 624	0·795	- 551	-0·061	-2,621	1·188	0·450	-0·19
0·590	7·573	-5911	2·647	$\bar{1}$·688	0·488	-1,713	+1·635	+ 249	0·827	- 455	+0·587	-2,707	1·048	0·410	-0·13
0·602	7·702	-6018	2·687	$\bar{1}$·728	0·535	-1,493	+1·044	- 240	0·889	- 283	+0·036	-1,787	1·008	0·398	-0·11
0·613	7·825	-6133	2·714	$\bar{1}$·755	0·569	-1,345	+0·482	- 767	0·928	- 179	-0·490	-1,195	0·972	0·387	-0·09
0·628	7·729	-5987	2·740	$\bar{1}$·781	0·604	-1,202	+0·921	- 97	0·962	- 93	-0·003	- 672	0·924	0·372	-0·07
0·652	7·668	-5916	2·738	$\bar{1}$·779	0·601	-1,213	+1·200	+ 227	0·922	- 193	+0·350	-1,594	0·850	0·348	-0·02
0·680	7·477	-5659	2·761	$\bar{1}$·802	0·634	-1,087	+2·074	+1,402	0·932	- 168	+1·308	-1,641	0·766	0·320	+0·02
0·827	7·898	-6004	2·890	$\bar{1}$·931	0·853	- 379	+0·171	- 174	1·031	+ 73	-0·206	+2,441	0·377	0·173	+0·31

Table 3 - Partial and Integral Thermodynamic Properties of Zn/Cu Alloys - Liquid State - 1200°K

x_{Zn}	$\frac{x_{Zn}}{x_{Cu}}$	$\Delta\bar{S}^{x}_{Zn}$	ΔA (Graph5)	$\Delta\bar{S}^{x}_{Cu}$	ΔS^{x}_{m}	$\Delta\bar{H}_{Zn}$	ΔA (Graph5)	$\Delta\bar{H}_{Cu}$	ΔH_{m}	ΔG^{x}_{m}	$\Delta\bar{G}^{x}_{Zn}$	$\Delta\bar{G}^{x}_{Cu}$	a_{Cu}	γ_{Cu}
0·000	0·000	0·000	0·000	0·000	0·000	-4,600	0	0	0	0	—	0	1·000	0·00
0·100	0·111	-0·420	-0·023	+0·023	—	-4,470	+ 7	- 7	—	—	—	- 35	0·887	0·90
0·175	0·212	-0·850	-0·070	+0·093	—	-4,430	+ 23	- 30	—	—	—	- 142	0·777	0·82
0·254	0·341	-1·226	-0·116	+0·209	-0·155	-4,210	+ 36	- 66	-1,118	- 932	-2,749	- 317	0·653	0·74
0·304	0·437	-1·511	-0·111	+0·320	-0·236	-4,102	+ 42	- 108	-1,322	-1,039	-2,289	- 492	0·566	0·69
0·412	0·701	-0·448	+0·605	-0·285	-0·353	-2,030	+1,178	-1,285	-1,593	-1,169	-1,496	- 944	0·396	0·58
0·433	0·764	-0·427	+0·015	-0·300	-0·355	-1,937	+ 70	-1,356	-1,608	-1,182	-1,426	- 996	0·374	0·56
0·446	0·812	-0·663	-0·202	-0·098	-0·360	-2,123	- 147	-1,209	-1,618	-1,186	-1,303	-1,091	0·349	0·55
0·460	0·852	-1·144	-0·364	+0·286	-0·372	-2,436	- 260	- 949	-1,632	-1,186	-1,063	-1,292	0·314	0·54
0·477	0·912	-1·310	-0·146	+0·432	-0·399	-2,684	- 219	- 730	-1,662	-1,193	-1,112	-1,248	0·310	0·52
0·493	0·972	-0·891	+0·395	+0·037	-0·420	-2,079	+ 570	-1,300	-1,684	-1,180	-1,010	-1,344	0·289	0·56
0·550	1·220	-0·061	+0·910	-0·673	-0·427	- 624	+1,596	-2,896	-1,646	-1,134	- 551	-1,848	0·207	0·41
0·590	1·439	+0·667	+0·862	-1·735	-0·365	+ 249	+1,162	-4,058	-1,517	-1,079	- 455	-1,976	0·179	0·41
0·602	1·513	+0·036	-0·812	-0·922	-0·345	- 240	- 723	-3,335	-1,471	-1,057	- 283	-2,229	0·156	0·31
0·613	1·584	-0·490	-0·815	-0·107	-0·340	- 767	- 816	-2,519	-1,445	-1,037	- 179	-2,391	0·142	0·31
0·628	1·688	-0·003	+0·797	-0·904	-0·338	- 97	+1,096	-3,615	-1,396	- 990	- 93	-2,530	0·129	0·31
0·652	1·874	+0·350	+0·629	-1·533	-0·305	+ 227	+ 579	-4,194	-1,312	- 946	- 193	-2,356	0·129	0·3
0·680	2·125	+1·308	+1·915	-3·448	-0·214	+1,402	+2,249	-6,443	-1,109	- 852	- 168	-2,305	0·122	0·3
0·827	4·780	-0·206	-5·226	+1·778	+0·138	- 174	-5,441	-1,002	- 317	- 151	+ 73	-3,136	0·046	0·1

ϕ Results obtained by extrapolation of $\Delta\bar{S}^{x}_{Zn}$ and $\Delta\bar{H}_{Zn}$ values in Graph 5.

Table 4 - Derivation of Partial Thermodynamic Properties of Zinc in Zn/Cu Alloys -Solid State

N_{Zn}	$\frac{N_{Zn}}{N_{Cu}}$	Constants		1000°K									1100°K	
		A	B	$\log p_{Zn}$	$\log a_{Zn}$	a_{Zn}	$\Delta\bar{G}_{Zn}$	$\Delta\bar{S}_{Zn}$	$\Delta\bar{H}_{Zn}$	$\Delta\bar{G}^{x}_{Zn}$	$\Delta\bar{S}^{x}_{Zn}$	Phase	$\log a_{Zn}$	$\Delta\bar{G}^{x}$
0·254	0·341	7·882	-7082	0·800	$\bar{2}$·675	0·047	-6,062	+3·501	-2,561	-3,339	+0·778	α	$\bar{2}$·727	-3,412
0·304	0·437	8·279	-7308	0·971	$\bar{2}$·846	0·070	-5,260	+1·685	-3,595	-2,914	-0·681		$\bar{2}$·918	-2,843
0·412	0·701	8·214	-7039	1·175	$\bar{1}$·050	0·112	-4,346	+1·982	-2,364	-2,584	+0·220	β	$\bar{1}$·090	-2,602
0·433	0·764	8·457	-7307	1·240	$\bar{1}$·115	0·130	-4,049	+0·459	-3,590	-2,366	-1·204		$\bar{1}$·187	-2,264
0·448	0·812	8·077	-6758	1·319	$\bar{1}$·194	0·156	-3,687	+2·609	-1,078	-2,092	+1·014		$\bar{1}$·216	-2,169
0·460	0·852	8·130	-6755	1·375	$\bar{1}$·250	0·178	-3,431	+2·366	-1,065	-1,888	+0·823		$\bar{1}$·272	-1,968
0·477	0·912	8·367	-6961	1·386	$\bar{1}$·261	0·182	-3,381	+1·282	-2,099	-1,910	-0·189		$\bar{1}$·304	-1,887
0·493	0·972	8·153	-6735	1·418	$\bar{1}$·293	0·196	-3.235	+2·261	- 974	-1,830	+0·856		$\bar{1}$·313	-1,912
0·550	1·222	-	-	1·550	$\bar{1}$·425	0·266	-2631	-	-	-1,443	-	$\beta+\gamma$	—	—
0·590	1·439	8·504	-6933	1·571	$\bar{1}$·446	0·279	-2,536	+0·655	-1,881	-1,488	-0·393	γ	$\bar{1}$·464	-1,444
0·602	1·513	8·627	-7005	1·622	$\bar{1}$·497	0·314	-2,301	+0·092	-2,209	-1,293	-0·916		$\bar{1}$·542	-1,196
0·613	1·584	8·652	-6954	1·698	$\bar{1}$·573	0·374	-1,954	-0·022	-1,976	- 982	-0·994		$\bar{1}$·618	- 881
0·628	1·688	8·521	-6768	1·753	$\bar{1}$·628	0·425	-1,702	+0·577	-1,125	- 778	-0·347		$\bar{1}$·651	- 740
0·652	1·874	8·209	-6412	1·797	$\bar{1}$·672	0·470	-1,500	+2·005	+ 505	- 650	+1·155		$\bar{1}$·663	- 760
0·680	2·125	8·000	-6155	1·845	$\bar{1}$·720	0·525	-1,281	+2·961	+1,680	- 515	+2·195		$\bar{1}$·688	- 730

Table 5 - Derivation of Partial Molar Thermodynamic Properties of Copper in Zn/Cu Alloys Solid State

N_{Zn}	$\frac{N_{Zn}}{N_{Cu}}$	1100°K				1000°K								Phase	N_{Cu}
		$\Delta\bar{G}^{x}_{Zn}$	ΔA (GRAPHS 13 & 14)	$\Delta\bar{G}^{x}_{Cu}$	$\Delta\bar{G}_{Cu}$	$\Delta\bar{G}^{x}_{Zn}$	ΔA (GRAPHS 12, 14 & 15)	$\Delta\bar{G}^{x}_{Cu}$	$\Delta\bar{G}_{Cu}$	$\Delta\bar{S}^{x}_{Zn}$	ΔA (GRAPH 15)	$\Delta\bar{S}^{x}_{Cu}$	$\Delta\bar{H}_{Cu}$		
0·333	0·499	-2,525†	+830	- 830	-1,715									α	0·667
0·350	0·538					-2430§	+885	- 885							0·650
0·383	0·621	-2,830	0	- 660	-1,715									β	0·617
0·405	0·681					-2720	0	- 709	1,741						0·595
0·412	0·701	-2,602	+151	- 811		-2584	+ 94	- 803				+0·08	- 723		0·588
0·433	0·764	-2,264	+248	-1,059		-2386	+145	- 948				+1·11	+ 182		0·567
0·448	0·812	-2,189	+ 59	-1,116		-2092	+232	-1,180				-0·62	-1,800		0·552
0·460	0·852	-1,968	+184	-1,302		-1,868	+170	-1,350				-0·48	-1,830		0·540
0·477	0·912	-1,887	+ 71	-1,373		-1,910	- 20	-1,330				+0·42	- 900		0·523
0·493	0·972	-1,912	- 24	-1,349		-1,830	+ 75	-1,405				-0·56	-1,965		0·507
0·523	1·095					-1,450*	+393	-1,798	-3,269						0·477
0·554	1·242	-1,306	+671	-2,020	-3,748										0·446
0·575	1·350					-1,639*	0	-1,569	-3,269					γ	0·425
0·590	1·439	-1,444		-1835	-3,784	-1,488	+210	-1,779		-0·393	0	+0·56	-1,219		0·410
0·602	1·513					-1,283	+288	-2,067		-0·916	-0·765	+1·33	- 737		0·398
0·613	1·584					- 982	+482	-2,549		-0·994	-0·121	+1·45	-1,099		0·387
0·628	1·688					- 778	+334	-2,883		-0·347	+1·058	+0·39	-2,493		0·372
0·652	1·874					- 650	+228	-3,111		+1·155	+2·674	-2·28	-5,391		0·348
0·680	2·125					- 515	+270	-3,381		+2·195	+2·079	-4·36	-7,741		0·320

§ Value obtained by extrapolation in Graph 12
† " " " " " " 13
* " " " calculation after extrapolation in Graph 9.

Table 6 - Summary of Partial and Integral Molar Thermodynamic Functions of Zinc/Copper Alloys Solid State (1000°K)

N_{Zn}	Partial Molar Functions of Zinc			Partial Molar Functions of Copper			Integral Molar Functions			Phase	N_{Cu}
	ΔG^{E}_{Zn}	ΔS^{E}_{Zn}	ΔH^{E}_{Zn}	ΔG^{E}_{Cu}	ΔS^{E}_{Cu}	ΔH^{E}_{Cu}	ΔG^{E}_{m}	ΔS^{E}_{m}	ΔH^{E}_{m}		
0·412	-2,564	+0·220	-2,364	- 803	+0·08	- 723	-1537	+0·138	-1,399	β	0·588
0·433	-2,386	-1·204	-3,590	- 948	+1·11	+ 162	-1571	+0·108	-1,462		0·567
0·448	-2,092	+1·014	-1,078	-1,180	-0·62	-1,800	-1568	+0·112	-1,477		0·552
0·460	-1,888	+0·823	-1,065	-1,350	-0·48	-1,830	-1597	+0·120	-1,478		0·540
0·477	-1,910	-0·189	-2,099	-1,330	+0·43	- 900	-1607	+0·135	-1,472		0·523
0·493	-1,830	+0·856	- 974	-1,405	-0·56	-1,965	-1614	+0·138	-1,476		0·507
0·590	-1,488	-0·393	-1,881	-1,779	+0·56	-1,219	-1607	-0·002	-1,610	γ	0·410
0·602	-1,293	-0·916	-2,209	-2,067	+1·33	- 737	-1601	-0·022	-1,623		0·398
0·613	- 982	-0·994	-1,976	-2,549	+1·45	-1,099	-1588	-0·046	-1,636		0·387
0·628	- 778	-0·347	-1,125	-2,883	+0·39	-2,483	-1561	-0·073	-1,634		0·372
0·652	- 650	+1·155	+ 505	-3,111	-2·28	-5,391	-1507	-0·040	-1,547		0·348
0·680	- 515	+2·195	+1,680	-3,361	-4·36	-7,741	-1432	+0·097	-1,335		0·320

Table 7 - Corrected Results of Other Workers - (a) Liquid Zinc/Copper Alloys

N_{Zn}	Constants A	Constants B	Corrected $\log p_{Zn}$	Corrected $\log p_{Zn_0}$	log a	a	$\Delta\bar{G}^{x}_{Zn}$	$\Delta\bar{S}_{Zn}$	$\Delta\bar{S}^{i}_{Zn}$	$\Delta\bar{S}^{x}_{Zn}$	$\Delta\bar{H}_{Zn}$	α-function	Temp. °K.
						Everett, Jacobs and Kitchener (7)							
0·320			1·924	2·992	2·932	0·086	-3,166					-6846	1208
0·342			1·928	2·939	2·989	0·098	-2,979					-6890	1195
0·367			2·057	3·000	1·057	0·114	-2,812					-7017	1210
0·408			2·093	2·942	1·151	0·142	-2,515					-7175	1196
0·416			2·096	2·921	1·175	0·150	-2,419					-7091	1191
0·422			2·110	2·916	1·194	0·156	-2,347					-7025	1190
0·425			2·134	2·934	1·200	0·159	-2,338					-7072	1194
0·435			2·159	2·929	1·230	0·170	-2,232					-6992	1193
0·445			2·249	2·992	1·257	0·181	-2,161					-7016	1208
0·460			2·282	2·996	1·286	0·193	-2,086					-7178	1209
0·669			2·579	2·916	1·663	0·460	- 882					-8047	1190
0·753			2·715	2·916	1·799	0·630	- 425					-6966	1190
						Schneider and Schmid (10)							
0·428	8·010	-6875	2·281	2·959	1·322	0·210	-1,699	-0·37	+1·69	-2,06	-4,161	-5193	1200
0·580	7·994	-6480	2·594		1·635	0·432	- 705	-0·30	+1·08	-1·38	-2,361	-3997	
0·664	8·008	-6360	2·708		1·749	0·561	- 402	-0·36	+0·81	-1·17	-1,806	-3561	
0·714	8·015	-6300	2·765		1·806	0·640	- 262	-0·39	+0·67	-1·06	-1,534	-3202	
0·798	7·955	-6100	2·872		1·913	0·619	+ 6	-0·11	+0·45	-0·56	- 666	+1471	
						Leitgebel (25)							
0·828			2·881	2·950	1·931	0·853	+ 71					+2400	1198
0·883			2·881	2·909	1·972	0·938	+ 141					+10299	1188
	$E_{900°}$ (mV)	$\frac{dE}{dT}$ (μV/°)	$E_{1200°}$ (mV)	$\Delta\bar{G}_{Zn}$		Kleppa and Thalmayer (6)							
0·800	10·76	+9·1	13·49	-622		0·770	- 90	+0·42	+0·44	-0·02	- 118	-2250	1200
0·841	7·56	+6·7	9·57	-441		0·831	- 28	+0·31	+0·34	-0·03	- 70	-1108	
0·869	5·96	+7·4	8·18	-377		0·854	- 42	+0·34	+0·28	+0·06	+ 32	-2448	
0·893	4·52	+4·8	5·96	-275		0·891	- 5	+0·22	+0·23	-0·01	- 10	- 437	
0·915	3·18	+4·1	4·41	-203		0·918	+ 9	+0·19	+0·18	+0·01	+ 23	+1246	

Table 7 - Corrected Results of Other Workers - (b) Solid Zn/Cu Alloys

N_{Zn}	$\frac{N_{Zn}}{N_{Cu}}$	Constants A	Constants B	Corrected log p_{Zn}	1000°K log a_{Zn}	1000°K a_{Zn}	1000°K $\Delta\bar{G}^{x}_{Zn}$	1000°K $\Delta\bar{S}_{Zn}$	1000°K $\Delta\bar{S}^{i}_{Zn}$	1000°K $\Delta\bar{S}^{=}_{Zn}$	1000°K $\Delta\bar{H}_{Zn}$	1100°K log p_{Zn}	1100°K log a_{Zn}	1100°K $\Delta\bar{G}^{x}_{Zn}$	Phase
Argent and Wakemann (9)															
0·039	0·041	8·224	-8875	$\bar{1}$·394	$\bar{3}$·269	0·002	-6050	+1·93	+6·45	-5·48	-11,530	0·156	$\bar{3}$·439	-5,795	α
0·131	0·151	7·878	-7647	0·266	$\bar{2}$·141	0·014	-4467	+3·52	+4·04	-0·52	- 4,987	0·962	$\bar{2}$·209	-4,567	
0·169	0·203	8·456	-8018	0·463	$\bar{2}$·338	0·022	-4071	+0·87	+3·53	-2·66	- 6,731	1·167	$\bar{2}$·450	-3,913	
0·184	0·225	8·232	-7796	0·459	$\bar{2}$·334	0·022	-4258	+1·90	+3·36	-1·46	- 5,718	1·143	$\bar{2}$·426	-4,220	
0·207	0·261	7·899	-7266	0·658	$\bar{2}$·533	0·034	-3584	+3·42	+3·13	+0·29	-3,294	1·294	$\bar{2}$·577	-3,717	
0·242	0·319	8·443	-7679	0·789	$\bar{2}$·664	0·046	-3294	+0·93	+2·82	-1·89	- 5,184	1·462	$\bar{2}$·745	-3,214	
0·276	0·381	8·494	-7588	0·921	$\bar{2}$·796	0·063	-2951	+0·70	+2·56	-1·86	- 4,811	1·596	$\bar{2}$·879	-2,826	
0·328	0·488	8·513	-7388	1·140	$\bar{1}$·015	0·104	-2292	+0·61	+2·22	-1·61	- 3,902	1·797	$\bar{1}$·080	-2,193	
0·335	0·504	8·063	-6864	1·214	$\bar{1}$·089	0·123	-1995	+2·68	+2·17	+0·51	- 1,485	-	-	-	
0·341	0·517	8·139	-7006	1·148	$\bar{1}$·023	0·105	-2333	+2·32	+2·14	+0·18	- 2,153	-	-	-	
Hargreaves (8)															
0·012	0·012	6·215	-7132	$\bar{1}$·083	$\bar{4}$·958	0·001	-5129	+11·13	+8·79	+2·34	- 2,789	$\bar{1}$·731	$\bar{3}$·014	-5,087	α
0·052	0·055	6·980	-7366	$\bar{1}$·614	$\bar{3}$·489	0·003	-5614	+7·63	+5·87	+1·76	-3,854	0·284	$\bar{3}$·567	-5783	
0·094	0·104	7·653	-7732	$\bar{1}$·921	$\bar{3}$·796	0·006	-5357	+4·55	+4·70	-0·15	- 5,507	0·624	$\bar{3}$·907	-5366	
0·144	0·168	7·925	-7669	0·256	$\bar{2}$·131	0·014	-4700	+3·30	+3·85	-0·55	- 5,250	0·953	$\bar{2}$·236	-4640	
0·195	0·242	7·340	-6933	0·407	$\bar{2}$·282	0·019	-4612	+5·98	+3·25	+2·73	- 1,882	1·037	$\bar{2}$·320	-4879	
0·255	0·342	7·931	-7214	0·717	$\bar{2}$·592	0·039	-3730	+3·28	+2·72	+0·56	- 3,170	1·373	$\bar{2}$·656	-3778	
0·317	0·464	8·185	-7197	0·988	$\bar{2}$·863	0·073	-2920	+2·12	+2·28	-0·16	- 3,080	1·642	$\bar{2}$·925	-2890	
0·373		Single result at 968°K													$\alpha + \beta$
0·395		7·972	-6875	1·097	$\bar{2}$·967	0·093	-2880								$\alpha + \beta$
0·453		8·150	-6871	1·279	$\bar{1}$·154	0·143	-2297	+2·28	+1·57	+0·71	- 1,587				β
0·481		8·198	-6830	1·368	$\bar{1}$·243	0·175	-2009	+2·06	+1·45	+0·61	-1,399				
0·504		7·703	-6183	1·520	$\bar{1}$·395	0·248	-1406	+4·32	+1·36	+2·96	+ 1,554				
Herbenar, Siebert and Duffendack (12)															
0·052	0·055	7·937	-8390	$\bar{1}$·547	$\bar{3}$·422	0·003	-5920	+3·25	+5·87	-2·62		0·310	$\bar{3}$·593	-5753	α
0·107	0·120	7·966	-7975	$\bar{1}$·993	$\bar{3}$·868	0·007	-5313	+3·11	+4·44	-1·33		0·718	$\bar{2}$·001	-5176	
0·158	0·188	8·115	-7825	0·290	$\bar{2}$·165	0·015	-4729	+2·44	+3·67	-1·23		1·001	$\bar{2}$·284	-4604	
0·195	0·242	8·192	-7749	0·443	$\bar{2}$·318	0·021	-4447	+2·08	+3·25	-1·17		1·147	$\bar{2}$·430	-4329	
0·235	0·307	8·313	-7720	0·593	$\bar{2}$·468	0·029	-4124	+1·53	+2·88	-1·35		1·295	$\bar{2}$·578	-3992	
0·284	0·397	8·348	-7660	0·788	$\bar{2}$·663	0·046	-3615	+1·37	+2·50	-1·13		1·475	$\bar{2}$·758	-3500	

log p_{Zn} at 1000° = 2·125 and log p_{Zn} at 1100° = 2·717

Table 7 - Corrected Results of Other Workers - (b) Solid Zn/Cu Alloys (continued)

N_{Zn}	$\frac{N_{Zn}}{N_{Cu}}$	Constants A	Constants B	Corrected log p_{Zn}	1000°K log a_{Zn}	1000°K a_{Zn}	1000°K $\Delta\bar{G}^{x}_{Zn}$	1000°K $\Delta\bar{S}_{Zn}$	1000°K $\Delta\bar{S}^{i}_{Zn}$	1000°K $\Delta\bar{S}^{x}_{Zn}$	1000°K $\Delta\bar{H}_{Zn}$	1100°K log p_{Zn}	1100°K log a_{Zn}	1100°K $\Delta\bar{G}^{x}_{Zn}$	Phase
						Seith and Kraus (11)									
0·120	0·136	(8·667)	(-8795)	$\bar{1}$·872	$\bar{3}$·745	0·006	-6103	-0·09	+4·21	-4·30	-10,403	0·672	$\bar{3}$·955	-5657	α
0·180	0·220	(8·865)	(-8622)	0·243	$\bar{2}$·118	0·013	-5064	-1·00	+3·41	-4·41	- 9,474	1·027	$\bar{2}$·310	-4753	
0·230	0·299	(8·362)	(-7807)	0·555	$\bar{2}$·430	0·027	-4263	+1·31	+2·92	-1·61	- 5,873	1·265	$\bar{2}$·548	-4097	
0·290	0·408	(7·377)	(-6434)	0·943	$\bar{2}$·818	0·066	-2948	+5·81	+2·46	+2·35	- 598	1·528	$\bar{2}$·811	-3275	
0·330	0·493	(7·518)	(-6434)	1·084	$\bar{2}$·959	0·091	-2560	+5·17	+2·20	+2·97	+ 410	1·669	$\bar{2}$·952	-2852	
0·420	-	(7·402)	(-6146)	1·257	$\bar{1}$·132	0·134	-2243	+5·70	+1·72	+3·98	+ 1,737	-	-	-	β
0·440	-	(8·118)	(-6843)	1·275	$\bar{1}$·150	0·141	-2258	+2·42	+1·63	+0·79	- 1,468	-	-	-	β
		* $E_{775°}$ (mV)	* dE/dT (μV/°)	* $E_{1000°}$ (mV)	$\Delta\bar{G}_{Zn}$			Olander (5)							
0·444		84·5	-43	74·7	-4226	0·119		+0·85	+1·61	-0·76	-3,376				β
0·448		82·4	-51	70·8	-4045	0·131		+0·48	+1·60	-1·12	-3,565				
0·453		81·4	-50	70·1	-4010	0·133		+0·52	+1·57	-1·05	-3,490				
0·464		77·3	-55	64·8	-3768	0·150		+0·29	+1·53	-1·24	-3,478				
0·472		75·6	-58	62·4	-3658	0·159		+0·16	+1·49	-1·33	-3,498				
0·480		72·6	-54	60·3	-3562	0·166		+0·34	+1·46	-1·12	-3,222				
0·583		68·5	-92	47·6	-2975	0·224		-1·41	+1·07	-2·48	-4,385				γ
0·595		63·9	-90	43·5	-2784	0·246		-1·32	+1·03	-2·35	-4,104				
0·596		62·3	-84	43·2	-2773	0·247		-1·04	+1·03	-2·07	-3,813				
0·606		56·1	-84	37·0	-2487	0·286		-1·04	+1·00	-2·04	-3,527				
0·611		52·8	-83	34·0	-2345	0·307		-1·00	+0·98	-1·98	-3345				
0·616		49·3	-78	31·6	-2236	0·325		-0·77	+0·96	-1·73	-3,006				
0·618		47·7	-71	31·6	-2236	0·325		-0·44	+0·96	-1·40	-2,676				
0·619		48·3	-78	30·6	-2190	0·332		-0·77	+0·95	-1·72	-2,960				
0·630		40·4	-65	25·6	-1962	0·373		-0·17	+0·92	-1·09	-2132				
0·640		33·2	-53	21·2	-1755	0·413		+0·39	+0·89	-0·50	-1,365				
0·650		27·0	-46	16·6	-1543	0·460		+0·71	+0·86	-0·15	- 833				
0·659		21·2	-34	13·5	-1402	0·494		+1·26	+0·83	+0·43	- 142				
0·665		18·4	-44	8·4	-1167	0·556		+0·80	+0·81	-0·01	- 367				
0·666		17·9	-35	10·0	-1240	0·536		+1·22	+0·81	+0·41	- 20				

* These properties are referred to Zn (L) as standard state. $\log p_{Zn_o}$ 1000° = 2·125

GRAPHS.

GRAPH 1
LIQUID ALLOYS-1200°K

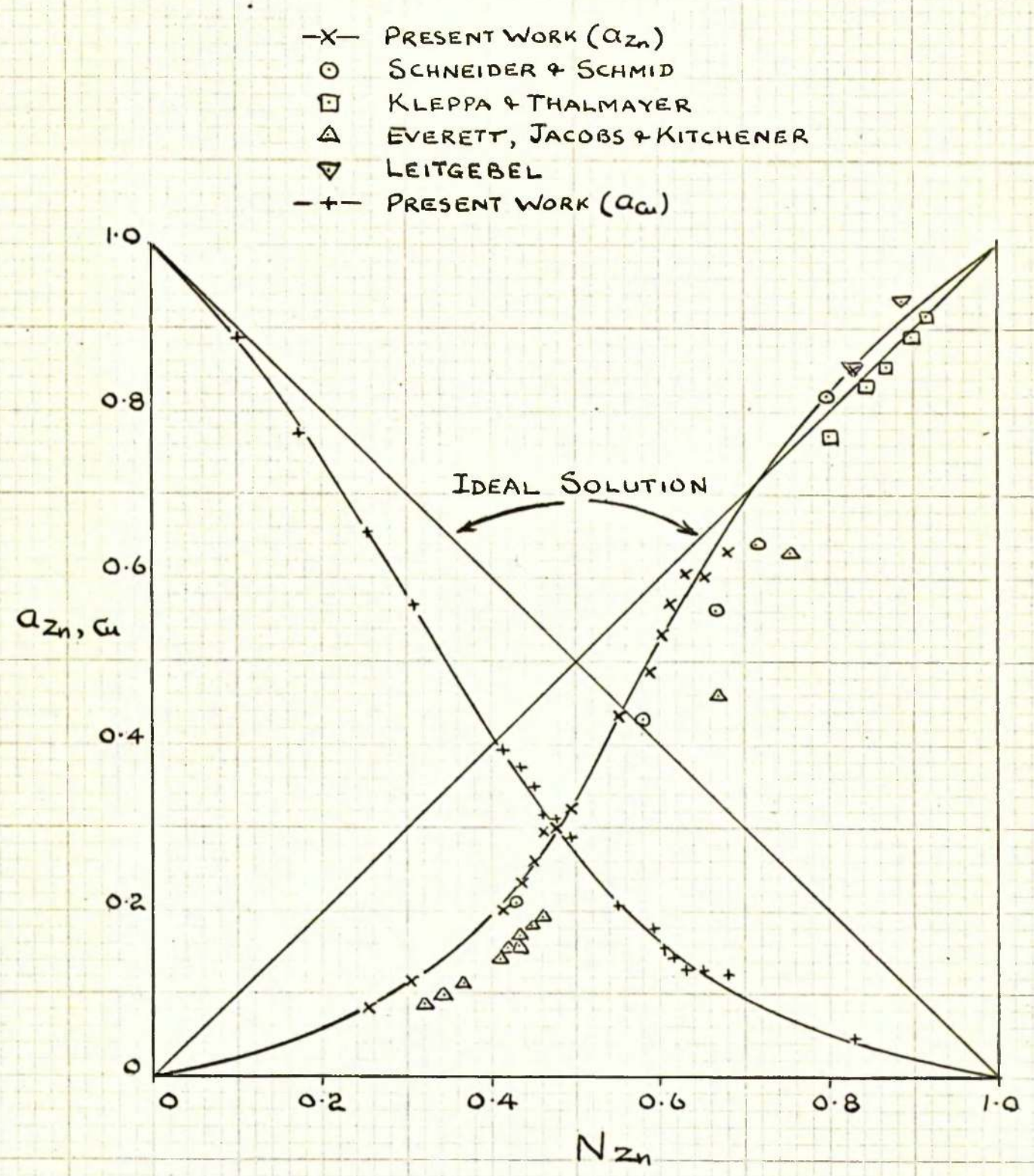

GRAPH 2
LIQUID ALLOYS - 1200°K

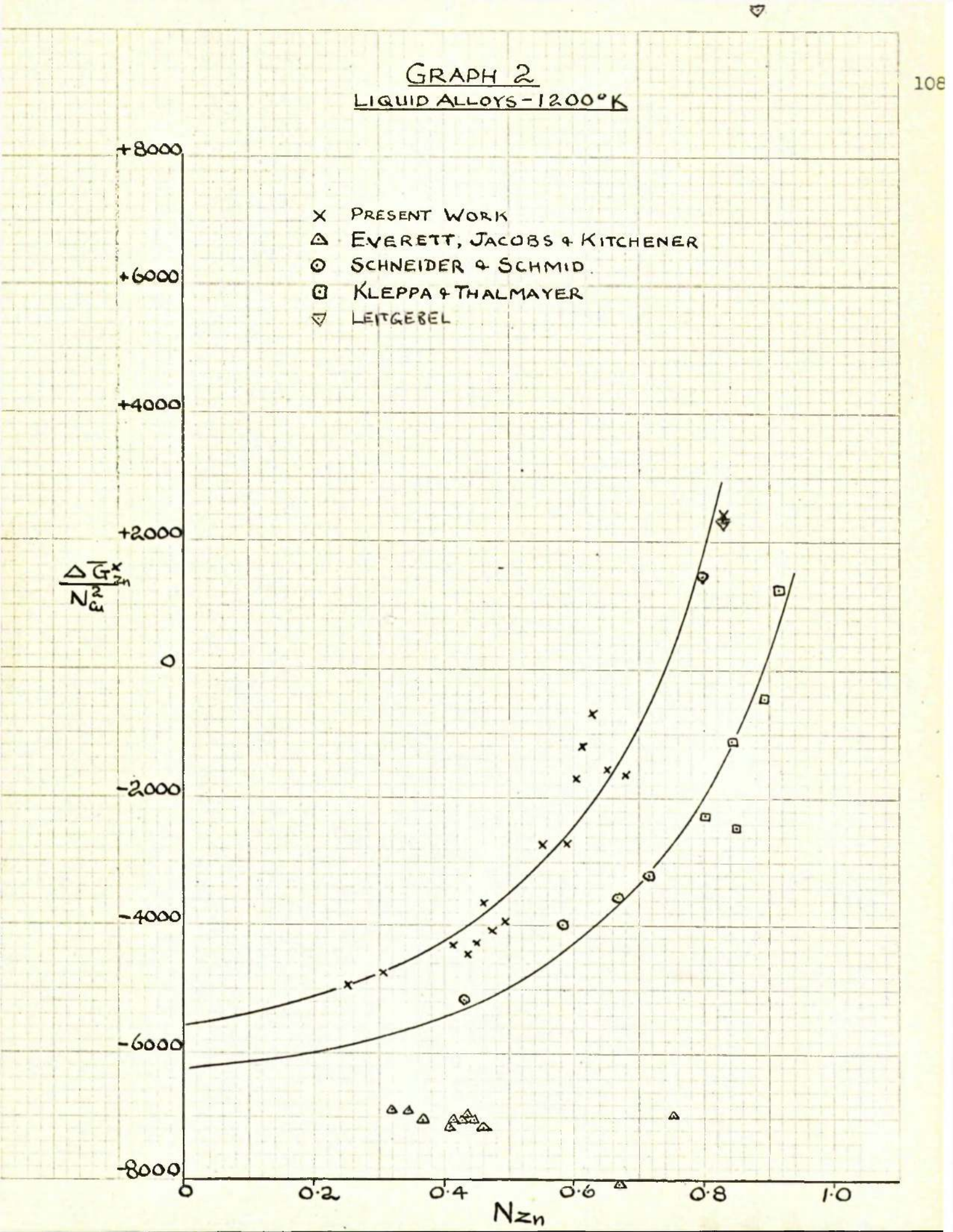

GRAPH 3

LIQUID ALLOYS - 1200°K

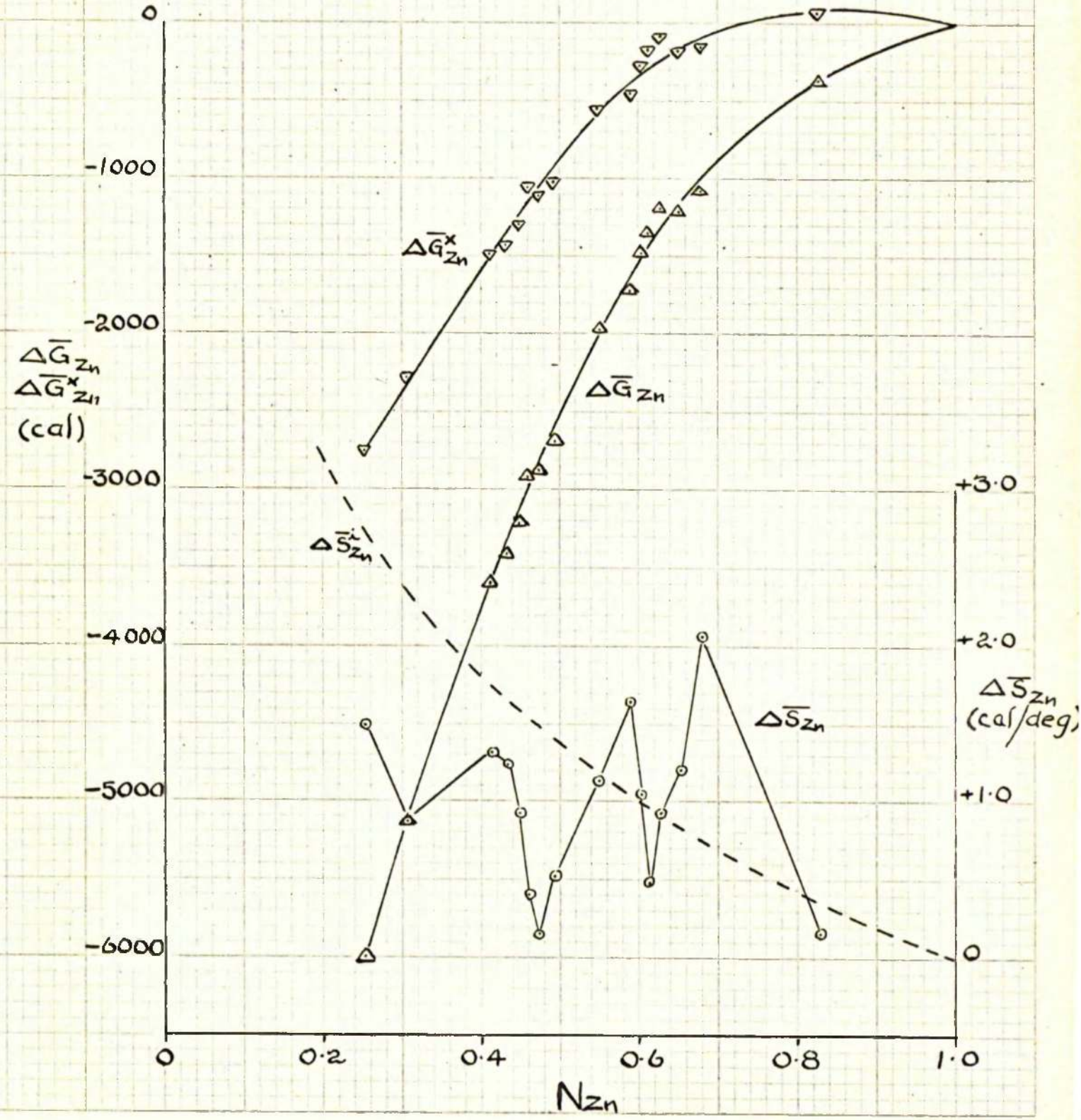

GRAPH 4
LIQUID ALLOYS - 1200°K

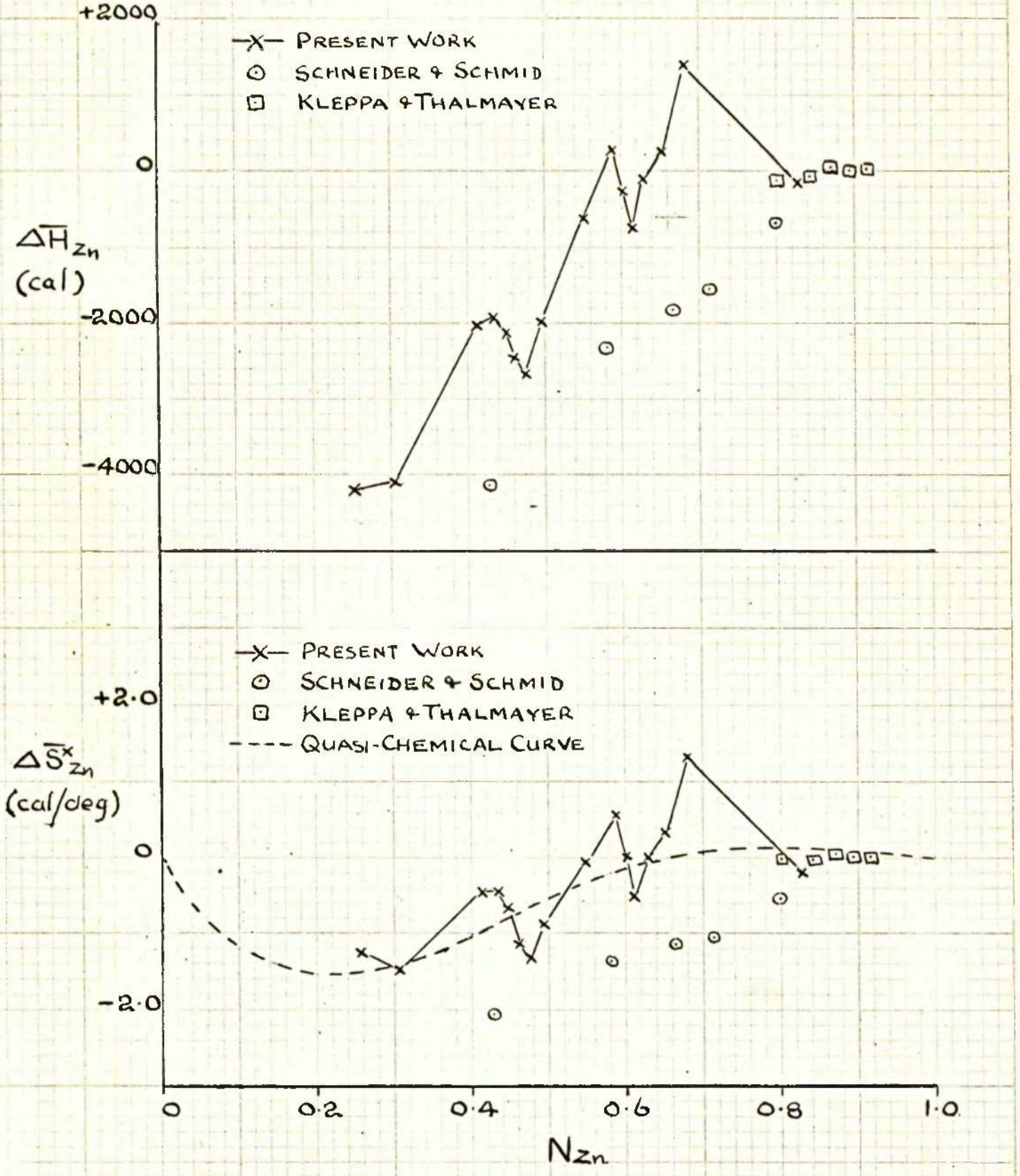

GRAPH 5

LIQUID ALLOYS - 1200°K.

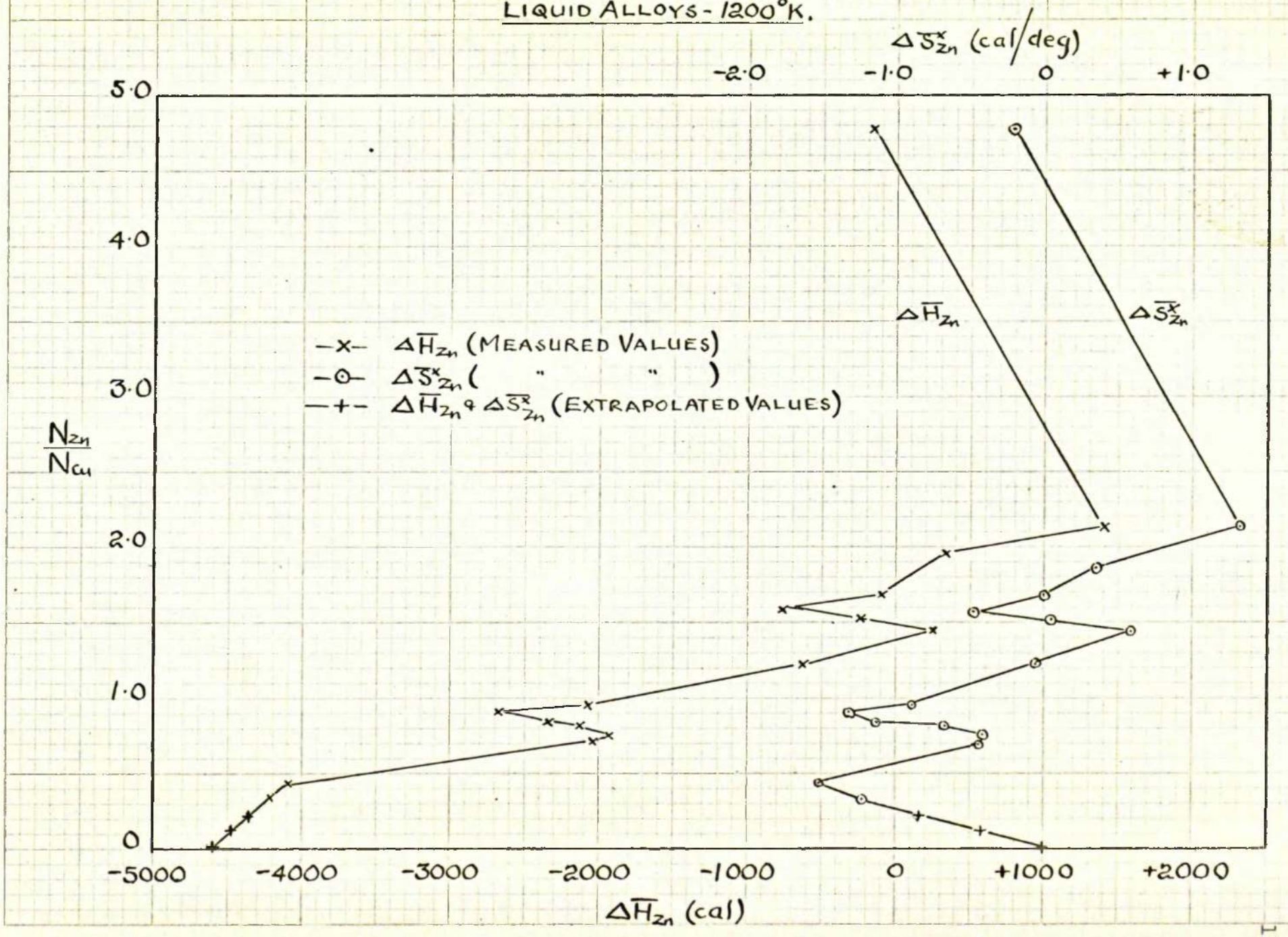

GRAPH 6

LIQUID ALLOYS - 1200°K

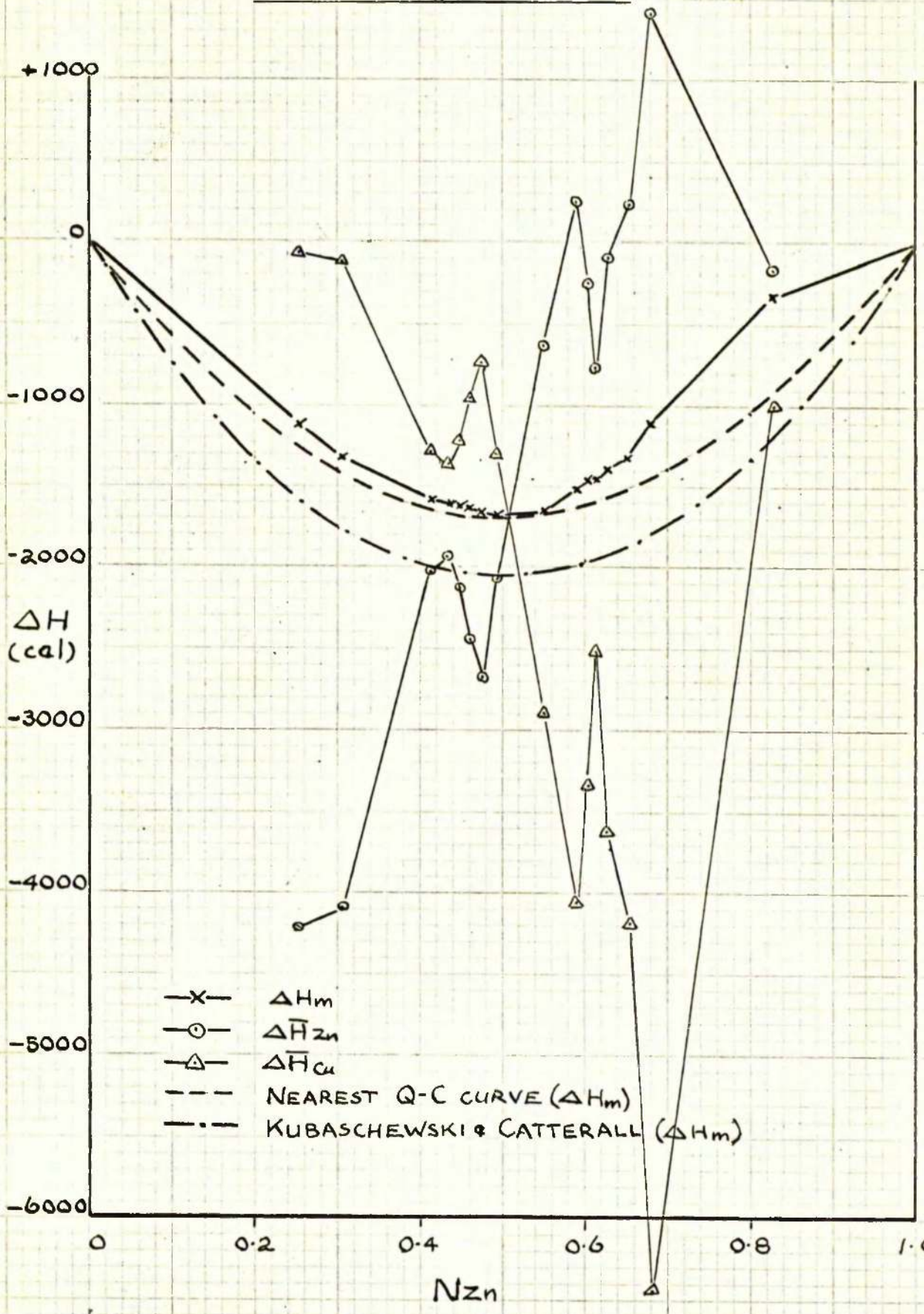

GRAPH 7.
LIQUID ALLOYS.

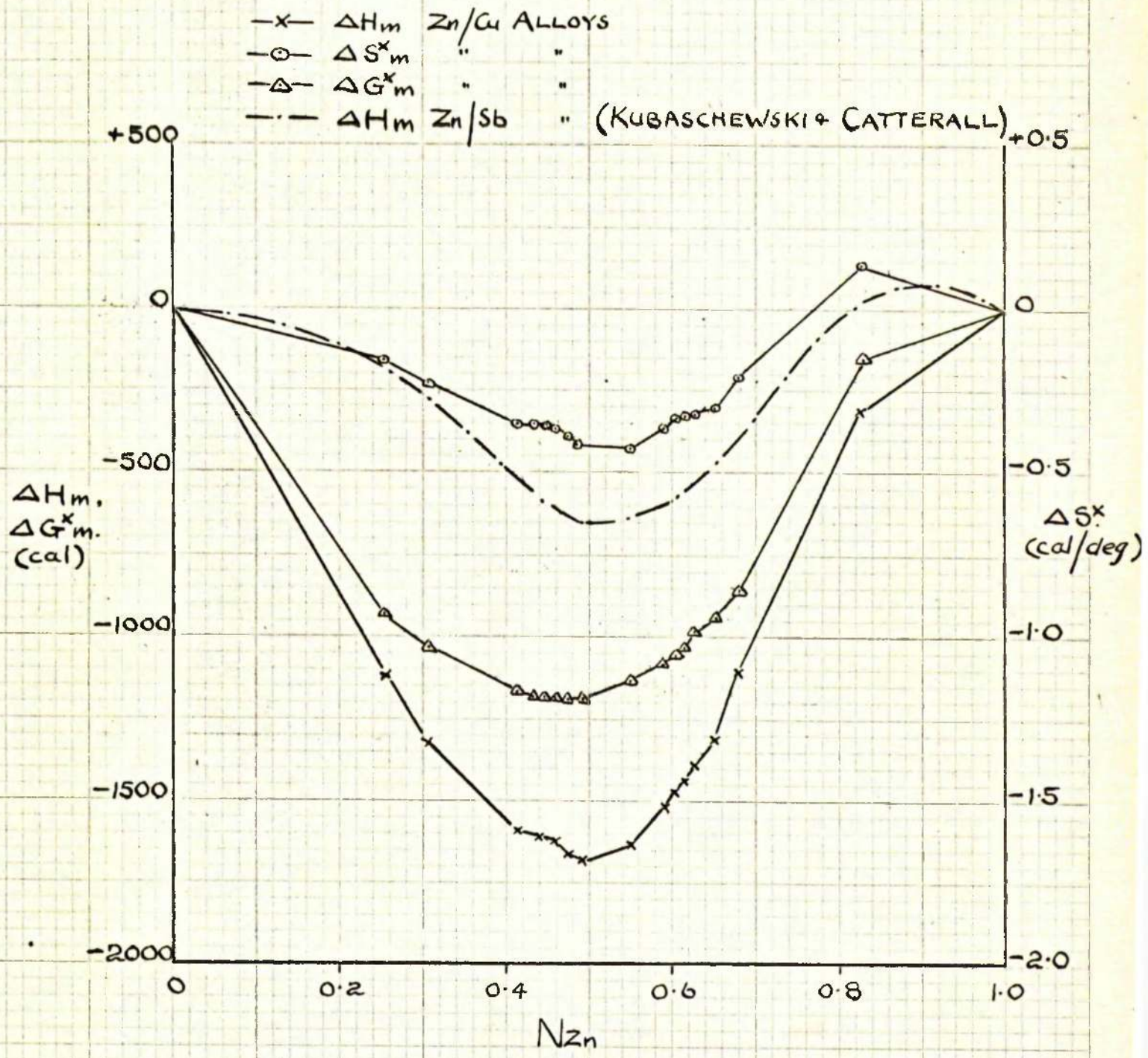

GRAPH 8
LIQUID ALLOYS - 1200°K

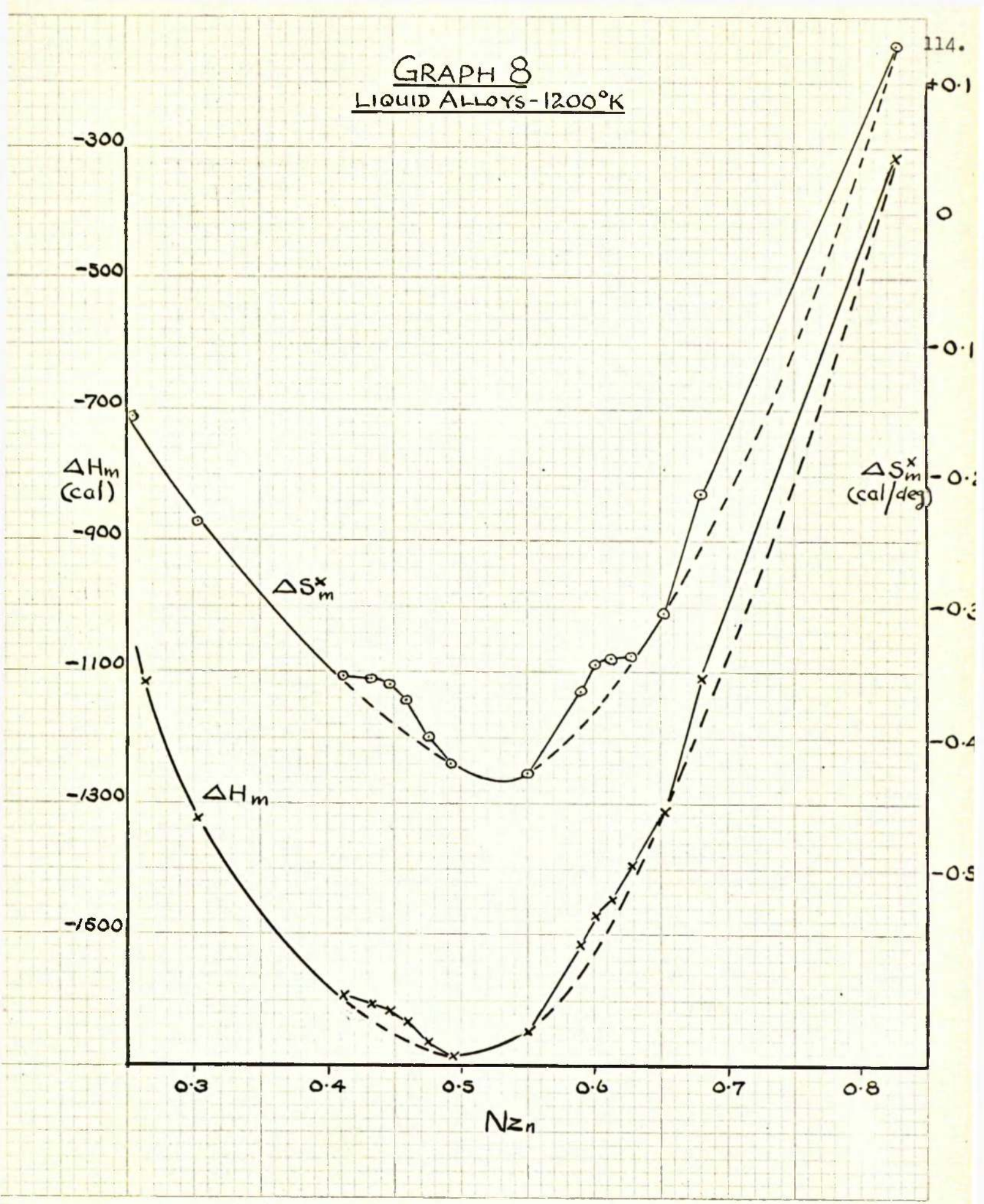

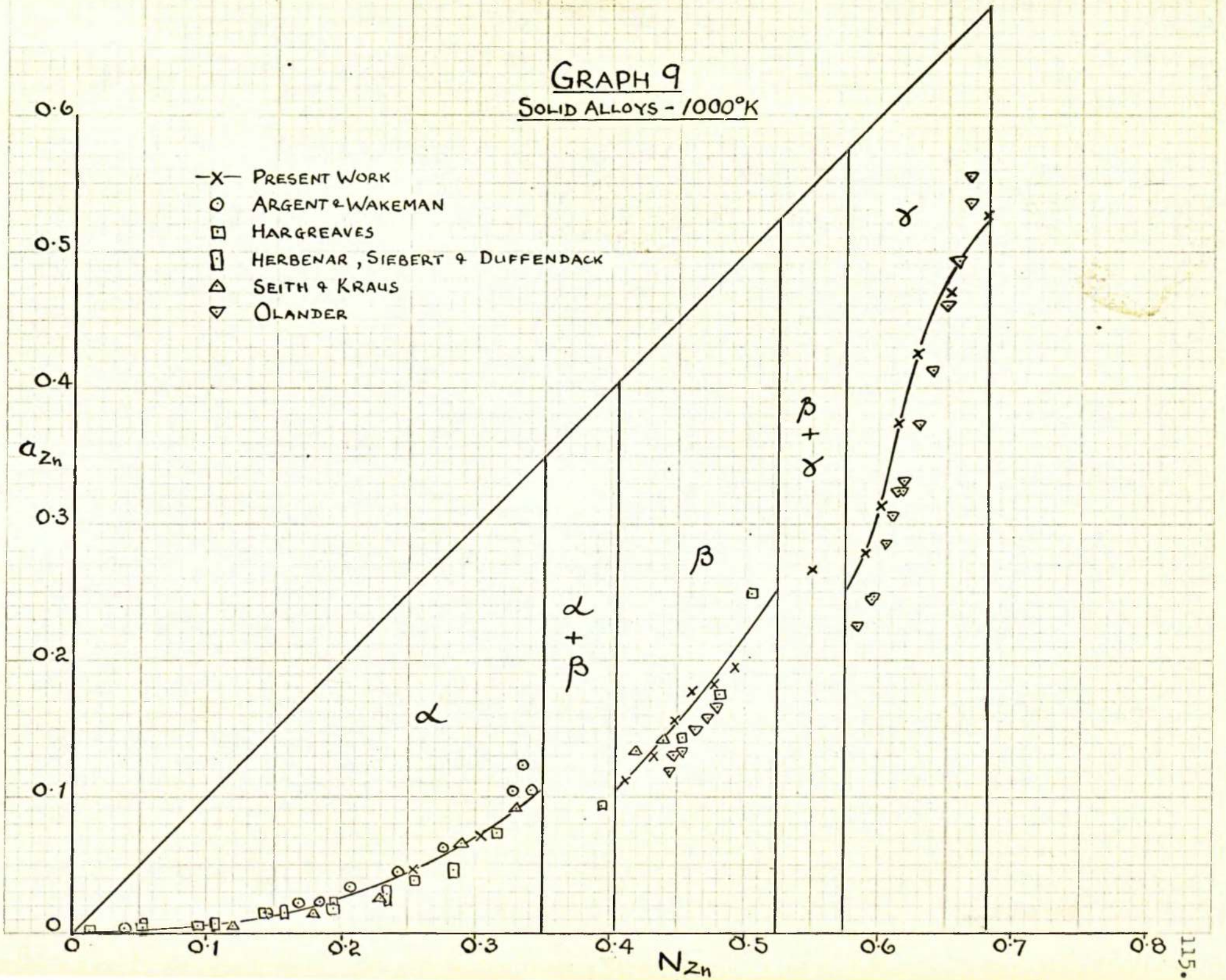
GRAPH 9
SOLID ALLOYS - 1000°K
—X— PRESENT WORK
ARGENT & WAKEMAN
HARGREAVES
HERBENAR, SIEBERT & DUFFENDACK
SEITH & KRAUS
OLANDER
a_{Zn}
N_{Zn}
0·6
0·5
0·4
0·3
0·2
0·1
0
0·1
0·2
0·3
0·4
0·5
0·6
0·7
0·8
α
α + β
β
β + γ
γ

GRAPH 10.

SOLID ALLOYS - 1000°K

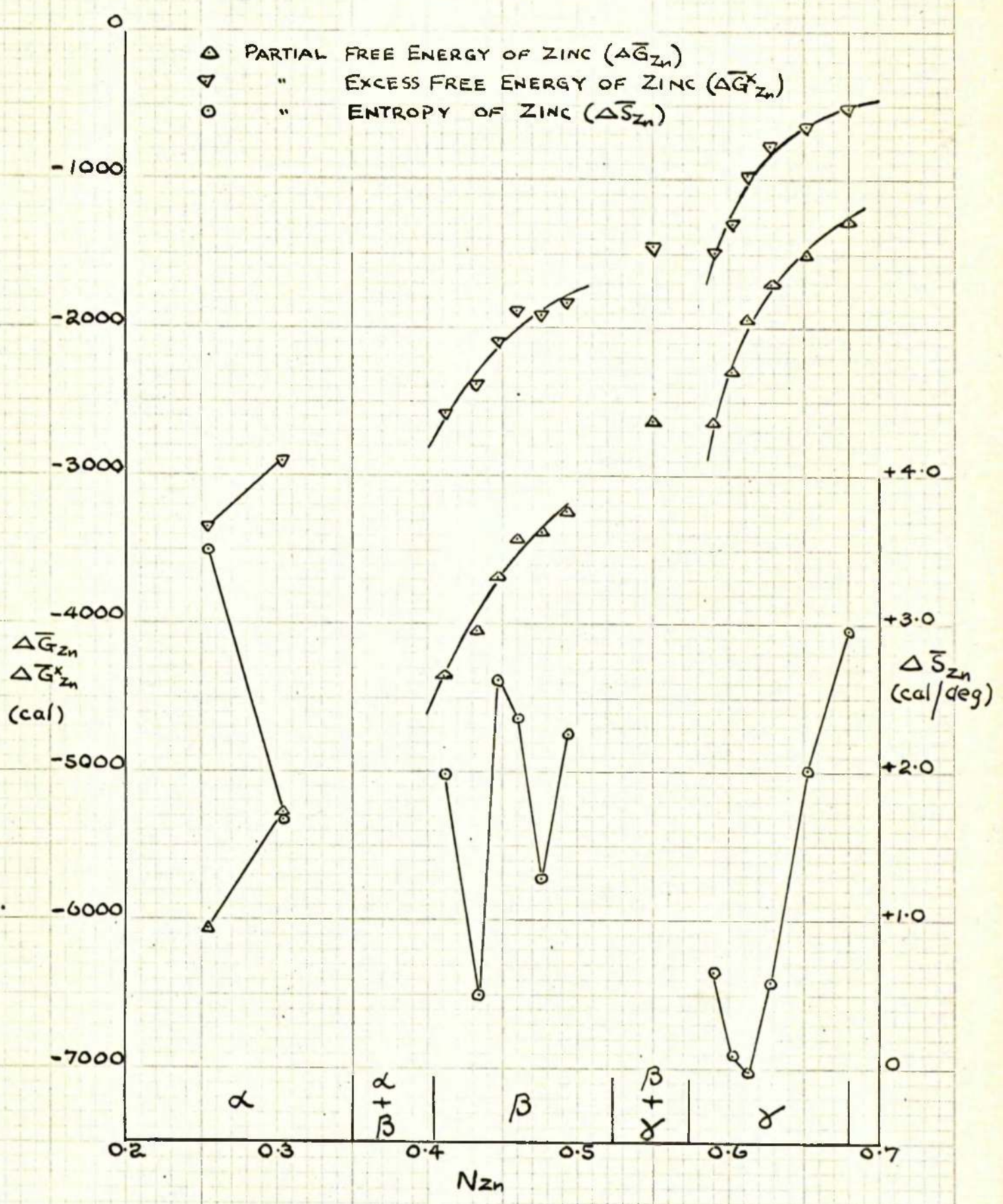

GRAPH 11

SOLID ALLOYS - 1000°K

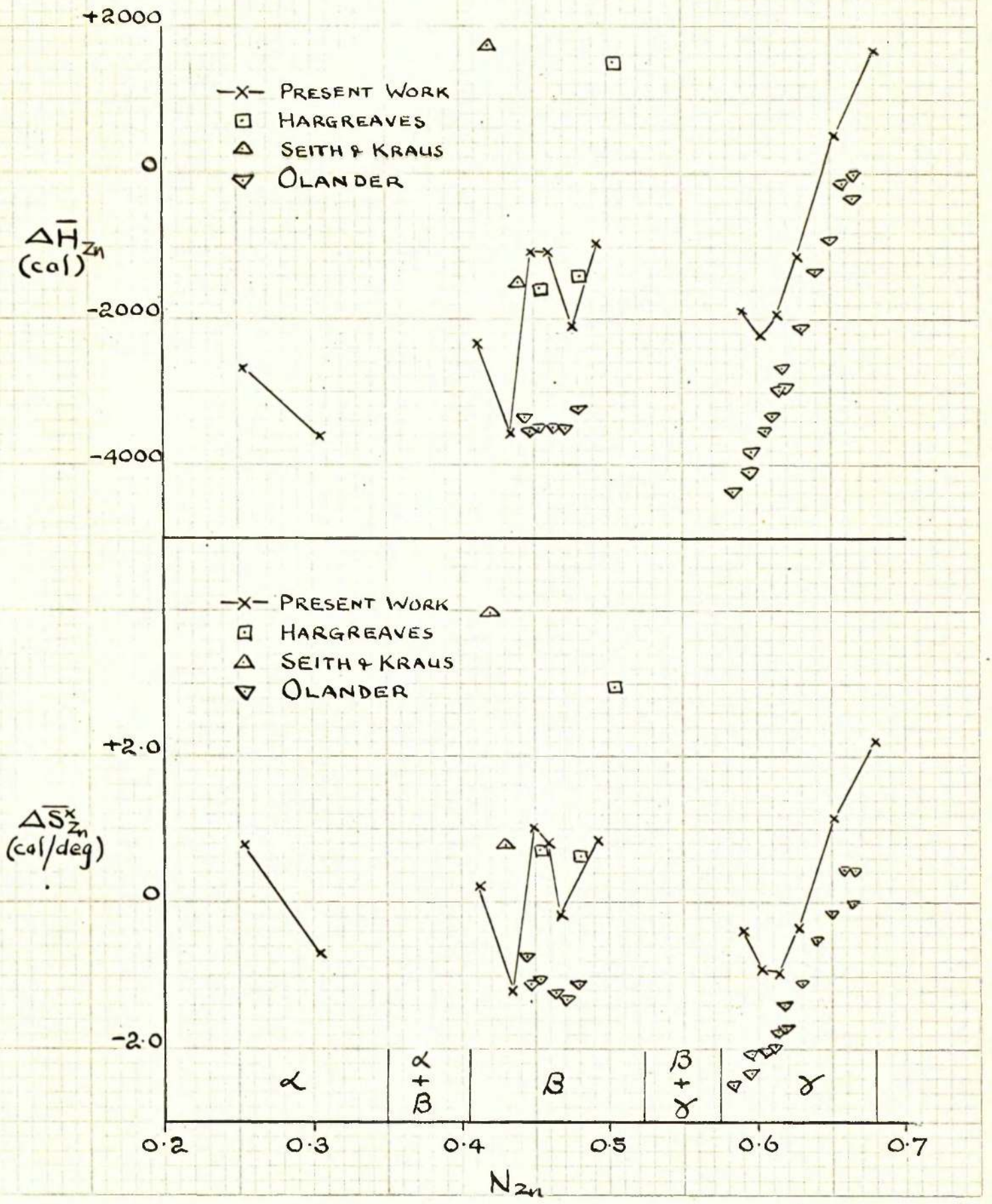

GRAPH 12

SOLID α-ALLOYS - 1000°K

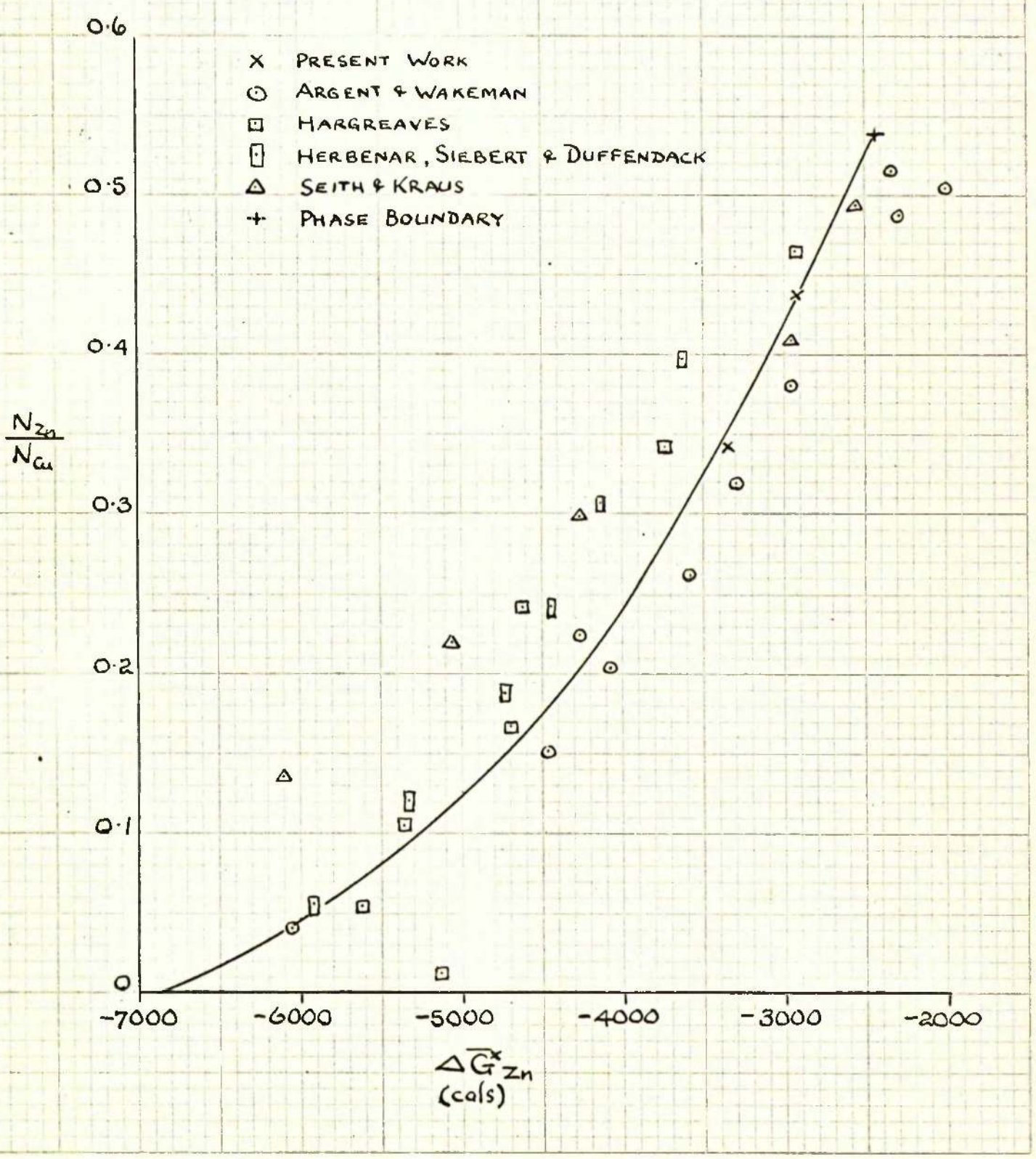

GRAPH 13.

SOLID α-ALLOYS - 1100°K.

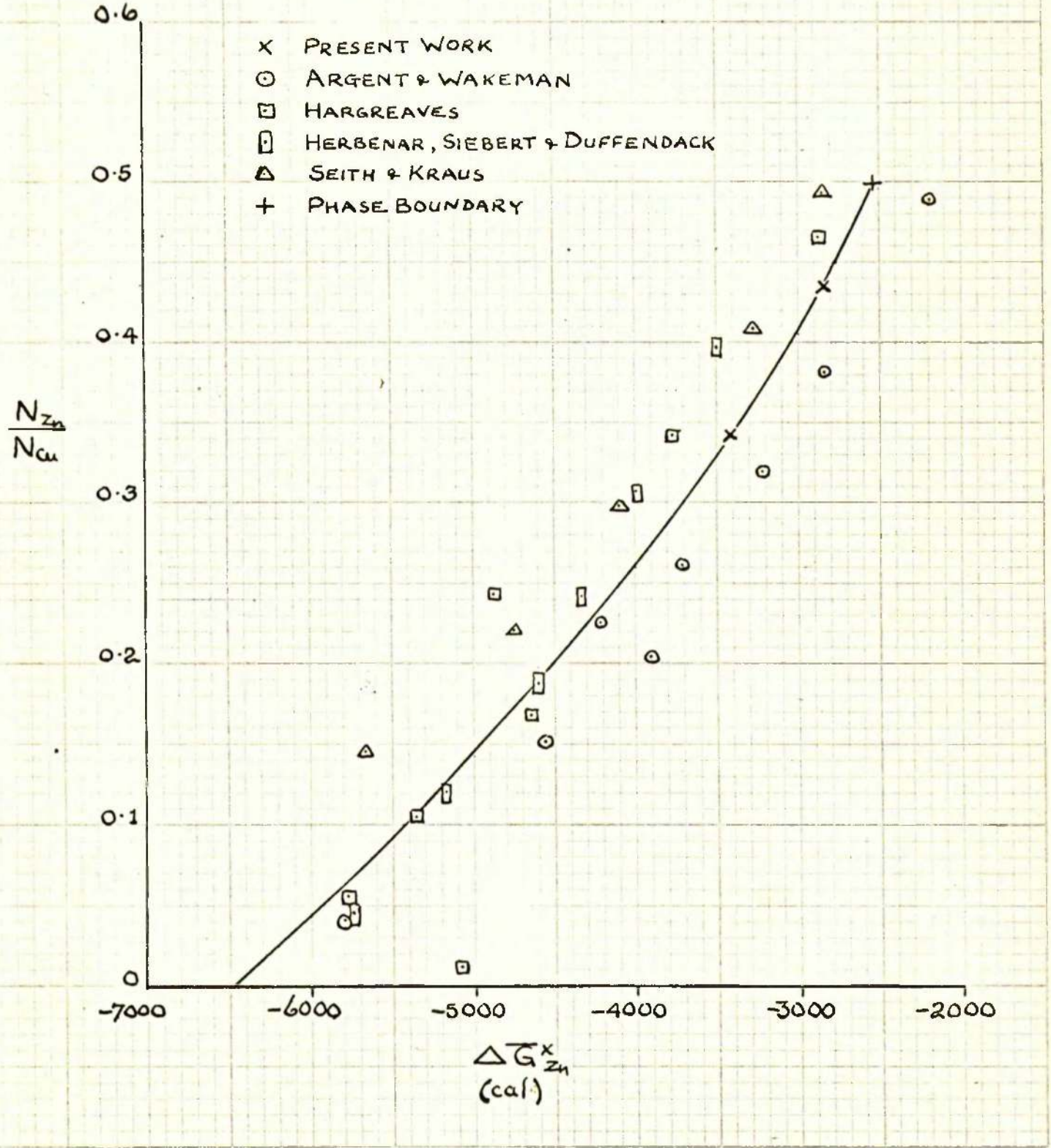

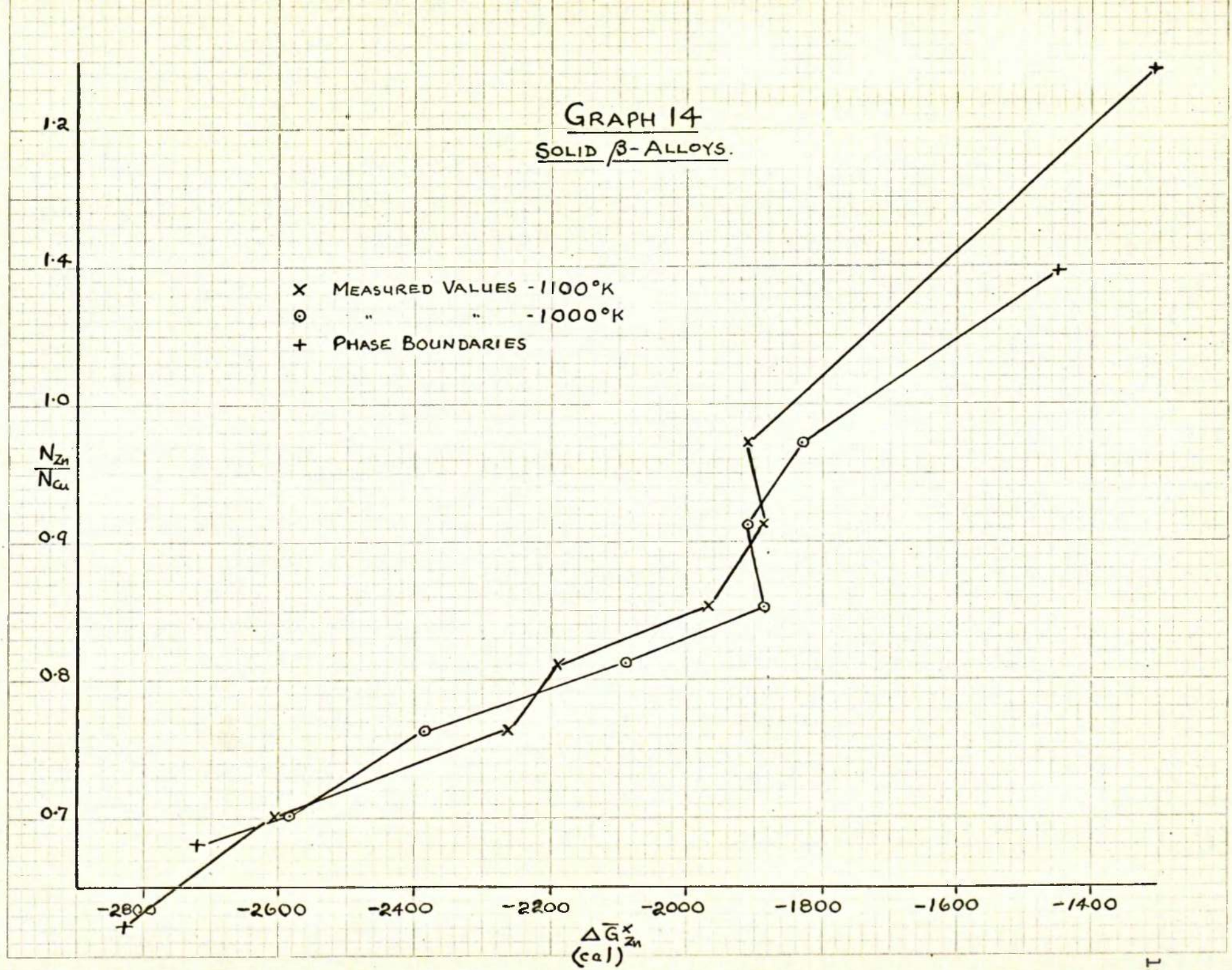
GRAPH 14
SOLID β-ALLOYS.
× MEASURED VALUES - 1100°K
⊙ " " - 1000°K
+ PHASE BOUNDARIES
1·2
1·4
1·0
0·9
0·8
0·7
$\frac{N_{Zn}}{N_{Cu}}$
-2800
-2600
-2400
-2200
-2000
-1800
-1600
-1400
$\Delta \bar{G}^{x}_{Zn}$ (cal)

GRAPH 15
SOLID γ-ALLOYS - 1000°K

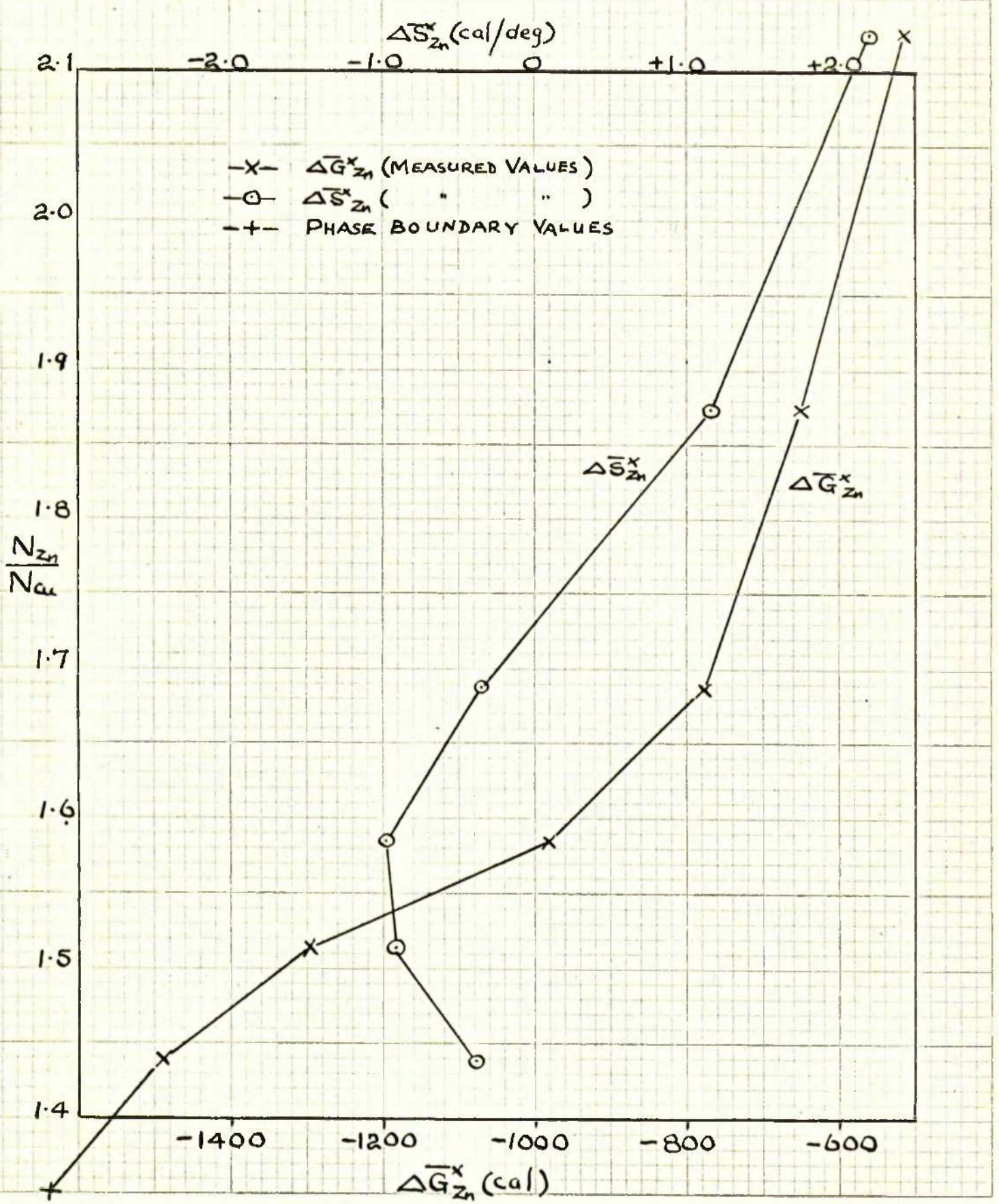

GRAPH 16
SOLID ALLOYS

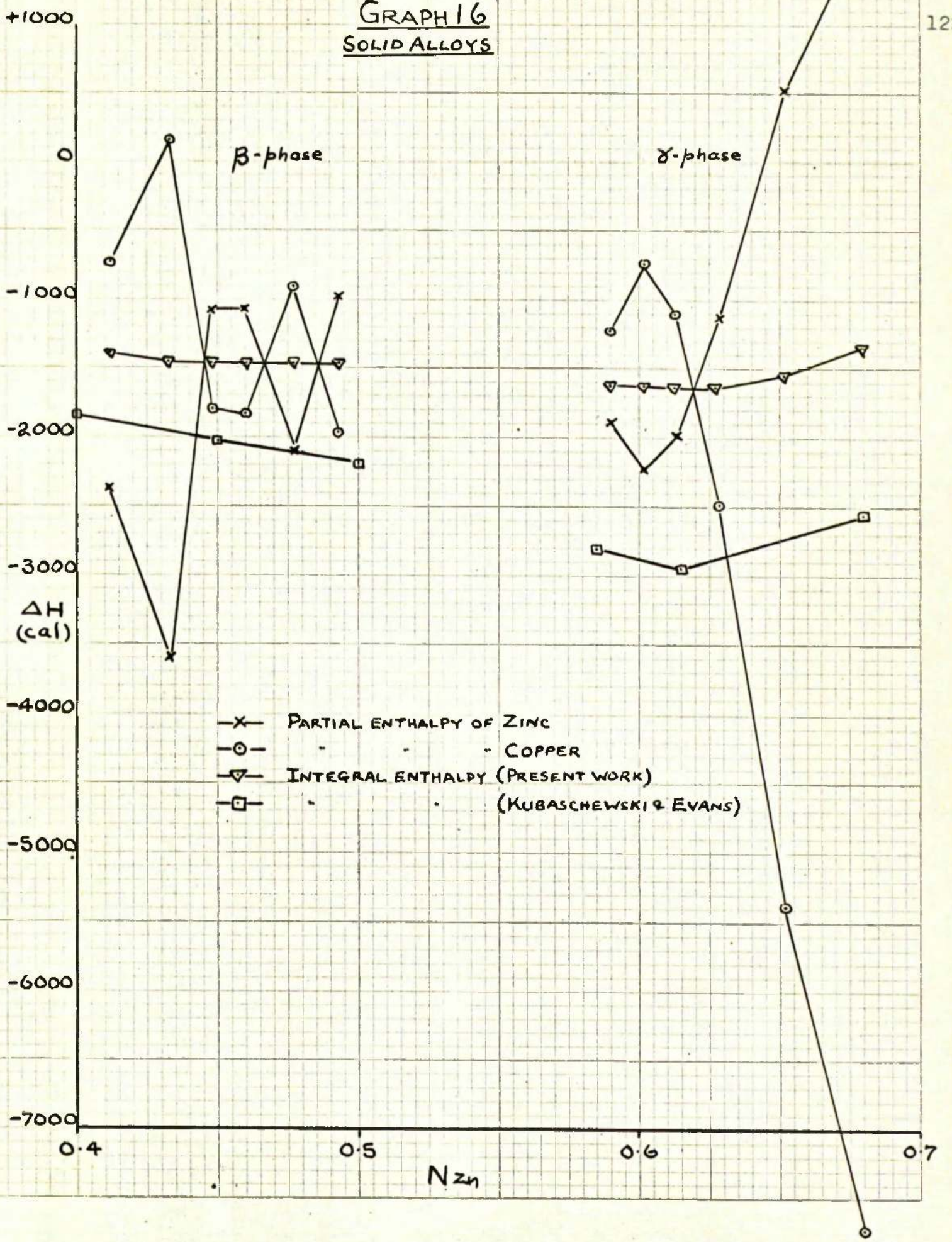

GRAPH 17

SOLID ALLOYS - 1000°K

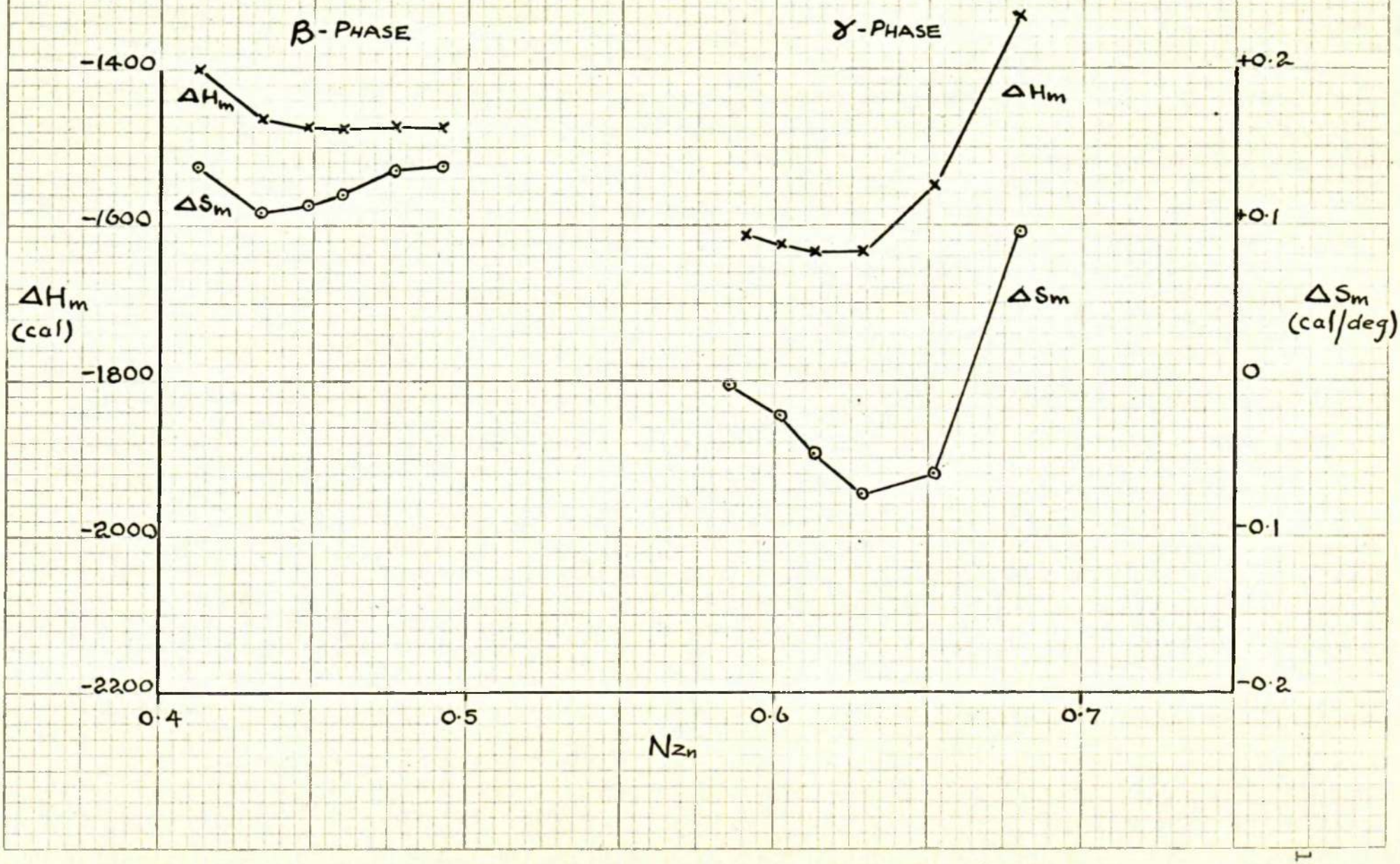

GRAPH 18.

LIQUID ALLOYS.

SYMBOL	SYSTEM	TEMP. °K	NoV FROM SLOPE	NoV FROM INTERCEPT	Z
×	Zn | Cu	1200	+1450	-90	12
+	Cu | Zn	1200	-570	-440	12
⊙	Zn | Sb	910	-1540	+10	10
⊡	Cd | Sb	773	-970	-280	10
▽	Tl | Au	1000	-370	-220	10
△	Al | Zn (K)	653	+250	+270	12

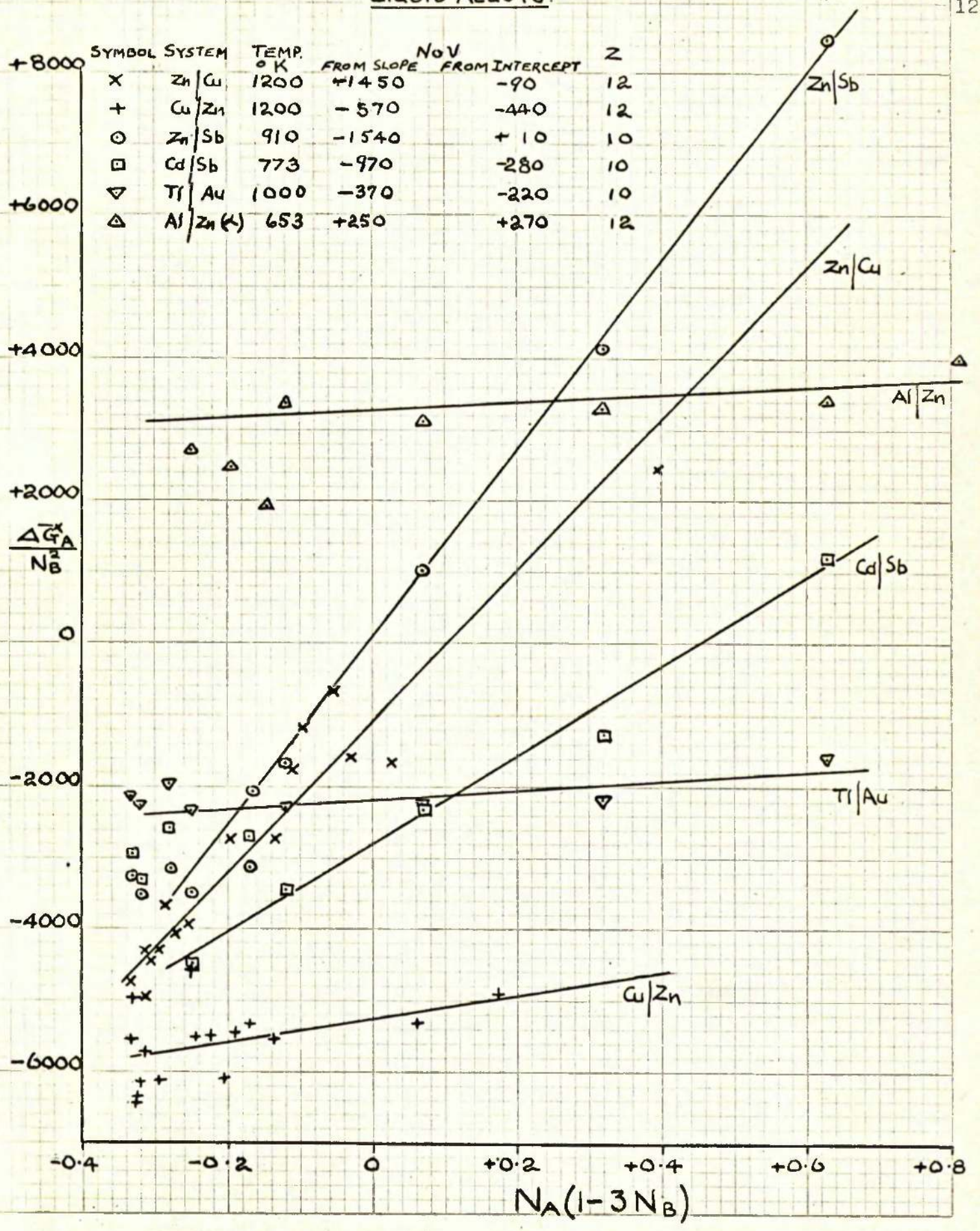

GRAPH 19.
LIQUID ALLOYS

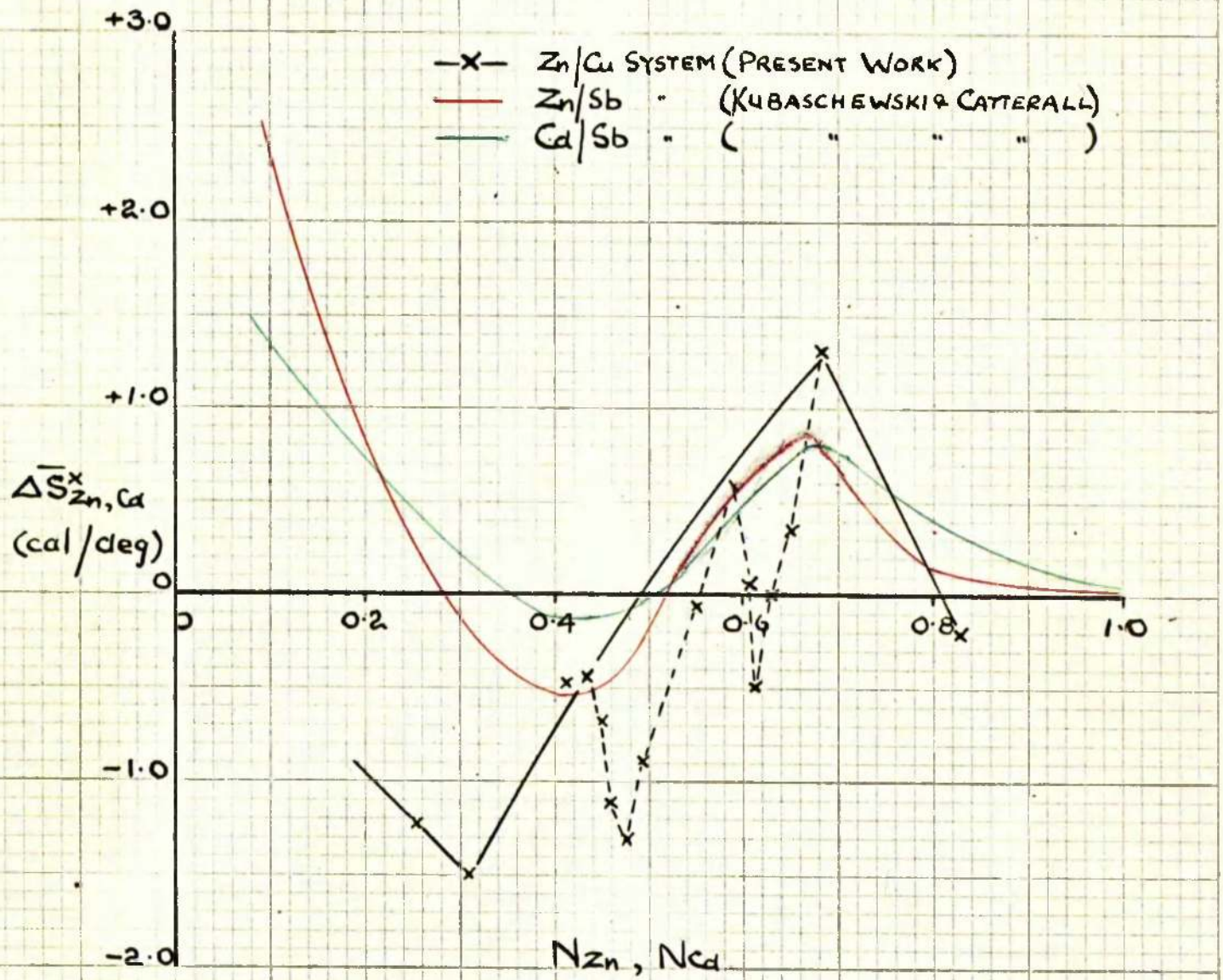

REFERENCES

REFERENCES

(1) J. Lumsden, "Thermodynamics of Alloys", Institute of Metals Monograph and Report Series No. 11 -(1952).

(2) O. Kubaschewski and J.A. Catterall, "Thermochemical Data of Alloys", Pergamon Press (1956).

(3) J.E. Hilliard, B.L. Averbach and M. Cohen, Acta. Met. Vol. 2 (1954) p. 621.

(4) O.J. Kleppa, "Liquid Metals and Solidification", A.S.M. Seminar, 39th National Metal Congress and Exposition (1957) p. 56.

(5) A. Olander, Zeits physik. Chem. (A) Vol. 164 (1933) p.428.

(6) O.J. Kleppa and C.E. Thalmayer, J. Phys. Chem., Vol. 63 (1959) p. 1953.

(7) L.H. Everett, F.W.M. Jacobs and J.A. Kitchener, Acta. Met. Vol 5 (1957) p. 261.

(8) R. Hargreaves, J. Inst. Metals, Vol. 64 (1939) p. 115.

(9) B.B. Argent and D.W. Wakeman, Trans. Far. Soc., Vol. 54 (1958) p. 799.

(10) A. Schneider and H. Schmid, Zeits, Electrochem, Vol. 48 (1942) p. 627.

(11) W. Seith and W. Kraus, Zeits. Electrochem. Vol. 44 (1938) p. 98

(12) A.W. Herbenar, C.A. Siebert and O.S. Duffendack, J. Metals Vol. 2 (1950) p.323.

(13) H.O. von Samson-Himmelstjerna, Zeits. Metallkunde Vol. 28 (1936) p. 197.

(14) F. Weibke, Zeits. anorg. Chem. Vol. 232 (1937) p. 289.

(15) F. Korber and W. Oelsen, Mitt. Kaiser Wilhelm Inst. Eisenforsch, Vol. 19 (1937), p.209.

(16) O. Kubaschewski and E.L. Evans, "Metallurgical Thermochemistry", Pergamon Press (1958).

(17) E.E. Underwood and B.L. Averbach, J. Metals, Vol. 3 (1951) p. 1198.

(18) Present work.

(19) P. Chiotti and K.J. Gill, Trans. A.I.M.E., Vol. 221 (1961), p. 873.

(20) K.K. Kelley, U.S. Bur. Mines Bull. 584 (1960).

(21) D.R. Stull and G.C. Sinke, "Thermodynamic Properties of the Elements", A.C.S. Wash. D.C. (1956).

(22) J.E. Vance and C.L. Whitman, J. Chem. Phys., Vol. 19 (1951) p.744.

(23) G.V. Raynor, "The Equilibrium Diagram of the System Copper-Zinc", Annotated Equilibrium Diagrams, No. 3, Inst. Metals (1955).

(24) Landolt-Börnstein, "Physikalische Chemische Tabellen II" Berlin (1923) p. 1338.

(25) W. Leitgebel, Zeits. anorg. Chem., Vol. 202 (1931) p. 305.

(26) O. Kubaschewski and E.L. Evans, "Metallurgical Thermochemistry" Pergamon Press, (1951).

(27) "International Critical Tables", Vol. 3 (1928) p. 204.

(28) A.C. Egerton, Phil. Mag.(vi) Vol. 33 (1917) p.33, Vol. 39 (1920) p.1.

(29) C.G. Maier, U.S. Bur. Mines Bull. 324 (1930)

(30) C.B. Alcock and G.W. Hooper, "Physical Chemistry of Process Metallurgy", Pt. 1. Vol. 7 Met. Soc. of A.I.M.E. (1959) p. 325.

(31) R.A. Swalin, "Thermodynamics of Solids", John Wiley and Sons, Inc., New York.

(32) E.A. Guggenheim, "Mixtures", Oxford University Press (1952).

A C K N O W L E D G M E N T S .

The author wishes to express his gratitude to Professor Emeritus Robert Hay for providing him, initially, with the opportunity to carry out this research and for his continued interest in the work. He is also indebted to Professor E. C. Ellwood for the continuation of these facilities and, along with Dr. John Taylor, for invaluable assistance and encouragement. The author also recalls with gratitude the help provided at the outset of the investigation by the late Dr. P. T. Carter.

Assistance given in the reproduction of diagrams by Mr. J. M. Steven and Messrs. Rank-Xerox, Ltd. of Queen Street, Glasgow is gratefully acknowledged.